

The maturation of the epithelial barrier in *Drosophila* wing imaginal discs is ecdysone dependent and is regulated to communicate the completion of regeneration

Danielle Frances DaCrema
McLean, Virginia

B.S. Biology and Chemistry, Christopher Newport University, 2013

A Dissertation presented to the Graduate Faculty of the
University of Virginia in Candidacy for the
Degree of Doctor of Philosophy

Department of Cell Biology

University of Virginia
December, 2020

Abstract

Regeneration is a highly coordinated process that results in the complete and scar-less restoration of damaged tissues. Over the last ten years we have improved our understanding of how tissues initiate and progress through regeneration, as well as how they coordinate regrowth with the growth of undamaged tissues. Still, little is known about how fully regenerated tissues communicate the completion of regeneration. Using the *Drosophila melanogaster* wing imaginal discs (adult wing precursors) as a regenerative model, I have found that one mechanism signaling the completion of regeneration is the re-establishment of epithelial barrier, which is disrupted during damage. The epithelial barrier is a semi-permeable diffusion barrier and a critical component of an epithelium. In the larval wing disc a functional barrier should separate the disc lumen from the larval hemolymph. However, one of the damage-response peptides, Dilp8, accumulates in the imaginal disc lumen following damage or exogenous overexpression even though it is only known to function in the brain and prothoracic gland. This indicates that some aspect of the imaginal disc epithelium contains Dilp8 in the lumen. My data indicate that the aspect of the disc providing this containment of Dilp8 is the epithelial barrier.

To investigate this, I used a phenotypic effect of Dilp8: Dilp8 causes a developmental delay, allowing the larvae to regenerate. This delay results from the inhibition of the production of the steroid hormone ecdysone in the brain and prothoracic gland. In Chapter 2, I show that disrupting the epithelial barrier by RNAi against the septate junction components Kune and Nr_x produces an extended Dilp8-mediated delay indicating that the barrier limits Dilp8 signaling. I observed the same result in damaged larvae, indicating that the barrier regulates the length of the regenerative response. Thus, the barrier is a mechanism to signal the completion of the regeneration.

To better understand this process, I characterized the functionality of the epithelial barrier in wing imaginal discs. I found that the epithelial barrier grows increasingly restrictive during the third instar between 92 and 116 hours after egg

deposition (h AED). Over time, the barrier becomes less permeable to the 10 kDa dextran used to assay barrier function. Interestingly, although the barrier becomes more exclusive, it is still functional at 92h AED, excluding significantly more dextran than a disrupted barrier. This change in function results from a change in the localization of the protein Coracle, a component of the septate junctions that form the epithelial barrier. Between 92h and 116h AED, Coracle shifts from being diffusely localized along the membrane to being localized only at the septate junctions. Diffusely localized Coracle is not necessary for the less restrictive barrier, as disruption by RNAi at 92h AED produces a barrier that excludes the dextran similarly to wild type controls.

In contrast, at 116h AED, Coracle localized only at the septate junctions is necessary for the more restrictive barrier, as Coracle disruption by RNAi also disrupts the barrier. The localization of Coracle is dependent on ecdysone, the same hormone that Dilp8 limits to produce developmental delay. Coracle localization at the septate junctions is significantly reduced in discs expressing a dominant-negative allele for the ecdysone receptor, and the barrier does not mature in these discs either. Inducing ecdysone signaling early causes the barrier to prematurely become more restrictive. These data indicate a model where a damaged tissue produces Dilp8, Dilp8 limits ecdysone in the brain and prothoracic gland, and then, once the tissue regenerates, the epithelial barrier begins to mature and limit Dilp8. This could act in a feedback loop where trapped Dilp8 results in higher levels of ecdysone which causes the barrier to mature more, which in turn traps more Dilp8.

I began to investigate this hypothesis in the Appendix. I first demonstrated that damage disrupts the epithelial barrier. Preliminary experiments indicate that the barrier is likely to recover after damage, but the timeframe of that recovery depends on when the larvae are damaged. *Drosophila* larvae lose the ability to regenerate during late larval development in response to rising ecdysone levels. When larvae are damaged with X-irradiation before regeneration is restricted, the barrier is disrupted and remains disrupted for an extended amount of time,

beginning to recover 48 hours after damage (the last timepoint collected). During this time the septate junction components are also depleted from the septate junctions. In contrast, when larvae are damaged after regeneration is restricted, the barrier is disrupted but recovers within 24 hours and the septate junctions are never depleted. These data preliminarily indicate that the barrier is downregulated during regeneration.

Overall, this work furthers our understanding of the hormonal regulation of the epithelial barrier during development and demonstrates how the restoration of a tissue's function can signal the completion of regeneration.

Acknowledgements

I would not be here without an incredibly supportive personal and professional network of people.

I'd like to start by thanking my advisor Adrian Halme. Adrian has been a wonderful mentor. He managed to adapt his mentoring to match the level of assistance that I needed to always challenged but never beyond my current abilities. This is an incredible and rare skill, one that I hope to emulate in the future. Another skill that Adrian has that is incredibly useful and that I hope I have inherited is the ability to ask the best question in a current situation. Adrian also gave me incredible latitude to explore various career options.

Next I would like to thank my thesis committee: Ann Sutherland, Michelle Bland, and Todd Stukenberg. Each has pushed me to be a better scientist and has supported me personally in one way or another. Ann convinced me to stay in grad school when I was considering quitting. Michelle always made me excited about my project again. Todd pushed me to quantify my data and without that quantification, I would have overlooked a critical component of this thesis.

I'd like to extend thanks my lab mates past and present (Faith Karanja, Cristina D'Ancona, Ryunosuke Yano, Subhashri Sahu, Rajan Bhandari, Rebecca Jaszczak, Jacob Jaszczak, and Jacob Wolpe) for always being there to talk about difficult problems or just to joke off in lab. And to the Cell Biology Department at UVA and especially the North Labs, always willing to share resources or equipment.

During my time in grad school, I've become very active in the science policy community at UVA and across the country. This would not have been possible without Michaela Rikard and Courtney Rogers who started the Science Policy Initiative at UVA (SPI) in 2016. From my work within SPI, I became involved at the national level with the National Science Policy Network (NSPN). With NSPN, I've had the opportunity to learn skills that I would not have easily been able to learn at UVA. The NSPN community inspired me to apply for the 2019 Christine Mirzayan Science and Technology Policy Fellowship at the National Academies of Sciences,

Engineering, and Medicine, to which I was accepted. Before doing the Mirzayan, I don't think I've ever met a group of people so eager to help each other succeed. I gained skills doing the Mirzayan and learned about career options, but this tight network is the most valuable experience I could have ever received.

My experience in the Mirzayan fellowship heavily influenced another project I worked on. I was part of a working group (along with Matthew Diasio, Holly Mayton, Michaela Rickard) that planned, designed, and developed a science policy fellowship in Virginia: the Commonwealth of Virginia Engineering and Science (COVES) Policy Fellowship. We worked with the Marlit Hayslett, Sonali Majumdar, and Phillip Trella at UVA and James Aylor at the Virginia Academy of Science, Engineering and Medicine to make COVES a reality. Thanks to all their efforts our 3-month fellowship just ended. We got funding for 6 fellows from 8 participating universities across Virginia. Our fellows worked in Virginia based science policy focused NGOs, in the policy offices of prominent scientific industries in Virginia, and in legislative and executive offices in Virginia. We have much to learn, but overall, this was a massive success! I'm thrilled to have been a part of it and look forward to future years.

As COVES became more and more a reality, I had the opportunity to co-write a white paper with other NSPN members (Matthew Diasio, Ryan Dudek, Coleman Harris, Meredith Schmehl, Caroline Schuerger, and Melody Tan) on how to implement similar fellowships across the United States. We've received great support on the paper and grew close in writing it.

I'd also like to thank my virtual support networks. TagBackTV's and Lady Wolf's YouTube communities are great places to relax at the end of a long day or to put on in the background during a long session of dissecting or imaging. These communities are always willing to throw around a few jokes or talk up anyone having a bad day. It's fantastic.

Along a similar vein, at the start of the COVID-19 pandemic, I joined a small virtual community of scholars (Write Here, Write Now) organized by Jazmine Scarlett. We have supported each other through the pandemic so far, through

thesis writing, job applications, and job losses. We also share drool-inducing recipes.

I'd like to thank my family. My parents, Regina O'Hare and John DaCrema, for always being interested in and excited by my work even if they didn't understand it, and for their moral and financial support throughout the years. They never pushed me to do more, but always gave me the latitude and means to do as much as I could manage. My best friend and sister by choice, Aurelia Khorsand, has never failed to make me laugh. I can always count on Aurelia to be there when I need her for anything from deep emotional support to thoughtful input on topics to lightness and levity to new explorations. Aurelia's parents, Susan and Ali Khorsand, are as much my parents as mine are. My pets have gotten me through grad school. Link is gives the best pupper hugs and can always make me smile. When I am with my family, I am the best version of myself.

Unfortunately, we've also had several deaths in the family during my time in grad school. Zelda was the first dog I raised from a puppy and passed away of old age in 2017, but I'll never forget coming home to those squirming puppy kisses. My aunts, Kathy McGraime and Mary Bagnell, and my grandmother, Vera DaCrema, also died during my time here. I was particularly close to my grandmother. She had a great sense of humor and a beautiful cackling laugh that she was never afraid to break out to anyone.

Last, but not least, I'd like to thank a multitude of friends and family who helped proofread this thesis, each of them proofread about 10 pages for clarity or checked my formatting for consistency. So big thanks to Regina O'Hare, Barbara Felitti, Reva Savkar, Bob Loser, Kristin Deason, Jon Fichthorn, Cindy Allgaier, Stephanie Pecaro, Susan Pecaio, John Brews, Michelle Victoria, Mariah Parker, Lisa Webb, Allen Tuller, Renee Shields, Jocelyn Day, Holland Dougherty, Becca Monteleone, Aurelia Khorsand, Noel Miller, Laura Fontenas, Joseph Ong, and Maria Porter.

Table of Contents

Abstract	i
Acknowledgements	iv
Table of Contents	vii
Abbreviations	x
List of Figures	xi
Chapter 1. <i>Drosophila melanogaster</i> as a model for the loss of regenerative ability and the development of the epithelial barrier.	1
1.1 Introduction	2
1.2 How is the completion of regeneration regulated?	4
1.3 <i>Drosophila melanogaster</i> as a regenerative model	7
1.4 Systemic responses to regeneration in <i>Drosophila</i>	9
1.5 Development and anatomy of wing imaginal discs	11
1.6 Epithelial barrier, vertebrates vs. invertebrates	15
1.7 Occluding junction components	19
1.8 Establishment of the epithelial barrier	22
1.9 Role of epithelial barrier regulation in tissue homeostasis	24
1.10 Conclusion and overview of thesis	25
Chapter 2. Ecdysone regulates the <i>Drosophila</i> imaginal disc epithelial barrier, determining the duration of regeneration checkpoint delay.	27
Abstract	28
2.1 Introduction	29
2.2 Results	30
2.2.1 The activity of Dilp8 is constrained by the imaginal disc epithelial barrier determining the duration of the regeneration checkpoint delay	30
2.2.2 The wing imaginal disc epithelial barrier becomes more restrictive during the last larval instar	34

	viii
2.2.3 Changes in epithelial barrier permeability correlate with changes in junctional protein expression and localization	42
2.2.4 Coracle is required to produce the changes in epithelial barrier permeability during the last larval instar	47
2.2.5 Ecdysone signaling promotes decreased epithelial barrier permeability and Coracle re-localization	54
2.2.6 The epithelial barrier regulates the end point of regeneration	58
2.3 Discussion	62
2.3.1 How is the end of regeneration determined?	62
2.3.2 Regulated maturation of the epithelial barrier	63
2.3.3 Could other signaling pathways be regulated by epithelial barrier maturation?	64
2.4 Materials and Methods	65
2.4.1 Drosophila stocks and husbandry	65
2.4.2 Pupariation time and developmental delay	66
2.4.3 Dissection and immunofluorescent staining	67
2.4.4 Imaging and statistical analysis	68
2.4.5 Dextran assay	68
2.4.6 Quantification of septate junction component localization	69
2.4.7 Genotypes	70
Appendix. Investigating epithelial barrier maturation and recovery during tissue regeneration.	74
Abstract	75
α.1 Introduction	76
α.2 Results	77
α.2.1 The epithelial barrier is disrupted following damage and may be restored prior to pupariation	77

α.2.2	Septate junction components are down-regulated during regeneration	82
α.3	Discussion	89
α.3.1	Disruption of the epithelial barrier following damage	89
α.3.2	Regulation of the epithelial barrier during regeneration	90
α.3.3	How is the end of regeneration determined?	91
α.4	Methods	91
α.4.1	Drosophila stocks, husbandry, and irradiation	92
α.4.2	Dissection and immunofluorescent staining	92
α.4.3	Imaging	93
α.4.4	Dextran assay	94
α.4.5	Genotypes	94
	Chapter 3. Conclusions, Discussion, and Future Directions.	96
3.1	Summary	97
3.2	Significance and implications	98
3.2.1	The role of epithelial barrier maturation in regeneration	98
3.2.2	The regulation and change of function of the epithelial barrier	99
3.2.3	The development of the barrier and ecdysone signaling	100
3.2.4	The role of the epithelial barrier in regulating signaling and developmental patterns	101
3.3	Proposal for future directions	102
3.3.1	How is epithelial barrier maturation regulated during regeneration?	102
3.3.2	How does tissue damage disrupt the epithelial barrier?	103
3.3.3	What is the role of Coracle in the less restrictive barrier?	105

3.3.4	How does ecdysone regulate Coracle localization and barrier maturation?	109 ^x
3.3.5	Does the mature barrier limit Dpp signaling in late third instar larvae?	111
3.3.6	What is the role of the less restrictive barrier?	112
3.4	Thesis conclusions and perspectives	113
References		115

List of Abbreviations

h AED	Hours after egg deposition
TARGET	Temporal and regional gene expression targeting
DEMISE	Dual expression method for induced site-specific eradication
EcR	Ecdysone Receptor
PTTH	Prothoracicotropic hormone
Dilp8	Drosophila Insulin-like Peptide 8
MAGUK	Membrane-associated guanylate kinase
PDZ	PSd/AP90, discs large, ZO-1
GUK	Guanylate kinase
PG	Prothoracic gland
Cora	Coracle
Nrx	Neurexin-IV
Ap	Apterous
Kune	Kune-Kune
Bx	Beadex
EtOH	Ethanol
20HE	20-hydroxyecdysone
Dpp	Decapentaplegic
Dcp1	Death Caspase-1
Usp	Ultraspiracle

List of Figures

Chapter 1. *Drosophila melanogaster* as a model for the loss of regenerative ability and the development of the epithelial barrier.

1-1	Larval wing imaginal disc anatomy.	14
1-2	Structure of occluding junctions in vertebrates and invertebrates.	18

Chapter 2. Ecdysone regulates the *Drosophila* imaginal discs epithelial barrier, determining the duration of regeneration checkpoint delay.

2-1	Dilp8 accumulates in the wing imaginal disc lumen.	32
2-2	The epithelial barrier limits Dilp8 signaling.	33
2-3	Explanation of the dextran assay for barrier function.	37
2-4	The wing disc epithelial barrier becomes more restrictive with progression through the third larval instar.	39
2-5	The epithelial barrier of wing imaginal discs grows more exclusionary to 70 kDa fluorescent dextran during the third instar.	40
2-6	The epithelial barrier matures between 92h and 116h AED, becoming more restrictive to 10 kDa fluorescein conjugated dextran.	41
2-7	The localization of septate junction components changes between 92h and 116h AED.	43
2-8	Complete images from Figure 2-7.	45
2-9	Method for junction quantification.	46
2-10	The role of Cora in epithelial barrier activity changes from 92h to 116h AED.	49
2-11	RNAi inhibition of septate junction components.	50
2-12	The localization of Nr _x and Kune is dependent on Cora at both 92h and 116h AED.	52
2-13	Ecdysone induces barrier maturation and Cora localization.	56
2-14	Ecdysone feeding induces barrier maturation early.	57

	xiii
2-15 Actin stain from discs in Figure 2-13.	58
2-16 The epithelial barrier regulates the end point of regeneration.	59
2-17 Coexpression of Eiger and RNAi against septate junction components does not significantly alter measured Dilp8 expression.	61
2-18 Nr _x limits Eiger-induced delay.	62

Appendix. Investigating epithelial barrier maturation and recovery during tissue regeneration.

Figure α -1. Damage disrupts the epithelial barrier, but it may recover before pupariation.	79
Figure α -2. Actin stain from discs in Figure α -1.	81
Figure α -3. Epithelial barrier of punctured imaginal discs.	81
Figure α -4. Nr _x is depleted and mislocalized following X-irradiation before but not after regeneration restriction.	85
Figure α -5. Actin stain from discs in Figure α -4.	
Figure α -6. Cora is depleted and mislocalized following X-irradiation before but not after regeneration restriction.	86
Figure α -7. Actin stain from discs in Figure α -6.	87

89

Chapter 3. Conclusions, Discussion, and Future Directions.

Figure 3-1. Kune protein levels following temporal knockdown.	108
Figure 3-2. Cora isoforms and binding site predictions.	110

Chapter 1

***Drosophila melanogaster* as a model for the loss of regenerative ability and the development of the epithelial barrier**

1.1 Introduction

Regeneration is commonly defined as the scar-less replacement of lost or damaged tissue with complete restoration of tissue mass and function. Many species can regenerate throughout their lifetime. Famously, planarian flatworms can regrow completely from small pieces of tissue as a result of clonogenic neoblasts distributed throughout the body (Wagner et al., 2011). Some vertebrate species like the axolotl salamander can completely regrow limbs below the shoulder joint. In axolotl blastemas (the region of regenerative activity), the stem cells that eventually regrow the tissues originate in the same embryonic region as the tissues that they eventually replace (Kragl et al., 2009).

However, in many animals, including many mammals, regenerative capacity is markedly reduced shortly after birth and/or limited to certain tissues. For instance, mammalian hearts can regenerate during the neonatal period from significant tissue loss that severely scars more developed hearts. In mice, this prenatal regenerative capacity was documented by experiments that removed 15% of the ventricular myocardium; complete and functional restoration of the lost tissue was observed within 21 days (Porrello et al., 2011; reviewed in Eschenhagen et al., 2017). In the young mice that are able to regenerate their heart tissue, the observed regeneration is histologically similar to zebrafish heart regeneration (Porrello et al., 2011; Poss et al., 2002). A large blood clot forms within a day, sealing the damaged area, which is followed by a large inflammatory response (Porrello et al., 2011). The lost tissue is replaced by cardiomyocytes that derive from other proliferating cardiomyocytes in the developing heart; the blood clot is gradually reabsorbed as the tissue is replaced (Porrello et al., 2011). When similar cardiac damage is produced in mice at post-natal day 7 or 21, the missing tissue is replaced with a fibrotic scar (Porrello et al., 2011). The cause of the change in regenerative ability is unknown but correlates with reduced proliferation of cardiomyocytes and an increased presence of binucleate cardiomyocytes (Porrello et al., 2011; reviewed in Eschenhagen et al., 2017). Binucleated cardiomyocytes in adult tissue proliferate but at a low rate (0.5-2% per year) and

overall levels remain stable (Ali et al., 2014; Bergmann et al., 2015; reviewed in Eschenhagen et al., 2017).

Mice can also regenerate up to 50% of the distal tips of their toes after amputation (Borgens, 1982; Han et al., 2008). Blastema formation in the regenerating distal mouse toe is dependent on Wnt activated differentiation of the nail stem cells and BMP-dependent ossification and proliferation of the remaining bone of the amputated digit (Han et al., 2008; Sensi and Marques-Souza, 2019; Takeo et al., 2013). The blastemas observed in the regenerating mouse toe are similar to blastemas observed during urodele amphibian limb regeneration. Like amphibians, the blastema derives from a heterogeneous population of ectoderm and mesoderm-derived progenitor cells, not pluripotent stem cell populations, and have high levels of *Msx1* expression that induces dedifferentiation (although amphibians also use *Msx2*) (Brockes and Kumar, 2005; Carlson et al., 1998; Han et al., 2008; Simon et al., 1995). Human children can also sometimes regrow finger tips scarlessly, including complete restoration of fingerprints (Illingworth, 1974). It is not known if the mechanism of digit regeneration in humans is the same as in mice, although it seems likely given similarities in characteristics of recovery from the injury and similarities between blastemas across species. It is also not known when or how this regenerative ability is lost in humans; the oldest child reported to regenerate their fingertips was 11 years old (Illingworth, 1974).

Some human tissues do retain their regenerative capacity into adulthood: occasionally the vas deferens will re-grow following sterilization and the individual will become fertile again (Girgis, 1975). The adult liver can regenerate if more than 50% of the hepatocytes remain (Katoonizadeh et al., 2006), and the highly organized endometrium is completely lost and then regenerates during the menstrual cycle (Graubert et al., 2001). However, in general, reproductive capacity greatly diminishes over a person's lifetime (reviewed in Yun, 2015). Bone density loss with age results from reduced proliferation and regeneration of tissues in the bones due to senescence of bone marrow stromal cells (Stenderup et al., 2003).

The great allure of regeneration and regenerative medicine is that it is so common in nature. We know that there are extensive similarities between human tissue regeneration and regeneration in other organisms. We know that some organisms are capable of extensive regeneration. It is easy to imagine a world in which we could use regenerative medicine to regain this potential in adult humans, which would have extensive impacts on medicine. Currently in the United States, heart disease is the leading cause of death (Heron, 2019), approximately 2 million people have a limb amputation (Ziegler-Graham et al., 2008), and annually between 30 and 40% of adults over 65 fall at least once and although many falls are low impact as a result of loss of bone density, these falls account for 87% of all bone fractures in the elderly population (Ambrose et al., 2015). Regenerative medicine could significantly reduce all of these instances and many, many more – if we knew how to implement it. However, there is much that we do not understand about how regeneration is initiated and regulated. One thing that we do understand, and see repeatedly across cancer biology, is that mis-regulation of many of the regenerative signals we know of can cause tumorous overgrowth and cancer (reviewed in Pesic and Greten, 2016). Therefore, if we ever wish to be able to utilize regenerative medicine to its fullest potential, it is absolutely critical to understand the regulation of regeneration.

1.2 How is the completion of regeneration regulated?

A poorly understood aspect of regeneration is how the completion of regeneration is communicated to the rest of the body. One cue that defines the endpoint of regeneration is the restoration of patterning during intercalary regeneration. Classic examples of patterning during intercalary regeneration are from amphibian and insect limb regeneration. When cockroach limbs are amputated at different sections and grafted them onto each other (Bohn, 1976). When an amputated distal tip of a limb is transplanted onto the base of a limb it regenerates the missing tissue to form a complete leg, without forming extra tissue (Bohn, 1976). However, when a limb that was amputated proximally is transplanted

onto a base of a limb with only the distal tip amputated, the tissue regenerates sections that would normally be found between the graft locations in the reverse direction (Bohn, 1976). If the transplanted sections are rotated, multiple limbs regenerate from the same base (French et al., 1976). The same results occur in axolotl limb regeneration (Maden, 1980). Work in crickets indicates that the positional memory of tissues is communicated in large part by epigenetic patterning of leg segments prior to amputation, specifically of the pattern of the methylation state of histone H3 lysine 27 within the cells of each segment (Hamada et al., 2015). In axolotl, the regeneration and positional identity are dependent on retinoic acid signaling in the blastema: loss of retinoic acid causes failure to regenerate while excess retinoic acid proximalizes the position of the regenerated tissue (Crawford and Stocum, 1988; Maden, 1997; reviewed in Stocum, 2017). In newt, retinoic acid regulates proximal identity by inducing expression of *prod 1* (newt CD59 ortholog), a GPI anchor that is presented at the cell surface (da Silva et al., 2002). The mechanism of Prod 1 in determining positional identity is not well understood, but correlates with EphA4 receptor, N-cadherin, and ephrin A in the blastema during regeneration of gecko tail and chick limb bud (Wada et al., 1998; Wang et al., 2011; Yajima et al., 1999; reviewed in Stocum, 2017). Although we do not understand the mechanism, these studies indicate that intrinsic properties of tissues can be and are used to determine regeneration completion.

Intercalary regeneration to restore patterning is clearly one cue to determine the endpoint of regeneration, but there are also other cues that may determine the regeneration target. For instance, upon removal of one of the mammalian kidney the other kidney doubles in weight and size, growing to take over the role of the missing kidney (reviewed in Malt, 1969 and Rojas-Canales et al., 2019). Compensatory growth begins within an hour and will continue until total functional capacity is about 75% of the total nephrons that were present in both kidneys (estimated 80% function) (Vuuren et al., 2012). More than 80% of the compensatory growth is primarily due to an increase in the size of existing cells, with the remaining portion resulting from proliferation (Johnson and Vera Roman,

1966; reviewed in Rojas-Canales et al., 2019). It is not clear how final tissue size is determined, however, hypertrophic kidney growth is also a characteristic of diabetic nephropathy, one of the most lethal complications of type 1 and type 2 diabetes (reviewed in Vallon and Thomson, 2012). In diabetic nephropathy, activation of the mTOR complex 1 initiates growth and deactivation of mTOR complex 1 and 2 causes cell death (Gödel et al., 2011; Inoki et al., 2011). This has led to the hypothesis that mTOR may also be involved in compensatory growth following kidney removal (Rojas-Canales et al., 2019).

Drosophila melanogaster larvae also have a mechanism for preventing overgrowth that we do not understand. Damage to one of the imaginal discs (precursors to adult organs) slows the growth of the organism and of the other imaginal discs to provide time for the damaged tissue to regenerate (mechanism discussed below) (Jaszczak et al., 2015; Smith-Bolton et al., 2009). However, overactivation of regenerative responses in response to perpetual damage in these tissues causes hyperplastic growths (Pérez-Garijo et al., 2009; reviewed in Worley et al., 2012). Despite the damage signaling, these larvae eventually pupate, indicating a mechanism for preventing these overgrowths (Katsuyama et al., 2015; reviewed in Fox et al., 2020).

If there is communication within the body to prevent overgrowth, there must also be a mechanism for sensing the completion of regeneration. There are few examples in the literature, but they do support this hypothesis. In adult *Drosophila* intestines (which retain the ability to regenerate), different modes of Decapentaplegic (*Drosophila* homolog of BMP) signaling initiates and then ends regeneration (Ayyaz et al., 2015; Tracy Cai et al., 2019; reviewed in Fox et al., 2020). Following damage, Decapentaplegic is secreted from gut associated hemocytes to induce proliferation of intestinal stem cells through the BMP type 1 receptor, Saxophone (Sax) (Ayyaz et al., 2015). Decapentaplegic also functions through the other BMP type 1 receptor, Thickveins, which induces intestinal stem cell quiescence (Guo et al., 2013). However, early in the regenerative period, Thickveins is internalized by the nucleoside diphosphate kinase Abnormal Wing

Disc and degraded by E3 ubiquitination (Cai et al., 2019). As a result, there is a shift towards Sax-induced proliferation in the tissue (Cai et al., 2019). As regeneration progresses, and tissue morphology is restored, Thickveins begins to localize at the cell surface and is activated by Decapentaplegic to induce quiescence again (Cai et al., 2019). Thus, the restoration of tissue homeostasis is sufficient to signal the completion of regeneration.

Regeneration and development share many similarities, and this may provide insights into the regulation of regeneration. For instance, during mouse development, thyroid hormone regulates the number, diameter, and contractile ability of muscle fibers through mitochondrial activity and myoblast proliferation (Dentice et al., 2014; Izumo et al., 1986; Mayerl et al., 2018; Rochard et al., 2000; Sugie and Verity, 1985). Following acute muscle injury, the thyroid hormone transporters MCT8 and OATP1C1 are necessary for regeneration and induce muscle stem cell differentiation, indicating that thyroid hormone is also necessary for regeneration in muscles (Mayerl et al., 2018). There are two thyroid receptors involved in development, the α - and β -receptors (Izumo et al., 1986; Sugie and Verity, 1985). It is not known if the β -receptors are necessary for muscle regeneration, but the α -receptor regulates mitochondrial activity and fiber size, likely through regulation of the proliferation rate (Pessemesse et al., 2019).

In my research presented in this thesis, I use *Drosophila* to investigate the development of the larval wing epithelial barrier and its impact on the duration of regeneration. In Chapter 2, I demonstrate that the epithelial barrier regulates the length of the regenerative period in *Drosophila* wing imaginal discs. In the Appendix I present preliminary data indicating that this is likely achieved by a regulated weakening, then re-development, of the barrier. This would indicate a model in which the restoration of a tissue's function may act as the method to communicate the endpoint of regeneration.

1.3 *Drosophila melanogaster* as a regenerative model

Drosophila imaginal discs are able to regenerate during larval development, but lose this ability before pupation (Bryant, 1971; Halme et al., 2010; Smith-Bolton

et al., 2009). Imaginal discs are specified during embryonic development and through extensive fate-mapping experiments we now understand how the imaginal discs are specified and develop into adult tissues (Bryant, 1971; Hadorn and Buck, 1962; Ursprung, 1962; reviewed in Worley et al., 2012). This well-characterized model, in combination with the short lifespan, high reproductive rate, and many genetic manipulation methods has led to numerous methods of studying damage and regeneration in *Drosophila* (reviewed in Fox et al., 2020).

Early experiments utilized surgical methods to cause damage to specific tissues (e.g. Bryant, 1971; Ursprung, 1962) or X-irradiation to produce DNA damage and apoptosis to across the animal (e.g. Abbott, 1983; Haynie and Bryant, 1977). X-irradiation is still used today (e.g. Jaszczak et al., 2015; Verghese and Su, 2016); however, damage to specific tissues can now be achieved through by a variety of genetic methods. One method is the temporal and regional gene expression targeting (TARGET) system (McGuire et al., 2004) (e.g. Harris et al., 2016; Smith-Bolton et al., 2009). TARGET utilizes the Gal4/UAS system to induce cell death along with a temperature sensitive allele of the Gal4 inhibitor Gal80 to control the time of damage (McGuire et al., 2004).

Other tools are available to assess genetic interactions. The Q-system functions the same way the Gal4/UAS system does to induce exogenous gene expression in a specific tissue and does not have cross reactivity with the Gal4/UAS system (Potter et al., 2010). As a result, these systems can be used together to induce specific expression in multiple places either separately or with overlap (e.g. Kashio et al., 2016). Another method to induce overlap is the dual expression method for induced site-specific eradication (DEMISE), which utilizes the Gal4/UAS system to induce expression of a gene of interest and the FLP/FRT system to induce genetic damage clonally (Cohen et al., 2018). In the Appendix, I use X-irradiation to induce damage and observe the response in the wing imaginal disc epithelial barrier.

Regardless of the damage method, regeneration of *Drosophila* imaginal discs depends on the activity of Wingless (*Drosophila* Wnt1 homolog) and

JAK/STAT signaling (Smith-Bolton et al., 2009; Verghese and Su, 2016). As mentioned above, Wnt is necessary for digit regeneration (Takeo et al., 2013) and the JAK/STAT pathway, which is highly conserved between *Drosophila* and vertebrates, is also known to be involved in vertebrate regeneration (reviewed in Herrera and Bach, 2019). Wingless plays roles in both normal development and in tissue regeneration (Schubiger et al., 2010; Smith-Bolton et al., 2009). In regenerating tissues, damage induces the phosphorylation of Basket (*Drosophila* JNK homolog) (Riesgo-Escovar et al., 1996; Sluss et al., 1996). Phosphorylated Basket activates the transcription factor AP-1 (Riesgo-Escovar et al., 1996; Sluss et al., 1996). AP-1 is a dimer of Jun-related antigen (*Drosophila* homolog of Jun) and Kayak (*Drosophila* homolog of Fos) that induces expression of multiple pro-apoptotic and regenerative genes, including Wingless (Chen et al., 2002; Harris et al., 2016; Hwang and Pallas, 2014; Perkins et al., 1990). Wingless is a morphogen that induces proliferative signals like Myc and JAK/STAT in neighboring cells to produce regenerative growth (Katsuyama et al., 2015; Rodrigues et al., 2012; Smith-Bolton et al., 2009). A primary cause of the loss of regenerative ability during late larval development is the epigenetic silencing of the enhancer region for *wingless* that AP-1 binds to following damage (Harris et al., 2016).

1.4 Systemic responses to regeneration in *Drosophila*

Damage to the imaginal tissues also slows the development of undamaged imaginal tissues and delays the larval transition to the pupal stage, thereby gaining more time to complete regeneration (Jaszczak et al., 2015; Smith-Bolton et al., 2009). These systemic responses to damage are the result of limiting the synthesis of ecdysone, a steroid hormone that is expressed and circulates at times of developmental transitions in insects to produce changes across the body (Burdette, 1962; Wigglesworth, 1951; Warren et al., 2002; Lavrynenko et al., 2015; reviewed in Pan et al., 2020). Ecdysone is synthesized from dietary cholesterol in the prothoracic gland and then converted to its functional form, 20-hydroxyecdysone, by the Halloween genes (*neverland*, *shroud*, *spooky*, *spookier*,

spookiest, cyp6t3, cyp6u1, phantom, disembodied, shadow, shade), so-called for the characteristic empty or ghost-like appearance of mutant embryos (reviewed in Gilbert, 2004; Pan et al., 2020).

Traditionally, 20-hydroxyecdysone was thought to enter cells from the hemolymph through simple diffusion like other steroid hormones; however, in 2018, Okamoto et al. identified a transporter, Ecdysone Importer, that is necessary for ecdysone-dependent signaling by ecdysone receptor (Okamoto et al., 2018). The ecdysone receptor is a dimeric nuclear receptor formed from one of the three splice isoforms of Ecdysone Receptor (EcR-A, EcR-B1, or EcR-B2) and Ultraspiracle (Hu et al., 2003; Koelle et al., 1991; Yao et al., 1992; Yao et al., 1993; reviewed in Schwedes and Carney, 2012). The ecdysone receptor has transcriptional regulatory functions with and without ecdysone binding (Cherbas et al., 2003). Ecdysone binding determines if the receptor acts as a transcriptional activator or as a transcriptional repressor (Cherbas et al., 2003). The ecdysone receptor splice isoforms determine to which genes the receptor dimer binds to the expression of the different splice isoforms are temporally and spatially regulated to provide specific control over the organismal and tissue responses to ecdysone production (Cherbas et al., 2003; Hu et al., 2003).

During the third larval instar, ecdysone is synthesized in three peaks – two small and one large – that cause an accumulation of 20-hydroxyecdysone in the larval hemolymph and causes numerous changes in preparation for pupation (Lavrynenko et al., 2015; McBrayer et al., 2007; Warren et al., 2002). The timing of the ecdysone peaks are regulated by prothoracicotropic hormone (PTTH) which is produced in PTTH-producing neurons; PTTH is not necessary for pupation but inhibition PTTH signaling delays development (McBrayer et al., 2007). One developmental change that ecdysone regulates is the limitation of regeneration capacity, which acts as a developmental checkpoint for pupation (Halme et al., 2010). Following damage before regeneration restriction, this regeneration checkpoint is delayed thereby providing more time to complete regeneration

(Halme et al., 2010; Smith-Bolton et al., 2009). At the same time, undamaged imaginal discs slow their development (Jaszczak et al., 2015).

The delay in developmental timing and undamaged disc growth both result from signaling by the relaxin peptide *Drosophila* insulin-like peptide 8 (Dilp8), which is produced and secreted by damaged imaginal tissues (Colombani et al., 2012; Garelli et al., 2012). Dilp8 binds to Lgr3 receptors in the brain and prothoracic gland to inhibit ecdysone production (Colombani et al., 2012; Colombani et al., 2015; Garelli et al., 2012; Garelli et al., 2015; Jaszczak et al., 2016; Vallejo et al., 2015, 3). Lgr3 is not expressed in the PTTH-producing neurons and Lgr3 activation in the prothoracic gland is not necessary to initiate regeneration checkpoint delay, indicating that there are likely additional steps to initiate regenerative delay (Jaszczak et al., 2016). However, growth control of the undamaged imaginal discs is regulated by Lgr3 expression in both the brain and prothoracic gland (Jaszczak et al., 2016). To do this, Dilp8 activation of Lgr3 expressed in the prothoracic gland activates nitric oxide synthase in the prothoracic gland, which in turn inhibits ecdysone biosynthesis by downregulating the expression of Halloween genes (Jaszczak et al., 2015; Jaszczak et al., 2016). Dilp8 is only known to function in the brain and prothoracic gland, but can be observed to accumulate in wing imaginal tissues (Colombani et al., 2012). This caused me to question if there are properties or characteristics of the wing imaginal disc that impact Dilp8.

1.5 Development and anatomy of wing imaginal discs

The imaginal discs are precursors to adult organs. The imaginal disc progenitor cells are specified during embryonic development (Cohen et al., 1993; reviewed in Ruiz-Losada et al., 2018). The wing imaginal disc is defined by *vestigial* activation in 20-70 progenitor cells; by the end of larval development the wing disc contains approximately 75,000 cells (Cohen et al., 1993; Mandaravally Madhavan and Schneiderman, 1977; Williams et al., 1991; reviewed in Klein, 2001; Baena-Lopez et al., 2012). During larval development, the wing disc is an epithelial sac formed of a pseudostratified epithelium (primary epithelium) and a

squamous epithelium (peripodial epithelium) that is connected to the larval epidermis by a thin stalk (Figure 1-1A,B) (Baena-López et al., 2003; Butler et al., 2003; Pastor-Pareja et al., 2004; Resino et al., 2002).

The primary epithelium has three major anatomical regions: the wing pouch, the hinge, and the notum (Figure 1-1B). The wing pouch is the precursor to the adult wing proper (reviewed in Beira and Paro, 2016; Butler et al., 2003). Thus, it is the adult wing that defines the dorsal, ventral, anterior, and posterior boundaries in the wing disc, so the center of the wing pouch is at the cross section of the dorsal-ventral and anterior-posterior boundaries (Figure 1-1B,C) (reviewed in Beira and Paro, 2016; Butler et al., 2003). During pupal development, the wing pouch everts along the dorsal-ventral boundary, rupturing the peripodial epithelium, which retracts down the sides of the expanding primary epithelium and later undergoes apoptosis (Aldaz et al., 2010; Fristrom and Fristrom, 1975; Pastor-Pareja et al., 2004). The hinge region surrounds the wing pouch and becomes the tissue connecting the adult wing to the thorax (Figure 1-1B) (reviewed in Beira and Paro, 2016; Butler et al., 2003). The notum is in the dorsal-most portion of the tissue and becomes part of the dorsal side of the adult thorax (Figure 1-1B) (reviewed in Beira and Paro, 2016; Butler et al., 2003).

Wing development is tightly regulated. The transcription factor *Apterous* is expressed dorsally starting during the second larval instar to drive differences between dorsal and ventral patterning while also promoting Notch signaling along the dorsal-ventral boundary (Figure 1-1C) (Cohen et al., 1992; Diaz-Benjumea and Cohen, 1993). This Notch signaling stabilizes then constrains *Vestigial* expression to the dorsal-ventral boundary (Figure 1-1D) (Williams et al., 1991; reviewed in Klein, 2001; Ruiz-Losada et al., 2018). Another transcription factor, *Engrailed*, is expressed in the posterior compartment to drive the differences between anterior and posterior patterning (Figure 1-1C) (Morata and Lawrence, 1975). *Engrailed* promotes expression of the morphogen *Hedgehog* while also blocking posterior cells from responding to *Hedgehog* (Tabata et al., 1992; Zecca et al., 1995). *Hedgehog* induces expression of another morphogen, *Decapentaplegic*, in

neighboring anterior cells (Hoffmann and Goodman, 1987; Nellen et al., 1996; Zecca et al., 1995). This results a stripe expression pattern of Decapentaplegic along the anterior side of the anterior-posterior axis, which in turn induces the expression of other spatially defining components in a gradient (Figure 1-1D) (Hoffmann and Goodman, 1987; Nellen et al., 1996; Zecca et al., 1995). Wingless is another critical morphogen and, in the second instar, is one of the driving factors that differentiates the wing pouch from the hinge and notum (Sharma, 1973; Sharma and Chopra, 1976; reviewed in Ruiz-Losada et al., 2018). By the third instar, *wingless* is expressed in the hinge just outside of the wing pouch and is also expressed along the dorsal-ventral boundary of the wing pouch (Figure 1-1D) (Sharma, 1973; Sharma and Chopra, 1976; reviewed in Swarup and Verheyen, 2012). The combination of Wingless, Decapentaplegic, and Notch in the wing pouch stabilizes Vestigial further and drives further specialization of the cells within the wing pouch (Figure 1-1D) (Couso et al., 1995; Klein and Arias, 1998a; Klein and Arias, 1998b; reviewed in Klein, 2001; Ruiz-Losada et al., 2018).

These morphogens are transmitted through cell-cell contacts and by secretion and diffusion in the lumen of the imaginal disc (Figure 1-1A) (Baena-López et al., 2003; Gibson et al., 2002; Strigini and Cohen, 2000). This luminal space is topologically separated from the hemolymph by the imaginal disc epithelial barrier (Pastor-Pareja et al., 2004). The epithelial barrier is a semi-permeable diffusion barrier formed between the epithelial cells of a tissue. When Colombani et al. observed an accumulation of Dilp8 in the imaginal disc, they observed it in the lumen (Colombani et al., 2012). This led me to investigate whether the epithelial barrier limits Dilp8 signaling by constraining Dilp8 within the lumen of the imaginal disc. In Chapter 2, I demonstrate that ecdysone-dependent changes in the wing imaginal disc epithelial barrier limit Dilp8 signaling.

Figure 1-1. Larval wing imaginal disc anatomy.

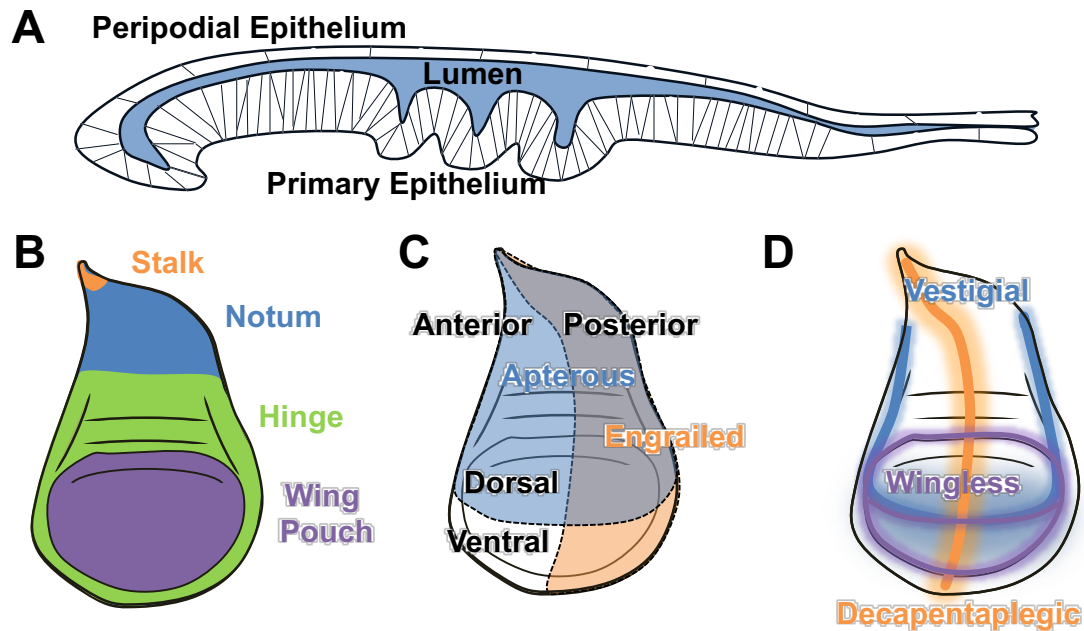


Figure 1-1. Larval wing imaginal disc anatomy. The wing imaginal disc is the larval precursor to the adult wing. Diagrams are of a wing imaginal disc in the third instar. (A) Cross section of the wing disc showing the two epithelial layers. The imaginal disc has a pseudostratified, primary epithelium and a squamous, peripodial epithelium. The lumen (blue) of the imaginal disc between the two epithelial layers is topologically separate from the larval hemolymph. (B) The wing imaginal discs are connected to the larval epidermis by a thin stalk region. The primary epithelium is the portion of the tissue that is retained into adulthood, and has three distinct parts: the notum (blue) which becomes part of the dorsal portion of the adult thorax, the hinge (green) which connects the wing to the thorax, and the wing pouch (purple) which becomes the wing proper. (C) The disc is divided into four compartments along the anterior-posterior and dorsal-ventral axes. Apterous (blue) is a transcription factor that drives dorsal gene expression. Engrailed (orange) is a transcription factor that drives posterior gene expression. (D) The wing pouch is differentiated by specific gene expression (only some key genes are shown). Decapentaplegic (orange) is expressed in a stripe on the anterior side of the *engrailed* boundary. Wingless (purple) is expressed in the hinge

just outside the wing pouch and also along the dorsal-ventral boundary of the wing pouch. Starting in the second instar, Vestigial (blue) expression is confined along the Apterous boundary. In the third instar, Vestigial expression is promoted and stabilized by Decapentaplegic and Wingless resulting in higher levels of Vestigial expression across a wider area in the wing pouch.

1.6 Epithelial barrier, vertebrates vs. invertebrates

Generally, the occluding junctions are the tight junctions of vertebrate epithelia (also known as zonula occludens) (Farquhar and Palade, 1963; Goodenough and Revel, 1970). The equivalent structure in invertebrates are septate junctions (Filshie and Flower, 1977). Tight and septate junctions are usually considered orthologs to each other (Green and Bergquist, 1982; reviewed in Izumi and Furuse, 2014). However, vertebrates do contain junctions, called paranodal septate junctions, that are anatomically more similar to septate junctions than to tight junctions. Paranodal septate junctions form on myelinated axons at the Nodes of Ranvier between the Schwann cells and the axon itself (Banerjee et al., 2006b; reviewed in Izumi and Furuse, 2014 and Banerjee et al., 2006a). Several of the mammalian homologs to invertebrate septate junction components localize specifically to the paranodal septate junctions, as discussed later.

Although considered orthologs, there are significant differences between tight junctions and septate junctions. Both tight junctions and septate junctions localize to the apical-lateral surface of cells, but tight junctions are formed apical to the adherens junctions whereas septate junctions are formed basal to the adherens junctions (reviewed in Tsukita et al., 2001). Tight junctions form through interlacing strands across the cell surface (Figure 1-2A). The strands fuse to the junctional strands of neighboring cells at kissing points (named because the intercellular space is not detectable in cross section) (Farquhar and Palade, 1963). This results in a mesh-like network across the cells' surfaces with bubbles of intercellular space (Claude and Goodenough, 1973). The number of tight junction strands that form the meshwork contributes to the functionality of the barrier.

Tissues with cells that have more strands have a greater transepithelial resistance, indicating that the barrier has increased selectivity and reduced permeability (Claude, 1978; Claude and Goodenough, 1973). Substrates that the barrier is permissive to are able to diffuse through the junctions at the kissing points, effectively moving from bubble to bubble (reviewed in Tsukita et al., 2001; Zihni et al., 2016). The way this diffusion occurs is less clear.

In the prevailing diffusion model, the protein model, members of the claudin protein class on the cell surface form dimers with the claudins of neighboring cells at the kissing points to form ion-conductive pores or channels (reviewed in Tsukita et al., 2001; Zihni et al., 2016). In both tight and septate junctions, the selective property of the junction is due to the activity of claudins (Balda et al., 1996; reviewed in Furuse and Tsukita, 2006). This model was first proposed based on similarities in the thickness of tight junctions and gap junctions observed via freeze fracture, differences in the charges of the extracellular components of various claudins, and the significant difference in transepithelial resistance in cell layers with disrupted and intact tight junctions (Claude, 1978; Claude and Goodenough, 1973; Staehelin, 1973; reviewed in Tsukita et al., 2001). More recently the model has received more concrete support by the determination of the first of the crystal structure of a claudin by Suzuki et al., 2014. Claudins were previously known to have four transmembrane domains and to sit with their C- and N-termini within the cell with two loop-like structures outside the cell (Furuse et al., 1998; reviewed in Furuse and Tsukita, 2006). Suzuki et al., 2014 resolved Claudin-15 with a resolution of 2.4 Å and found that the extracellular loops form a negatively charged β -sheet (Suzuki et al., 2014). In a follow up communication, they presented a model in which the β -sheets of claudin dimers within the same cell form a “half pipe,” and then bind to dimers of a neighboring cell to form the paracellular pore (Suzuki et al., 2015). The proposed pores are structurally very similar to those of gap junctions (Suzuki et al., 2015).

However, the protein model for diffusion does not address the role of non-claudin components in the barrier (reviewed in Zihni et al., 2016). Although

claudins are stable at the barrier, FRAP studies indicate that non-claudin components, such as Occludin and ZO-1, undergo rapid and constant diffusion around the tight junction strands (Shen et al., 2008; Shen, 2012; reviewed in Zihni et al., 2016). A second model for tight junction paracellular diffusion, called the hybrid model (or sometimes the lipid-protein model or the lipid model), addresses some of these concerns (reviewed in Zihni et al., 2016). The hybrid model proposed that in addition to these pores, the cell membranes of the neighboring cells fuse together at the kissing points (Kachar and Reese, 1982; Shen, 2012; reviewed in Zihni et al., 2016). This fusion was demonstrated at tight junctions by Kan, 1993 who visualized gold-labeled phospholipids in high concentrations at tight junction kissing points (Kan, 1993). This type of membrane fusion between cells is not energetically favorable; by this model the tight junction proteins stabilize the fusions (Chernomordik and Kozlov, 2005; da Silva and Kachar, 1982).

Septate junctions do not form this meshwork structure and do not have kissing points. Instead they form highly organized, parallel ribbon-like structures around the cell surface, with extracellular components that bind to the extracellular septate junction components of neighboring cells (Lane, 1979; Wood, 1959).¹ The extracellular regions, called septa, are evenly spaced 8-10 nm from each other and keep the cell membranes of the neighboring cells 15-20 nm apart; this gives septate junctions a unique ladder-like appearance in cross-section (Figure 1-2B) (Lane, 1979; Lane and Swales, 1982). Paranodal septate junctions in vertebrates also have this ladder-like structure (Banerjee et al., 2006b). The exact spacing and orientation of the ribbons relative to each other is the primary differentiating factor in the different types of septate junctions (reviewed in Green and Bergquist, 1982). *Drosophila* have two types of septate junctions, pleated and smooth septate junctions (Noirot-Timothee and Noirot, 1980).

¹ Wood, 1959 mistook the structures that they imaged for a new type of desmosome (“septate desmosomes”), they were re-classified gradually in the literature. By late 1970s the term “septate junctions” was used almost exclusively, and septate junctions were recognized as the occluding junctions of invertebrates.

Pleated septate junctions are found in ectoderm-derived tissues (Lane and Swales, 1982; Tepass and Hartenstein, 1994; reviewed in Izumi and Furuse, 2014). The ribbon structure of pleated septate junctions undulate or zig-zag as they wrap around the cell (Figure 1-2B) (Noirot-Timothee and Noirot, 1980). Although the *Drosophila* blood brain barrier is formed by pleated septate junctions, it is not clear if there are components, regulatory pathways, or assembly mechanisms that are specific to the blood brain barrier (Tepass and Hartenstein, 1994; reviewed in Banerjee et al., 2006a).

Smooth septate junctions have ribbon structures that do not undulate and are found in endoderm-derived tissues (e.g. midgut) (Lane and Swales, 1982; Tepass and Hartenstein, 1994; reviewed in Izumi and Furuse, 2014). Relatively little is known about the smooth septate junctions, but there are at least two septate junction components, Snakeskin and Mesh, that are specific to smooth septate junctions (Izumi et al., 2012). Since little is known about smooth septate junctions, I will focus on pleated septate junctions for the remainder of this thesis; all references to septate junctions will be to pleated septate junctions.

Figure 1-2. Structure of occluding junctions in vertebrates and invertebrates.

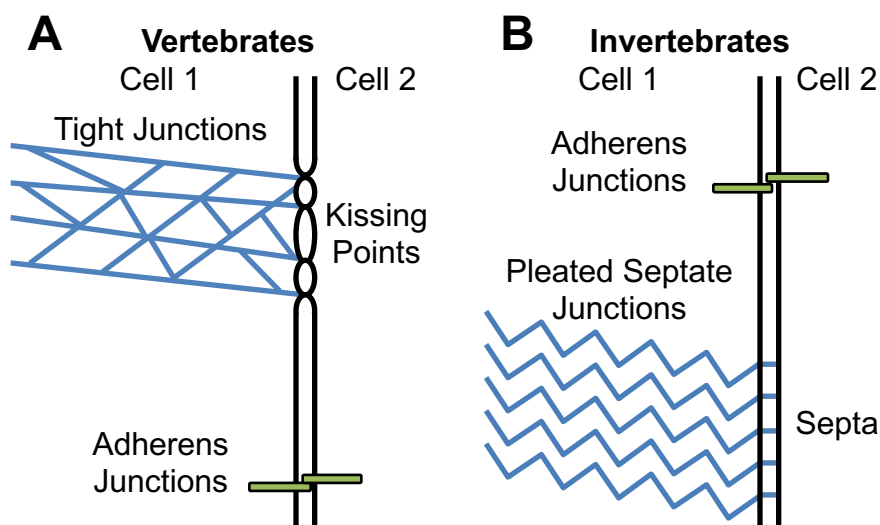


Figure 1-2. Structure of occluding junctions in vertebrates and invertebrates.

(A) Tight junctions are the occluding junctions of vertebrates. They form on the

apical lateral surface of cells and are apical to the adherens junctions. Tight junctions are formed by an interlacing network of strands that fuse to the tight junction strands of neighboring cells at kissing points. Intercellular space is not detectable at kissing points. (B) Septate junctions are the occluding junctions of invertebrates. They form on the apical lateral surface of cells and are basal to the adherens junctions. Pleated septate junctions are the most thoroughly studied type of septate junction. Pleated septate junctions form zig-zag or pleated structures across the cell that are evenly spaced and run approximately parallel to each other. To provide the excluding function of the barrier, the junctions have extracellular components that bind to the extracellular components of the septate junctions of neighboring cells. The bound extracellular components, called septa, keep the cell membranes of cells evenly spaced and are similar in appearance to the rungs in a ladder.

1.7 Occluding junction components

Humans express at least 24 claudins, with different claudins providing different selectivity for size and charge (reviewed in Furuse and Tsukita, 2006). By the protein model of diffusion, the selectivity of the barrier is dependent on the homo- and hetero-dimerization of claudins to provide highly specific selectivity based purely on claudin expression (Suzuki et al., 2015; reviewed in Turksen and Troy, 2004; Zihni et al., 2016). Claudins are differentially expressed in different organs and in different tissues of the same organ. For example, the adult lung expresses Claudins 3, 4, 5, 7, and 18 (Kaarteenaho et al., 2010; Niimi et al., 2001; reviewed in Schlingmann et al., 2015). The only other tissue Claudin-18 is found in is the stomach (Niimi et al., 2001). The kidney nephron expresses Claudins 1, 2, 3, 4, 6, 7, 8, 9, 10, 11, 14, 16, and 19 (reviewed in Angelow et al., 2008). However, only Claudin-10 has been found across all nephron tissues (Van Itallie et al., 2006), whereas Claudin-14 is only found in the collecting duct (Ben-Yosef et al., 2003). Claudins are also differentially expressed during development (discussed in section 1.8) and in response to stimuli (discussed in section 1.9),

and improper claudin expression is characteristic of numerous diseases and conditions including some forms of genetic deafness, Crohn's disease, and asthma (Ben-Yosef et al., 2003; Jin and Park, 2018; Zeissig et al., 2007). Tight junctions also utilize the protein Occludin, *Drosophila* do not have an *occludin* homolog, to contribute to the barrier (McCarthy et al., 1996). *Drosophila* have three confirmed claudins, Pickel (previously Megatrachea) (Behr et al., 2003), Sinuous (Wu et al., 2004), and Kune-kune (Nelson et al., 2010), and four proteins that are hypothesized to be claudins based on sequence similarity (Nelson et al., 2010). It is not known if *Drosophila* claudin expression is as tissue specific as mammalian claudins.

Claudin localization and function is dependent on other proteins referred to as the tight junction plaque in vertebrates (reviewed in Schneeberger and Lynch, 2004 and Zihni et al., 2016) and the septate junction core complex in invertebrates (reviewed in Rouka et al., 2020). The components of the tight junction plaque and the septate junction core complex differ, but many components contain the same protein domains indicating that similar tasks may be performed, but by different components. Many components of both the tight junction plaque and the septate junction core complex are in the MAGUK (membrane-associated guanylate kinase) superfamily (reviewed in González-Mariscal et al., 2000). These proteins contain at least one PDZ (PSd/AP90, discs large, ZO-1) domain that can bind to the actin cytoskeleton or to another PDZ domain (reviewed in González-Mariscal et al., 2000). *In vitro*, the PDZ domain of the tight junction MAGUK proteins ZO-1, ZO-2, and ZO-3 bind directly to Claudin-1 and Claudin-8 (Itoh et al., 1999). The PDZ domains of ZO-1 can also bind Occludin and Junctional adhesion molecule (Ebnet et al., 2000). Many other occluding junction proteins also contain one or more PDZ domains which are thought to be the mechanism of binding that provides structure to the junctions and connects them to the actin cytoskeleton (reviewed in González-Mariscal et al., 2000). The MAGUK proteins also contain at least one GUK (guanylate kinase) domain, while other proteins at the occluding junctions contain phosphatase domains. Other proteins are scaffolding proteins,

while others still are known to influence adhesion or polarity. These different structures at the junctions form cohesive, interdependent structures that also serve as signaling hubs for the cells (reviewed in Rouka et al., 2020; Schneeberger and Lynch, 2004; and Zihni et al., 2016).

Both tight and septate junctions have unique structures at cell corners, called tricellular junctions. Four components of the tricellular tight junctions have been identified: Tricellulin and Angulin-1, -2, and -3 (Higashi et al., 2013; Ikenouchi et al., 2005; Masuda et al., 2011; reviewed in Higashi and Chiba, 2020). The Angulins are PDZ-domain containing proteins that have differential expression across tissue types, leading to hypotheses that they are regulated similarly to Claudins, but this has not been tested (Higashi et al., 2013; reviewed in Higashi and Chiba, 2020). Angulin-1 and -2 were able to specifically recruit Tricellulin *in vitro* in mouse mammary epithelial cell culture (Higashi et al., 2013). ZO-1 also binds Tricellulin at its C-terminal end, and disruption of Tricellulin compromises barrier function (Ikenouchi et al., 2005). In tricellular septate junctions, the gap between cells is filled by the trimeric “plug” Bark beetle (previously Anakonda) (Byri et al., 2015). The connection to the bicellular septate junctions is achieved by Gliotactin (Auld et al., 1995; Sharifkhodaei et al., 2019). Gliotactin attaches to the ends of assembled the septate junction ribbons in embryonic development and is then localized to the tricellular junctions by Discs large and Scribble (Auld et al., 1995; Sharifkhodaei et al., 2019). At the tricellular junctions, Gliotactin binds to Bark Beetle; this has the effect of anchoring the ends of the septate junction ribbons (Sharifkhodaei et al., 2019).

The vast majority of the *Drosophila* homologs to the proteins in tight junction plaques localize to the adherens junctions not the septate junctions. The exception is DLG1 (mammal) / Discs large (*Drosophila*); Discs large localizes to bicellular septate junctions, but does not contribute to the barrier function at bicellular junctions (Oshima and Fehon, 2011; Woods et al., 1996). Discs large is, however, necessary for localizing Gliotactin to the tricellular septate junctions (Sharifkhodaei et al., 2019). Interestingly, the mammalian homolog of other MAGUK protein at the

septate junctions in *Drosophila*, *Varicose* (MMP6 in mammals), localizes to the Nodes of Ranvier, where the paranodal septate junctions are found (Banerjee et al., 2006b; Terada et al., 2012; Wu et al., 2007). In mammals, MMP6 is a matrix metalloproteinase that interacts with the 4.1 group protein (mammalian homolog of *Drosophila* core complex component Coracle) (Stevens and Page-McCaw, 2012; Wu et al., 2007). Neurexin-IV and Neuroglian also localize to these paranodal septate junctions (Banerjee et al., 2006b; Baumgartner et al., 1996; Bieber et al., 1989).

1.8 Establishment of the epithelial barrier

The mechanisms that regulate the assembly of occluding junctions and the establishment of the epithelial barrier are not well understood. In vertebrates, the adherens junctions form before the tight junctions. The adherens junctions recruit scaffolding proteins associated with tight junction plaques (e.g. ZO-1, -2) (Rajasekaran et al., 1996; reviewed in Rouka et al., 2020). These scaffolds then recruit adhesion proteins, like JAM-A, to the junctions (Haas et al., 2020; Monteiro et al., 2013; reviewed in Rouaud et al., 2020). Junctional assembly is part of the mechanism that polarizes cells (reviewed in Zihni et al., 2016). Little is known about how the barrier is established after this point. However, calcium signaling is critical. The junctions do not form in the absence of calcium, and adding calcium is sufficient to induce assembly (Cereijido et al., 1978). At least one thing that calcium does is induce G-protein coupled receptor 40 expression, which is sufficient to localize ZO-1 to the junctions (Moonwiryakit et al., 2018).

Drosophila septate junction assembly has been studied in the embryonic epidermis, foregut, hindgut, salivary glands, and trachea. The development of the septate junctions in these tissues can be observed by transmission electron microscopy between embryonic stages 14 and 17 (Tepass and Hartenstein, 1994). The components of the junctions begin to assemble before this point. The exclusivity function of the barrier is established by the end of stage 15, when tissues gain the ability to exclude fluorescent-conjugated dextran that is injected

into the embryonic hemocoel (Lamb et al., 1998; Paul et al., 2003). The establishment of the barrier has impacts on the functionality of these tissues. In septate junction mutants, the chitin deacetylases Vermiform and Serpentine do not accumulate in the tracheal lumen. In the epidermis, dorsal closure is dependent on septate junction formation (failure to close is embryonic lethal) (Fehon et al., 1994). The elongation of the salivary gland is also dependent on the septate junctions (Hall and Ward, 2016). Barrier establishment in the trachea regulates tube elongation and proper branching patterns (Luschnig et al., 2006; Wang et al., 2006). The specific mechanism is not known, but elongation and branching are controlled by the deposition of Vermiform and Serpentine within the trachea (Luschnig et al., 2006; Wang et al., 2006).

The septate junction components are diffusely localized along the surface of cells at stage 12, but most components are tightly localized at the septate junctions by the end of stage 14 (Bätz et al., 2014; Hall and Ward, 2016; Oshima and Fehon, 2011). Coracle is one of the last core complex components to localize at the septate junctions. Between stage 12 and 14, Coracle does localize increasingly more to the septate junctions, but it is not exclusively localized to the septate junctions until stage 17 (Hall and Ward, 2016). The regulatory mechanisms that recruit the core complex components to the septate junctions are poorly understood. However, four Ly6 proteins, Crooked, Coiled, Crimped, and Boudin, are known to regulate several core complex components during embryonic development (Hijazi et al., 2009; Nilton et al., 2010). Crooked and Coiled localize to intracellular vesicles and are necessary for the formation of the barrier in embryonic trachea (Nilton et al., 2010). In mutants for *crooked* or *coiled*, the core complex components Neurexin-IV and Coracle are localized in intracellular vesicles, indicating that it is likely that Crooked and Coiled regulate the deposition of Neurexin-IV and Coracle at the junctions (Nilton et al., 2010). It is not known if Crimped and Boudin also localize to intracellular vesicles, but both are also necessary for the formation of the epithelial barrier in embryonic trachea (Hijazi et

al., 2009; Nilton et al., 2010). Loss of *boudin* also causes the mislocalization of the core complex component Neuroglian (Hijazi et al., 2009).

1.9 Role of epithelial barrier regulation in tissue homeostasis

Once the epithelial barrier is established, it is regulated to best adapt to the needs of the tissue. In vertebrates, steroid hormones and transcription factors are known to regulate tight junction component expression. In mammals, decreases in progesterone and corticosterone in the mammary duct induces a tightening of the epithelial barrier that is necessary for milk secretion (Nguyen et al., 2001). This correlates with the upregulation of Claudin 1, 3, and 4 in the mammary epithelia (Baumgartner et al., 2017). Adding Vitamin D to cultured cornea epithelial cell lines increases Occludin expression and transepithelial resistance, indicating a tightening of the barrier (Yin et al., 2011; reviewed in Zhang et al., 2013). The tightening effect continues for at least 5 hours, but is discernable within 1 hour relative to controls (Yin et al., 2011). However, the opposite effect was observed in cultured intestinal epithelia – transepithelial resistance decreased after the addition of Vitamin D (Chirayath et al., 1998; reviewed in Zhang et al., 2013). The transcription factor Grainyhead-like 2 induces expression of Claudins 3 and 4 in liver progenitor cell lines (Senga et al., 2012).

Barrier regulation after establishment has not been explored much in *Drosophila*. However, the microRNA miR-184 expression is known to down-regulate the expression of the bicellular septate junction components Neurexin-IV, Coracle, and Macroglobulin complement related as well as the tricellular septate junction component Gliotactin, by triggering the degradation of the component mRNAs (Kertesz et al., 2007; Sharifkhodaei et al., 2016). Overexpression of Gliotactin triggers miRNA-184 expression, which then reduces expression of Gliotactin (indicating that Gliotactin is self-regulatory) as well as the expression of Neurexin-IV, Coracle, and Macroglobulin complement related (Sharifkhodaei et al., 2016). miRNA-184 is also expressed throughout the embryo, in the larval wing imaginal discs, in the adult female germline, and in response to the expression of

three pro-apoptotic genes, *head involution defect*, *reaper*, and *grim-reaper* (Kertesz et al., 2007). In Chapter 2, I demonstrate that in wing imaginal discs the steroid hormone ecdysone induces Coracle localization to septate junctions which results in a further restriction of the epithelial barrier.

Interestingly, the *Drosophila* homolog of Grainyhead-like 2, Grainy head, also regulates septate junction component expression (Narasimha et al., 2008). Grainy head induces expression of Coracle, Fasciclin III, and Sinuous during dorsal closure in the embryo, but is not necessary for the barrier function in the embryonic trachea (Narasimha et al., 2008). Grainy head is also expressed in the larval wing imaginal discs, and transgenic expression of Grainy head mutants in the wing discs cause a mislocalization of Coracle and Fasciclin III; it is not clear what impact this has on the epithelial barrier (Narasimha et al., 2008).

Certain types of cell death may also affect the epithelial barrier, but specific mechanisms are not known. In mice when apoptosis occurs in an epithelial sheet, the cells around the dying cell form an epithelial barrier with each other before extruding the dying cell from the cell layer (Rosenblatt et al., 2001). As a result, the functionality of the barrier is not compromised (Rosenblatt et al., 2001). However, apoptosis is non-inflammatory, and inflammatory diseases (e.g. Crohn's disease, asthma) are associated with weaker epithelial barriers (Hardyman et al., 2013; Xu et al., 2019; Zeissig et al., 2007; Xie et al., 2020; Duszyc et al., 2017). While it has not been explicitly studied, inflammatory forms of cell death like necrosis are likely to have different impacts on the barrier than apoptosis does.

1.10 Conclusion and overview of thesis

Here I have outlined the importance of regulating regeneration and communicating the status of regenerating tissues within the body. I have discussed what is known about regeneration, the loss of regenerative ability, and regeneration regulation, then outlined a significant gap in our understanding of how the completion of regeneration is communicated. Considerable progress has been made towards understanding regeneration in *Drosophila* since the discovery of

Dilp8 (Colombani et al., 2012; Garelli et al., 2012; reviewed in Fox et al., 2020). Interestingly, Dilp8 accumulates in the wing imaginal disc lumen even though it functions in the brain and PG (Colombani et al., 2012), leading me to question if the epithelial barrier of the wing disc sequesters Dilp8 in the imaginal disc lumen and if this influences Dilp8 signaling. I next discussed the role of the epithelial barrier, how the barrier differs in vertebrates and invertebrates, how the barrier is established and regulated, and discussed gaps in our understanding of barrier establishment and regulation.

In Chapter 2, I show that Dilp8 signaling is indeed limited by the epithelial barrier. I next explore how the barrier functions in the wing imaginal disc, and find that it grows more restrictive during the third instar. I observe that this maturation of barrier function is in response to the localization of the core complex component Coracle to septate junctions. I also find that this localization of Coracle is dependent on ecdysone, the hormone that regulates the loss of regenerative ability in *Drosophila* (Halme et al., 2010). Then I determine that the mature and restrictive barrier serves as a mechanism to communicate the completion of regeneration. I explore this more in the Appendix, where I present preliminary data that indicate that the barrier and septate junction components may be down-regulated in regenerating tissues. In Chapter 3 (Discussion), I explore the connections between the data presented in the Appendix and in Chapter 2, and the implications of this work on the fields of regenerative biology and epithelial barrier development.

Chapter 2

Ecdysone regulates the larval imaginal disc epithelial barrier, determining the length of regeneration checkpoint delay

Note to reader: This chapter is based on a paper submitted for publication to *Development*, where it is under major revision. The submitted version is available open access on BioRxiv (doi: 10.11.01/2020.07.16.207704). The differences between this chapter and the submitted version are based on some of the reviewer requested edits to the text of the document. The format of the document has also been changed to match the rest of this thesis. Some of the experiments presented here were performed by my co-authors, but even in these experiments I provided critical analysis.

Full author list: Danielle DaCrema, Rajan Bhandari, Faith Karanja, Ryunosuke Yano, Adrian Halme.

Abstract

Regeneration of *Drosophila* imaginal discs, larval precursors to adult tissues, produces a systemic response, a regeneration checkpoint that coordinates regenerative growth with developmental progression. This regeneration checkpoint is coordinated by the release of the relaxin-family peptide Dilp8 from regenerating tissues and functions in the brain and prothoracic gland. However, secreted Dilp8 protein is detected within the imaginal disc lumen. The disc epithelium should separate the lumen from the larval hemolymph, and therefore the brain and prothoracic gland. Here we demonstrate that following damage the imaginal disc epithelial barrier limits Dilp8 signaling and regeneration checkpoint delay. We also find that the barrier becomes decreasingly permeable during the second half of the third instar. This change in barrier permeability is driven by the steroid hormone ecdysone and correlates with changes in localization of Coracle, a component of the septate junctions that is required for the late-larval, impermeable epithelial barrier. Based on these observations, we propose that the imaginal disc epithelial barrier regulates the duration of the regenerative checkpoint, providing a mechanism by which tissue function can signal the completion of regeneration.

2.1 Introduction

Drosophila melanogaster imaginal discs, larval precursors to adult organs, can regenerate after damage early in development, but lose this regenerative ability prior to pupariation (Halme et al., 2010). Following damage, regenerating imaginal discs activate a regeneration checkpoint through release of the relaxin peptide *Drosophila* insulin-like peptide 8 (Dilp8) (Colombani et al., 2012; Garelli et al., 2012). Dilp8 functions in the brain and the prothoracic gland (PG) by binding to the relaxin receptor (Lgr3), which inhibits the synthesis of the steroid hormone ecdysone (Colombani et al., 2015; Garelli et al., 2015; Jaszczak et al., 2016; Vallejo et al., 2015). Ecdysone triggers many of the developmental events that characterize the end of larval development and pupariation, including regeneration restriction (Hackney and Cherbas, 2014; Halme et al., 2010). Therefore, the inhibition of ecdysone synthesis during the regeneration checkpoint extends the larval phase, coordinating regeneration with developmental progression (Halme et al., 2010; Jaszczak et al., 2016). However, it is unclear what events determine the duration of the regenerative checkpoint and signal the completion of regeneration, allowing the larvae to enter pupation and progress through development to the adult stage.

Colombani et al. observed Dilp8 in the luminal space of the wing imaginal discs, between the primary epithelium and the peripodial epithelium (Colombani et al., 2012). Since the imaginal discs derive from the larval epidermis, emerging like an inflating balloon into the larval body cavity, this luminal space is topologically separated from the hemolymph by the imaginal disc epithelia (Pastor-Pareja et al., 2004). This led us to hypothesize that the imaginal disc epithelial barrier activity might regulate Dilp8 signaling by preventing access of Dilp8 in the disc lumen to the larval hemolymph, thus blocking signaling through the Lgr3 receptors in the brain and PG.

The epithelial barrier is a semi-permeable diffusion barrier between adjacent epithelial cells and is formed by tight junctions in vertebrates and septate junctions in invertebrates (Tepass et al., 2001). Claudin proteins determine

epithelial barrier exclusivity by homo- and heterodimerizing with the claudins of neighboring cells (Furuse and Tsukita, 2006). The claudins are localized to and stabilized at the junctions by a large core complex (Izumi and Furuse, 2014). However, the assembly and function of each member of the septate junction complex is not well understood. One subcomplex of the septate junction includes Coracle (Cora), a member of the Protein 4.1 superfamily (Fehon et al., 1994), and Neurexin-IV (Nrx) (Baumgartner et al., 1996). *In vivo*, Cora and Nrx both localize to the septate junctions and are necessary for stabilization of claudins at the septate junction and barrier activity (Baumgartner et al., 1996; Fehon et al., 1994; Genova and Fehon, 2003).

Here we describe experiments demonstrating that the epithelial barrier of wing imaginal discs matures during the third instar in response to increasing ecdysone levels and a re-localization of Coracle along the lateral membrane. This mature, prepupal epithelial barrier limits Dilp8 signaling and determines the duration of the developmental checkpoint after damage.

2.2 Results

2.2.1 The activity of Dilp8 is constrained by the imaginal disc epithelial barrier, determining the duration of the regeneration checkpoint delay

Previously, Colombani et al. observed that Dilp8 protein could be detected in the luminal space between the primary wing disc epithelium and the peripodial epithelium, within a region of the imaginal disc that is topologically separate from the larval hemolymph (Colombani et al., 2012; Pastor-Pareja et al., 2004). We recapitulated these findings by exogenously expressing a FLAG epitope-tagged allele of Dilp8 (Garelli et al., 2012) in wing imaginal discs with *apterous-Gal4* (*Ap-Gal4*) to induce expression in the dorsal half of the tissue (Cohen et al., 1992). We detected an accumulation of Dilp8::FLAG in the lumen of the wing imaginal discs (Figure 2-1). This observation led us to hypothesize that this luminal localization might limit Dilp8 signaling by preventing access to Lgr3 receptors in the brain and prothoracic gland, targets of Dilp8 to regulate growth and developmental timing

(Colombani et al., 2015; Garelli et al., 2015; Vallejo et al., 2015).

As the imaginal disc is an epithelial tissue, we examined whether disruption of the epithelial barrier would produce increased developmental checkpoint signaling when Dilp8 is expressed in the wing disc. To test whether the imaginal disc epithelial barrier constrains Dilp8 signaling, we expressed Dilp8 in the wing imaginal disc and measured the effect on developmental checkpoint delay when co-expressing an RNAi construct against a necessary component of the imaginal disc epithelial barrier, the claudin *kune-kune* (*kune^{RNAi}*, see Figure 2-4A,B and 2-11B,C for demonstrations of RNAi activity) (Nelson et al., 2010). We used *beadex-Gal4* (*Bx-Gal4*), to express either *dilp8::FLAG*, *kune^{RNAi}*, or both constructs in the pouch region of the wing disc (Milán et al., 1998) and measured developmental checkpoint delay relative to *lacZ* expressing control larvae. While *Bx > dilp8::FLAG* and *Bx > kune^{RNAi}* expression each produce a short delay in development relative to control larvae (13 and 10 hours respectively), the co-expression of Dilp8::FLAG and *kune^{RNAi}*, produces a strong genetic interaction and a synergistic effect on delay (40 hours; Figure 2-2A). The disruption of septate junction components is linked to perturbations of the Hippo pathway and epithelial proliferation, which could induce endogenous Dilp8 signaling (Khadiikar and Tanentzapf, 2019; Lee et al., 2020). To confirm the synergistic effect on delay is not due to increased activity at the endogenous *dilp8* locus, we examined the effect of co-expression of Dilp8::FLAG and *kune^{RNAi}* in a homozygous *dilp8* hypomorphic genetic background. Even without functional endogenous copies of the *dilp8* gene, we still observe a strong genetic interaction between Dilp8::FLAG and *kune^{RNAi}* and synergistic effect on developmental checkpoint delay (Figure 2-2B). We generated similar synergistic interactions when we co-expressed Dilp8::FLAG and targeted Neurexin-IV (Nrx), another necessary component of the imaginal disc septate junction (Baumgartner et al., 1996) (Figure 2-2). As we did not assess the mechanism of Dilp8 secretion, these data do not exclude the possibility of Dilp8 release through the basal surfaces of the tissue. However, these data indicate that disrupting the epithelial barrier through either of two distinct genetic targets can

produce synergistic extension of delay during Dilp8 expression. These results support the hypothesis that the epithelial barrier limits Dilp8 signaling from the wing imaginal disc by retaining at least a portion of Dilp8 in the wing disc lumen.

Figure 2-1. Dilp8 accumulates in the wing imaginal disc lumen.

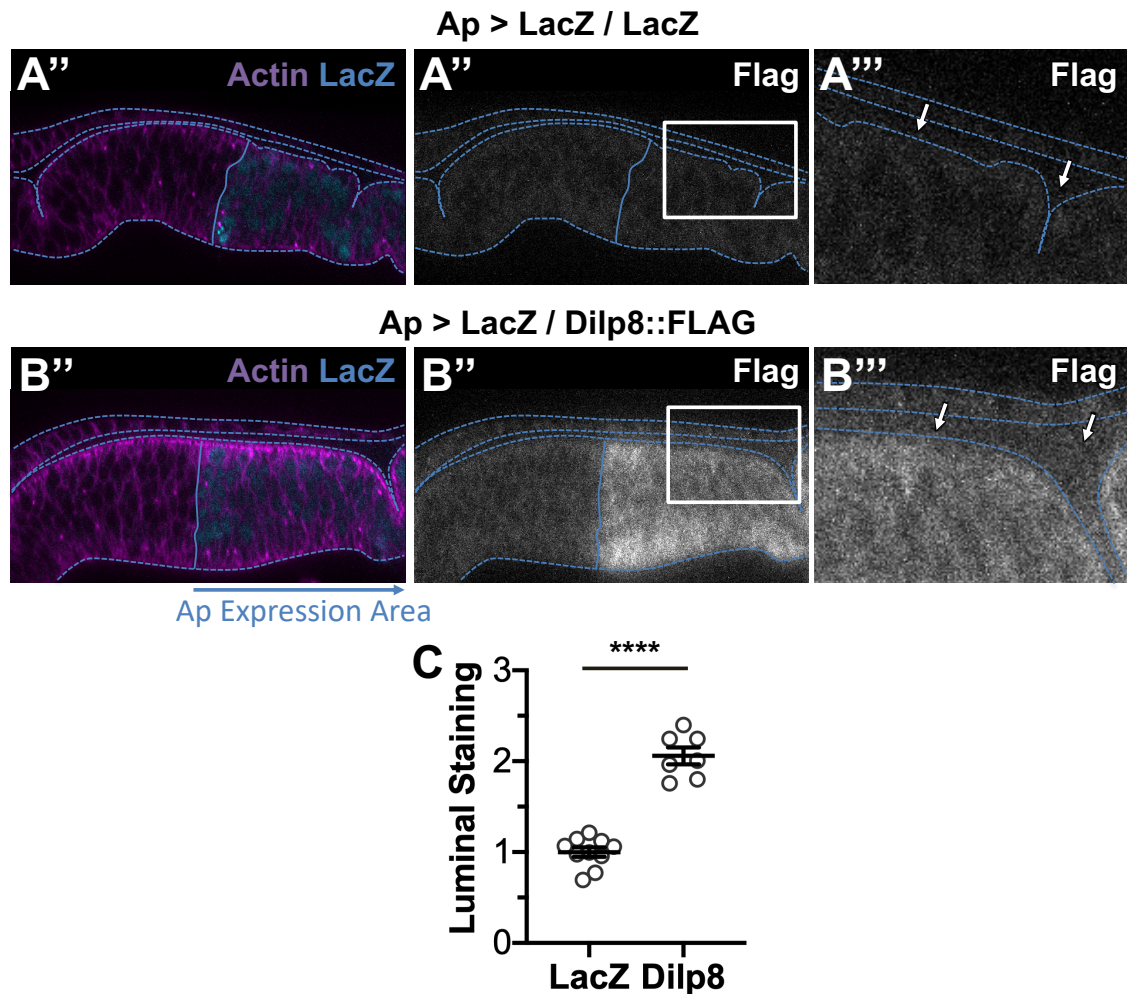


Figure 2-1. Dilp8 accumulates in the wing imaginal disc lumen. Ap-Gal4 was used to express (A) LacZ (wild type control) or (B) LacZ and Dilp8::FLAG in the dorsal region of wing imaginal discs. (A-B) Images are XZ cross-sections of wing imaginal discs in the pouch region of the disc. Dotted blue lines indicate disc area as defined by Actin (rhodamine phalloidin staining). Solid blue lines indicate the dorsal-ventral boundary, as defined by LacZ expression (β -Gal staining). White arrows indicate lumen. Representative images are oriented dorsal on the right. (A)

No FLAG is observed in *Ap > lacZ / lacZ* expressing discs either in (A'') the expression region or (A''') the lumen. (B) FLAG is observed in *Ap > lacZ / dilp8::FLAG* expressing discs in the (B'') expression region and (B''') the lumen. (C) Quantification of FLAG in the lumen, normalized to *Ap > LacZ* expression. Graph represent mean \pm SEM, with individual points indicating values of single images. $n = (\text{LacZ}) 10$ and $(\text{Dilp8}) 7$ discs. **** $p < 0.0001$ by unpaired t-test.

Figure 2-2. The epithelial barrier limits Dilp8 signaling.

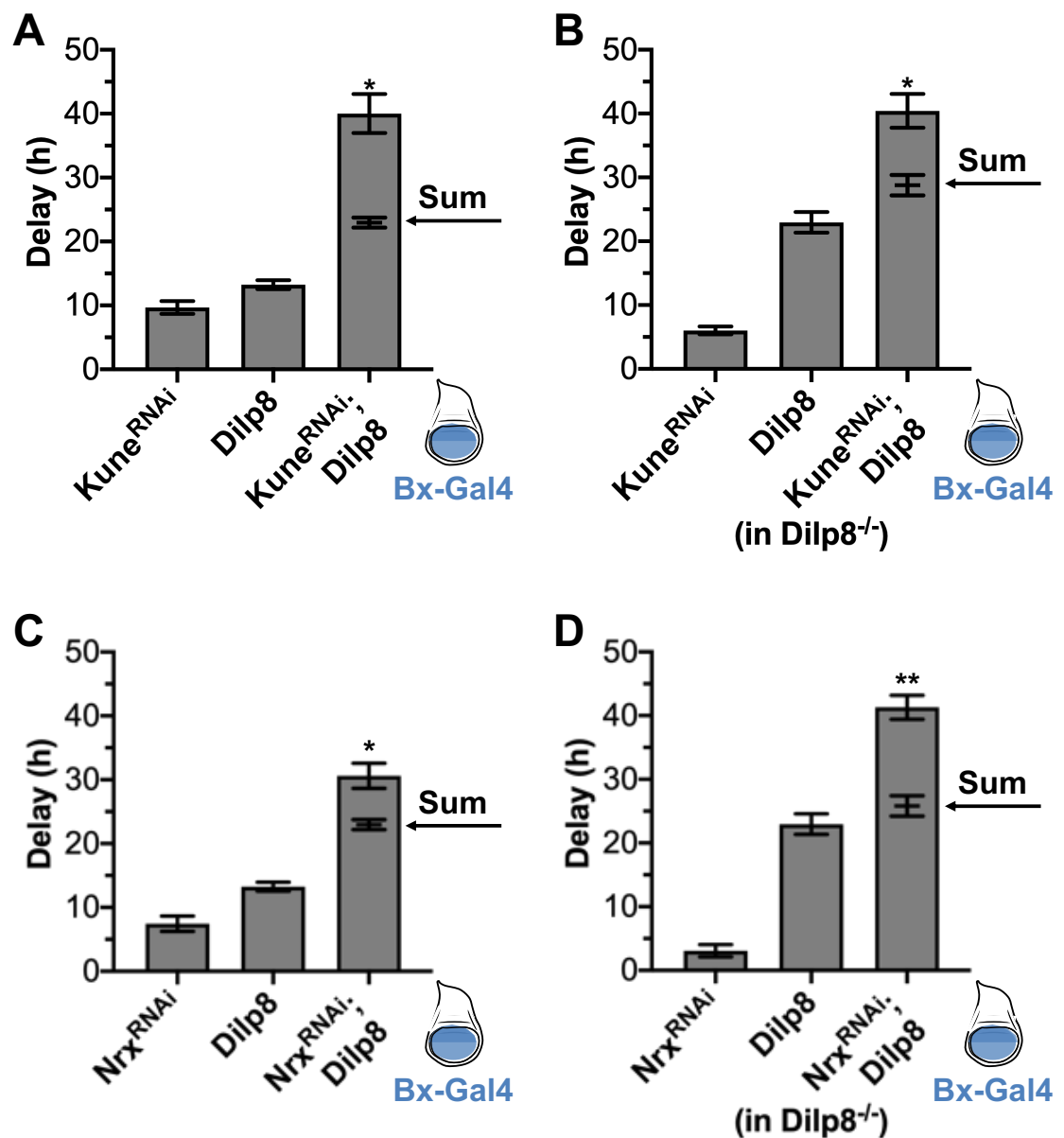


Figure 2-2. The epithelial barrier limits Dilp8 signaling. (A) Co-expression of *kune^{RNAi}* and Dilp8 induces synergistic delay. Ectopic expression of either *kune^{RNAi}*, Dilp8, or co-expression of *kune^{RNAi}* and Dilp8 (*kune^{RNAi}*; Dilp8) induce developmental delay compared to LacZ controls when expressed in the wing imaginal disc under Bx-Gal4 (expression region in blue). The delay induced by co-expression of *kune^{RNAi}* and Dilp8 (*kune^{RNAi}*; Dilp8) is significantly more than the sum of the delay induced by *kune^{RNAi}* and Dilp8 expressed alone (sum indicated by arrow). (B) This trend holds true when endogenous Dilp8 is limited by expression in a Dilp8 hypomorphic background (Dilp8^{M100727}/Dilp8^{M100727}; Garelli et al., 2012). (C) Likewise, co-expression of *nrx^{RNAi}* and Dilp8 induces synergistic delay. Ectopic expression of *nrx^{RNAi}*, Dilp8, and co-expression of *nrx^{RNAi}* and Dilp8 (*nrx^{RNAi}*; Dilp8) induce developmental delay compared to LacZ controls when expressed in the wing imaginal disc under Bx-Gal4 (expression region in blue). The delay induced by co-expression of *nrx^{RNAi}* and Dilp8 (*nrx^{RNAi}*; Dilp8) is significantly more than the sum of the delay induced by *nrx^{RNAi}* and Dilp8 expressed alone (sum indicated by arrow). (D) This trend holds true when endogenous Dilp8 is limited by expression in a Dilp8 hypomorphic background (Dilp8^{M100727}/Dilp8^{M100727}; Garelli et al., 2012). Data were collected from at least three independent experiments with a minimum of 20 larvae per experimental condition, bars represent mean \pm SEM, * $p < 0.05$, ** $p < 0.01$ from one-tailed sample t-test comparing the additive value and observed delay.

2.2.2 The wing imaginal disc epithelial barrier becomes more restrictive during the last larval instar

The experiments above demonstrate that the wing disc epithelial barrier can limit Dilp8 signaling. However, Dilp8 expression in the wing disc produces developmental delay even when the wing disc epithelial barrier is not disrupted (Figure 1A,B; Colombani et al., 2012; Garelli et al., 2012). Additionally, basal levels of Dilp8 expression in the developing wing disc regulate tissue symmetry through communication with Lgr3 in the brain (Colombani et al., 2012; Garelli et al., 2012;

Garelli et al., 2015; Vallejo et al., 2015). To reconcile these observations with the sequestration of Dilp8 in the wing disc lumen during in late third instar larvae, we hypothesized that there may be changes in the epithelial barrier permeability during development. To examine this, we developed a quantitative method for measuring epithelial barrier permeability that is an extension of a method described in Lamb et al. 1998, in which the ability of fluorophore-conjugated dextran to enter into the lumen of a tissue was used to assess epithelial barrier function (Lamb et al., 1998). For our assay, we incubated inverted larval carcasses for 30 minutes in solution containing fluorescein-conjugated dextran prior to paraformaldehyde fixation. We mounted and imaged the fixed imaginal discs, then measured the fluorescein signal in the lumen of the imaginal discs to quantify epithelial barrier permeability (see Materials and Methods and Figure 2-3 for a more complete description of this assay).

When we examined late third instar imaginal discs (116 hours After Egg Deposition; h AED), we observed that very little fluorescent signal is detected in the wing disc lumen (Figure 2-4A). To determine whether exclusion of dextran from late larval wing discs is dependent on epithelial barrier function, we measured fluorescence in imaginal discs that had been punctured with a forceps tip prior to incubation with fluorescently-labeled dextran. As expected, we observed that puncturing the wing disc led to a substantial increase in luminal fluorescence detected in these discs after fixation (Figure 2-4A), demonstrating that an intact epithelium is necessary for the exclusion of dextran from the lumen of late third instar wing discs. We then tested whether this exclusion reflected the activity of the epithelial barrier by measuring dextran infiltration into wing discs expressing *kune^{RNAi}* (*Ap > kune^{RNAi}*). Consistent with a critical role for the claudin Kune in wing epithelial barrier function, we observed an equivalent amount of fluorescence infiltration into 116h AED *Ap > kune^{RNAi}* discs as we observed in punctured discs (Figure 2-4A). Therefore, loss of *kune* appears to completely disrupt the epithelial barrier in late third instar wing discs.

To characterize the epithelial barrier in earlier wing discs, we examined wing

discs 24 hours earlier in development (92h AED, about the middle of the third and last larval instar), a time when disc damage and/or Dilp8 expression is still capable of producing developmental delay. In 92h AED discs we observe that physical puncture and *kune*^{RNAi} expression both produce increases in dextran infiltration into the wing disc lumen (Figure 2-4B), similar to what we observed at 116h AED. This indicates that wing imaginal discs in the middle of the third instar have a functioning epithelial barrier mediated by *kune*. However, we also noticed that the level of dextran infiltration into control 92h AED wing discs is much higher than the fluorescence observed in the same tissues at 116h AED (compare Figure 2-4A and B), suggesting that the epithelial barrier of the wing disc grows more restrictive as the larvae approach the end of the third instar.

This change in barrier permeability from 92h to 116h AED is also observed with 70 kDa dextran (Figure 2-5), suggesting that the change in permeability does not reflect a change in size selectivity of the barrier. To further characterize the maturation of the more restrictive barrier, we used our quantitative barrier permeability assay to examine dextran infiltration at six-hour intervals between 92h AED and 116h AED. We normalized the fluorescence intensity to discs of equivalently staged larvae with barriers disrupted by *kune*^{RNAi} expression. Consistent with our earlier observations at 92h and 116h AED, as the wing disc develops, we see a progressive decrease in dextran in the lumen (Figure 2-4C, for an illustration of the individual fluorescence distributions, see Figure 2-6). This suggests that barrier permeability decreases over time to limit the infiltration of dextran into the lumen of this tissue.

Based on these observations, we conclude that the wing disc epithelial barrier limits diffusion throughout the third instar since we see an increase in permeability in punctured or *kune*^{RNAi} expressing discs at earlier stages. However, we see a substantial difference in permeability of the barrier between earlier and later discs, with the wing disc epithelial barrier becoming progressively less permeable as larvae advance through the third instar.

Figure 2-3. Explanation of the dextran assay for barrier function.

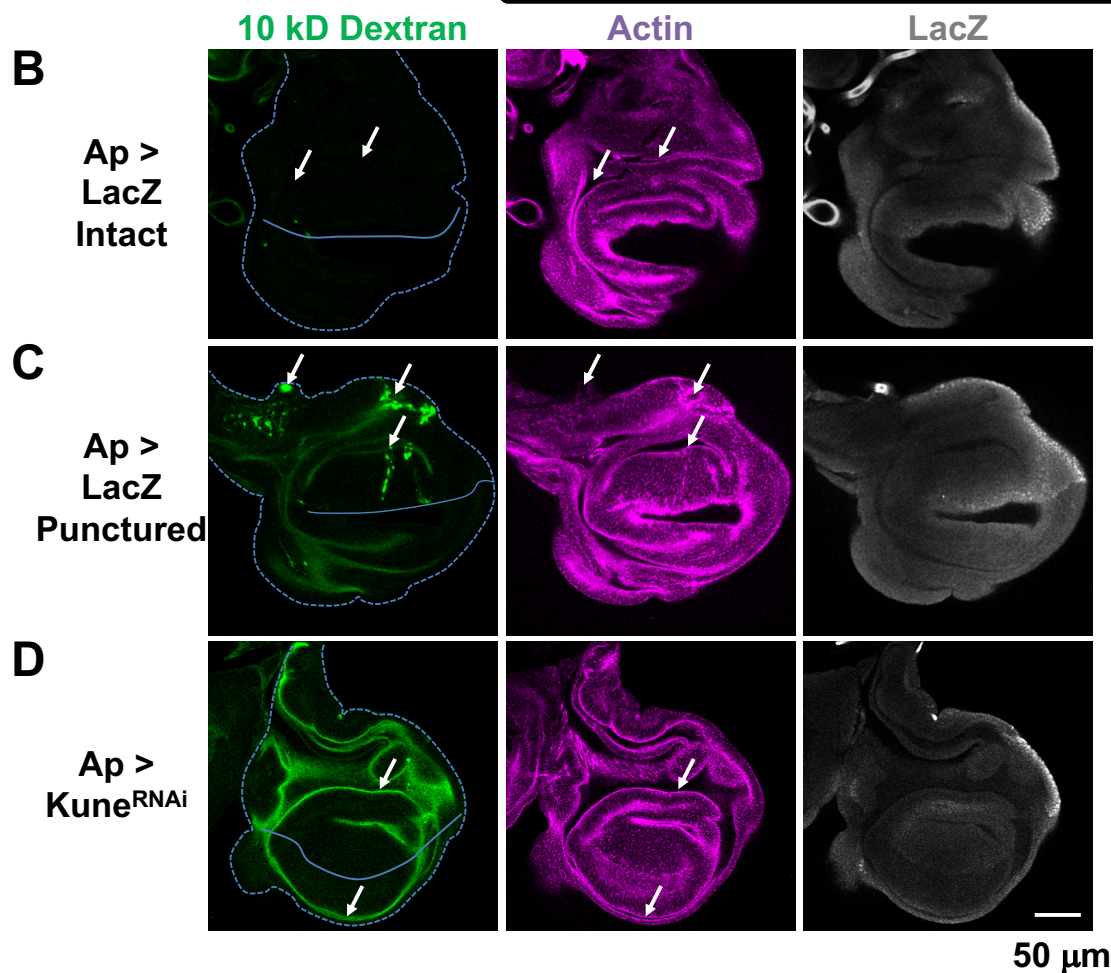
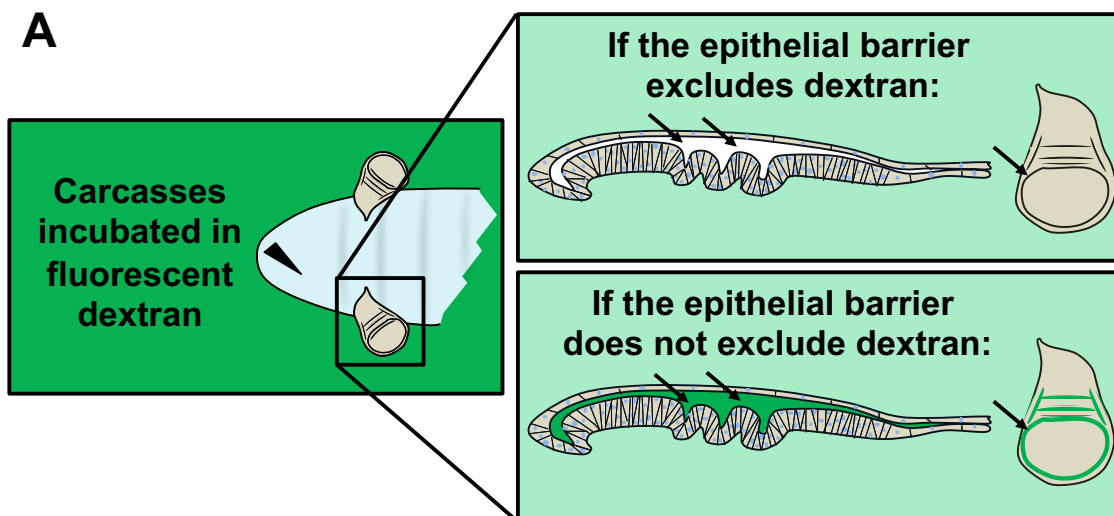


Figure 2-3. Explanation of the dextran assay for barrier function. (A) Carcasses are inverted and cleaned, then incubated in a fluorescence conjugated dextran for 30 minutes before fixation, the discs were then stained, mounted, and imaged (full description in methods). If the epithelial barrier excludes the dextran, no dextran should be observable in the lumen of the imaginal disc. If the epithelial barrier does not exclude the dextran or the tissue integrity is disrupted, dextran should be observable in the lumen. (B-D) Representative images after 10 kDa fluorescein-conjugated dextran incubation (from the experiment quantified in Figure 2-4A). Ap-Gal4 was used to express LacZ (*Ap > lacZ*) or Kune^{RNAi} (*Ap > une^{RNAi}*). Dextran is observed in punctured LacZ expressing discs (C) and Kune^{RNAi} expressing discs (D), but not in intact LacZ expressing discs (A). Disc area is indicated by the dashed line, as defined by Actin staining (rhodamine phalloidin). Area of expression is dorsal (oriented up) of the solid line, as defined by LacZ staining (β -Gal). Note that *lacZ* expressing discs express two copies of *lacZ* while *kune^{RNAi}* expressing discs have one copy so β -Gal staining is not comparable between images. Additionally, this LacZ allele has a nuclear localization sequence (LacZ.NZ), but the images are taken along the best plane for dextran quantification. This frequently results in β -Gal staining being out-of-plane. Due to the curvature of the disc the outside edge of the tissue may be in better focus but the differences along the dorsal-ventral boundary are still distinguishable. Arrows indicate: (A) areas of the lumen with no distinguishable dextran fluorescence; (B) areas where damage during dissection (puncturing) has disrupted epithelial barrier integrity, allowing dextran to enter the cells and the imaginal disc lumen; and (C) luminal dextran is observed in both the dorsal lumen (Kune^{RNAi} expressing area, oriented up) and also in the ventral lumen (non-expressing area, oriented down), indicating that the lumen is contiguous. Images are single slices.

Figure 2-4. The wing disc epithelial barrier becomes more restrictive with progression through the third larval instar.

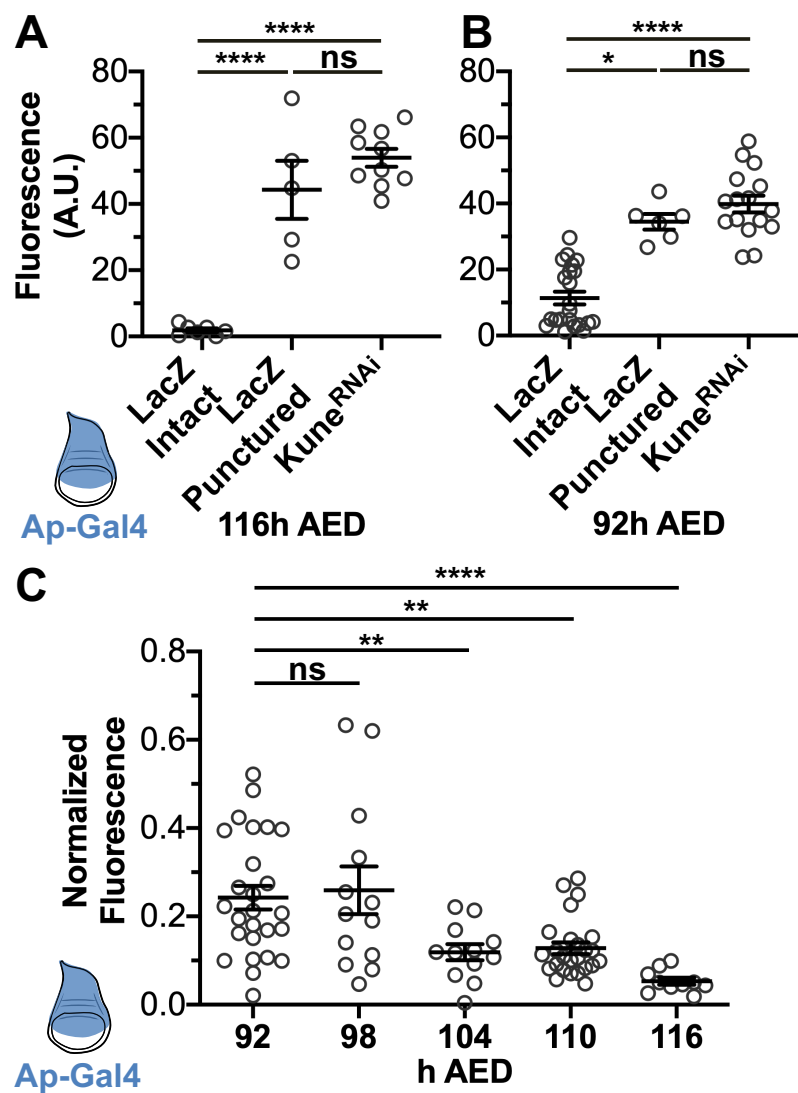


Figure 2-4. The wing disc epithelial barrier becomes more restrictive with progression through the third larval instar. (A-B) The wing imaginal disc epithelial barrier excludes 10 kDa dextran and the function of the barrier is dependent on Kune at both (A) 116h and (B) 92h AED. LacZ and Kune^{RNAi} were expressed in the imaginal disc with Ap-Gal4 (expression area diagramed in blue). Imaginal discs were incubated in 10 kDa fluorescein-conjugated dextran for 30 minutes prior to (see methods for details). Luminal intensity was measured in the LacZ controls, LacZ controls that were punctured during dissection prior to fixing,

and the Kune^{RNAi} expressing discs. (C) The maturation of the epithelial barrier occurs gradually from 92h to 116h AED. Every 6 hours from 92h and 116h AED, barrier function was measured, as previously described, in wing imaginal discs expressing LacZ or Kune^{RNAi} with Ap-Gal4. Data indicate luminal intensity of intact LacZ expressing discs normalized to the mean luminal intensity of the Kune^{RNAi} expressing discs from the same timepoint, Kune^{RNAi} data represented in Figure 2-8. (A-C) Graphs represent mean \pm SEM, with individual points indicating values of single images. Left to right, n = (A) 7, 5, 10, (B) 22, 6, 16, (C) 26, 13, 12, 25, 10. (A-C) ns not significant, * p < 0.05, ** p < 0.01, **** p < 0.0001 as calculated by (A,C) Brown-Forsythe and Welch ANOVA with Dunnett's T3 test for multiple comparisons or (B) one-way ANOVA with Tukey test for multiple comparisons.

Figure 2-5. The epithelial barrier of wing imaginal discs grows more exclusionary to 70 kDa fluorescent dextran during the third instar.

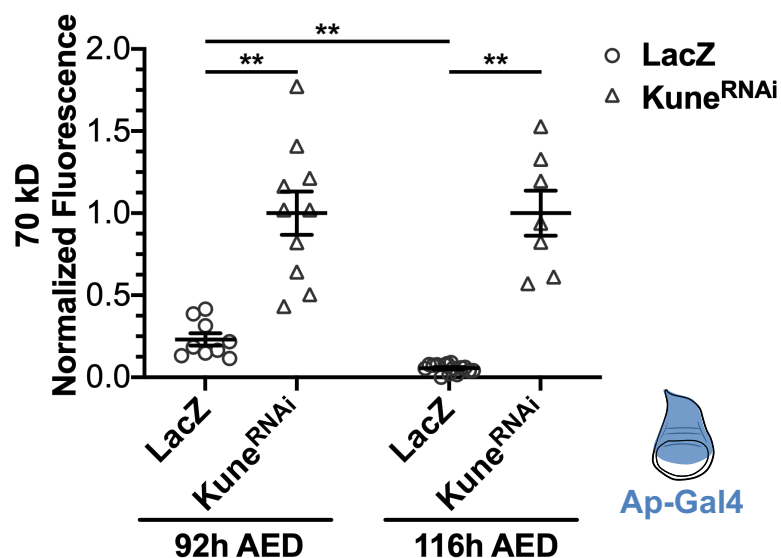


Figure 2-5. The epithelial barrier of wing imaginal discs grow more exclusionary to 70 kDa fluorescent dextran during the third instar. The function of the epithelial barrier to exclude 70 kDa Texas Red conjugated dextran was measured, as previously described, at 92h and 116h AED in wing imaginal discs expressing LacZ or Kune^{RNAi} by Ap-Gal4 (expression area diagramed in blue). Data are normalized to the mean luminal intensity of the Kune^{RNAi} expressing

discs. Graph represents mean \pm SEM, with individual points indicating values of single images. Left to right, $n = 9, 10, 15, 7$. ** $p < 0.01$ as calculated by Brown-Forsythe and Welch ANOVA with Dunnett's T3 test for multiple comparisons.

Figure 2-6. The epithelial barrier matures between 92h and 116h AED, becoming more restrictive to 10 kDa fluorescein conjugated dextran.

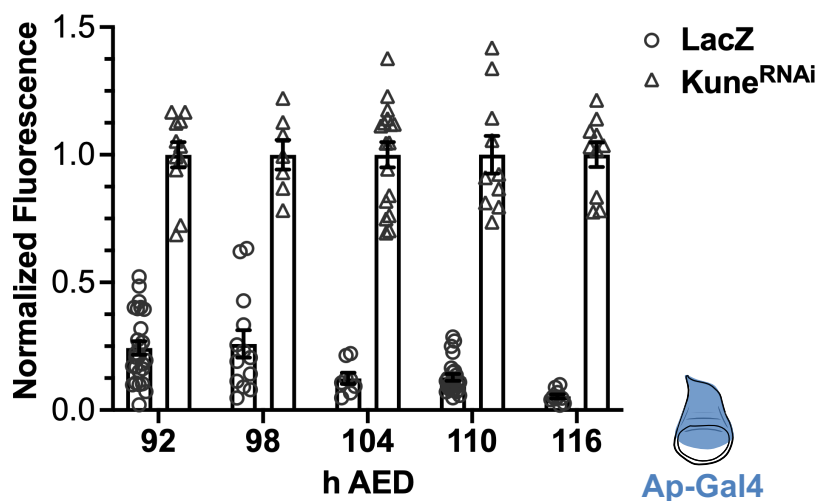


Figure 2-6. The epithelial barrier matures between 92h and 116h AED, becoming more restrictive to 10 kDa fluorescein conjugated dextran. These are the complete data from Figure 2-2C, including data from Kune^{RNAi} expressing discs: the barrier function of wing imaginal discs expressing LacZ or Kune^{RNAi} by Ap-Gal4 was measured every 6 hours between 92h and 116h AED. Data indicate luminal intensity of intact LacZ expressing discs normalized to the mean luminal intensity of the Kune^{RNAi} expressing discs from the same timepoint. Graphs represent mean \pm SEM, with individual points indicating values of single images. Significance between LacZ expressing discs at each timepoint is indicated in Figure 2-2C. Left to right, $n = (92\text{h AED}) 26, 11, (98\text{h AED}) 13, 7, (104\text{h AED}) 12, 17, (110\text{h AED}) 25, 10, (116\text{h AED}) 10, 11$.

2.2.3 Changes in epithelial barrier permeability correlate with changes in junctional protein expression and localization

The changes that we observe in barrier permeability during the last larval instar could be attributable to changes in localization and/or activity of different components of the epithelial barrier. To address this, we examined the localization of three major components of the epithelial barrier: the claudin Kune, which forms the intercellular component of the junctional barrier (Nelson et al., 2010), along with Cora and NrX which together regulate the function of pleated septate junctions in ectoderm-derived tissues such as the imaginal discs (Baumgartner et al., 1996; Lamb et al., 1998). Using indirect immunofluorescent staining with a Kune protein-directed antibody (Nelson et al., 2010), we observed that Kune protein is localized to the apical region of the lateral membrane throughout the third instar (Figure 2-7C,D; Figure 2-8D,E), which is the region of septate junctions localization in imaginal tissues (Lamb et al., 1998; Ward IV et al., 2001). We also observed that there is a substantial increase in localized Kune signal at the septate junction in late third instar discs (116h AED) when compared to earlier (92h AED) discs (Figure 2-7E, quantification method described in Materials and Methods and diagrammed in Figure 2-9). To localize NrX, we used a functional NrX-GFP fusion (Buszczak et al., 2007; Morin et al., 2001). Like Kune, NrX-GFP also localizes to the septate junctions throughout the third instar and increases in signal intensity from 92 to 116 hAED (Figure 2-7F-H; Figure 2-8F,G). In contrast to Kune and NrX-GFP, the localization of Cora is more dynamic. At 92h AED, Cora is localized either approximately uniformly along the entire length lateral membrane, without selectivity for the septate junction, or with slight selectivity for the septate junctions (Figure 2-7I,K; Figure 2-8H). However, by 116h AED, Cora localization shifts to become restricted to the apical-lateral localization at the septate junctions, as we observed for Kune and NrX-GFP (Figure 2-7J,K; Figure 2-8I).

These changes in septate junction component localization correlate with the maturation of the disc epithelial barrier. In particular, we observe an increase in Kune localization at the septate junction, and a refinement of Cora localization,

from a uniform distribution along the lateral membrane to the apical site of the septate junction, that correlates with the developmental changes in septate junction permeability that we have measured.

Figure 2-7. The localization of septate junction components changes between 92h and 116h AED.

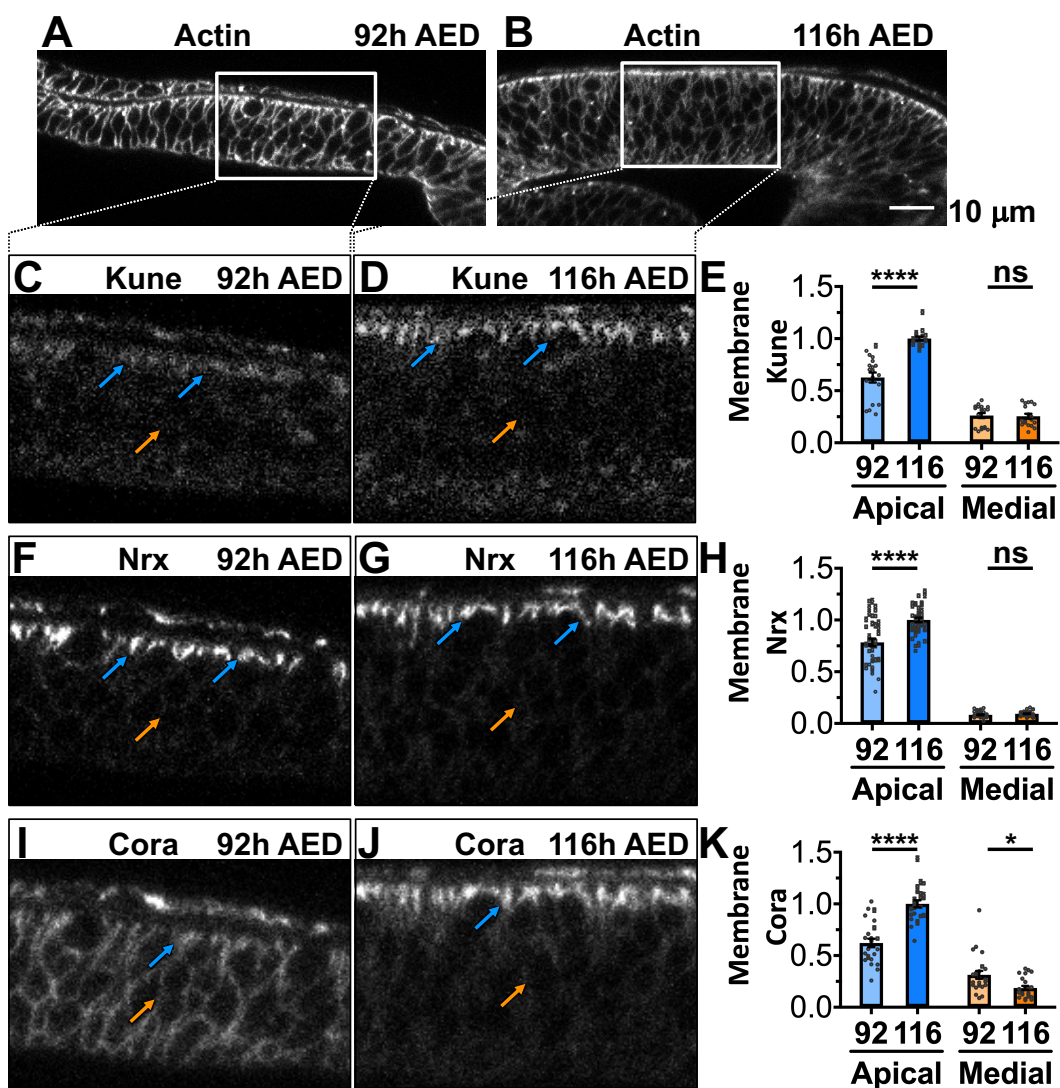


Figure 2-7. The localization of septate junction components changes between 92h and 116h AED. (A-B) Disc area was determined by Actin (rhodamine phalloidin) staining at (A) 92h and (B) 116h AED. The box represents the area of focus for images in C, F and I for the 92h AED disc and D, G, and J for

the 116h AED disc. Blue arrows indicate apical-lateral localization, orange arrows indicate medial-lateral localization (or lack thereof). (C,D) Representative images of Kune localization at (C) 92h and (D) 116h AED showing of apical-lateral Kune localization. (E) Quantification of Kune localized along the apical-lateral and medial-lateral membrane. Normalization is to the mean apical-lateral Kune membrane intensity at 116h AED. Thus, normalization represents intensity relative to localization at the mature septate junction. (F,G) Representative images of NrX localization at 92h (F) and 116h (G) AED showing apical-lateral localization. (H) Quantification of NrX localized along the apical-lateral and medial-lateral membrane, normalized to apical-lateral NrX membrane intensity at 116h AED. (I,J) Representative images of Cora localization at (I) 92h and (J) 116h AED showing diffuse Cora localization at 92h AED, and apical-lateral Cora localization at 116h AED. (K) Quantification of Cora localized along the apical-lateral and medial-lateral membrane, normalized to mean apical-lateral Cora membrane intensity at 116h AED. (C,D,F,G,I,J) Full images in Figure 2-8. (E,H,K) Individual points represent mean \pm SEM for each image, with the n considered to be the number of cell-cell contacts across the region measured. Bars represent mean \pm SEM across the images, with the n considered to be the number of images measured. Details of the quantification method are explained in the Methods Section and Figure 2-9. n = (E) 19, 92h AED and 18, 116h AED images, (H) 39, 92h AED and 41, 116h AED images, and (K) 24, 92h AED and 24, 116h AED images. ns not significant, * $p < 0.05$, **** $p < 0.0001$ as calculated by unpaired, two-tailed t-test, except for apical-lateral Kune, which had unequal variance, in this case significance was calculated by unpaired, two-tailed t-test with Welch's correction.

Figure 2-8. Complete images from Figure 2-7.

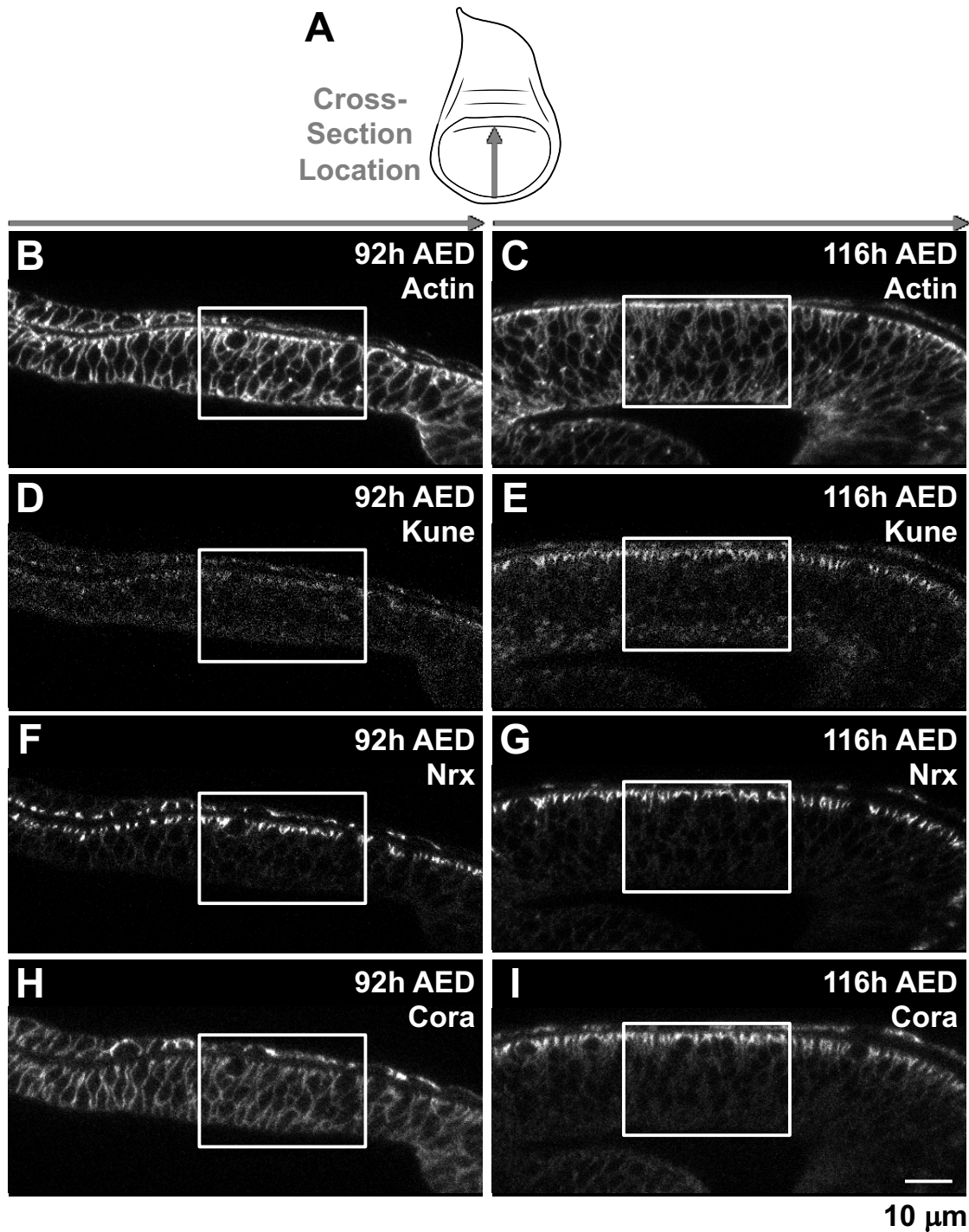


Figure 2-8. Complete images from Figure 2-7. (A) Approximate area and orientation of XZ image locations in the wing imaginal discs. Gray arrow in the cartoon aligns with the grey arrows above B-I. (B-I) Representative XZ images at

92h and 116h AED, the region zoomed into in Figure 2-7 is indicated (white box). Images are: (B-C) Actin (rhodamine phalloidin; corresponds to Figure 2-7A,B), (D-E) Kune (Anti-Kune; corresponds to Figure 2-7C-E), (F-G) Nrj (Nrj-GFP; corresponds to Figure 2-7F-H); and (H-I) Cora (Anti-Cora; corresponds to Figure 2-7 I-K).

Figure 2-9. Method for junction quantification.

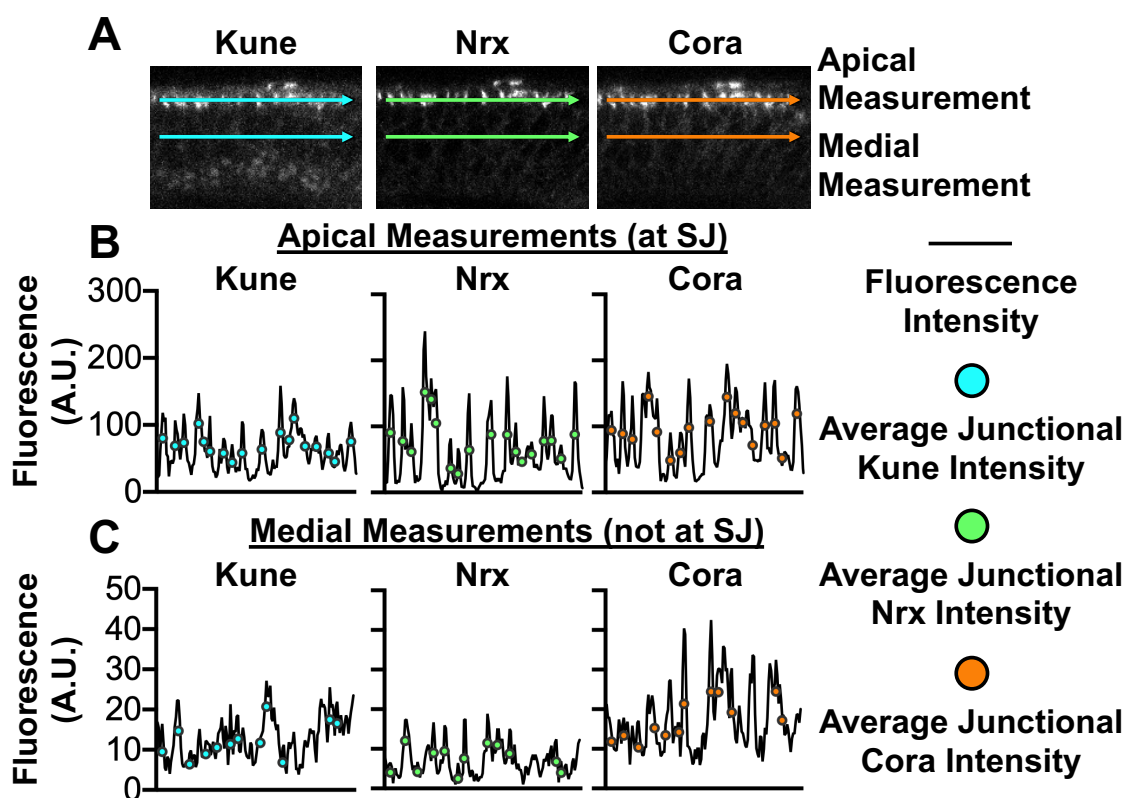


Figure 2-9. Method for junction quantification. (A) Lines were drawn apically bisecting the region of brightest septate junction (SJ) staining, and medially. (B-C) Fluorescence intensity across each line were measured with plot profile. Areas of the membrane (septate junction if apical) were identified as local maxima (peak) within a 7-pixel range, the 3 prior and following the pixel in question. We adjusted these data in three steps, further described in Materials and Methods, to reduce false identification of a peak being localized at a membrane due to imaging or staining issues (e.g. non-specific staining, image noise), especially with regard to

Anti-Kune and Anti-Cora staining. The average junctional intensity was taken as the mean of the 7-pixel range.

2.2.4 Coracle is required to produce the changes in epithelial barrier permeability during the last larval instar

To determine whether Cora activity is important for the observed decrease in septate junction permeability during the last larval instar, we examined the effect of *cora*^{RNAi} expression on wing imaginal disc barrier permeability. At 92h AED *Ap* > *cora*^{RNAi} expression has little impact on the wing epithelial barrier permeability. The barrier activity in Cora knockdown discs is similar to control discs, with much greater selectivity than *Ap* > *kune*^{RNAi} expressing discs, which have no functioning barrier (Figure 2-10A). In contrast, in late third instar wing imaginal discs (116h AED) *Ap* > *cora*^{RNAi} expressing discs exhibit a completely disrupted epithelial barrier, comparable to that seen in *Ap* > *kune*^{RNAi} expressing discs (Figure 2-10B). Therefore, as the third instar progresses, there is a change in the role of Cora for septate junction barrier activity: 92h AED wing discs have a weaker, somewhat permeable, barrier activity that requires Kune, but does not depend on Cora, whereas 116h AED wing discs have a more restrictive barrier activity that is completely dependent on both Kune and Cora.

Cora, Kune, and Nr_x localize interdependently at the septate junctions during the development of the embryonic tracheal epithelium (Nelson et al., 2010; Oshima and Fehon, 2011). We examined whether the same interdependence occurs in the wing imaginal disc, and whether it changes during development. To do this, we visualized the localization of Cora, Kune, and Nr_x-GFP in discs in which we had knocked down each of these components using RNAi targeting constructs driven by *Ap-Gal4*. Predictably, when we expressed RNAi lines targeting Cora, Kune, and Nr_x, we saw a loss of expression of the targeted gene product in the dorsal compartment of both 92 and 116h AED wing discs (Figure 2-11), demonstrating the efficacy of the RNAi constructs. We then examined the interdependence for localization of these three septate junction proteins at 92h and

116h AED wing discs (Figure 2-12 A-F). At 92h AED, the localization of Cora along the lateral membrane is unaffected by RNAi targeted knockdown of either Kune ($Ap > kune^{RNAi}$, Figure 2-12A) or Nr x ($Ap > nrx^{RNAi}$, Figure 2-12C). However, the localization of Cora at the septate junctions at 116h AED is disrupted by RNAi targeted knockdown of either Kune ($Ap > kune^{RNAi}$, Figure 2-12B) or Nr x ($Ap > nrx^{RNAi}$, Figure 2-12D). Therefore, the early, diffuse localization of Cora along the lateral membrane does not require the activity of either Kune or Nr x , but its refinement to the septate junction at the end of the larval period depends on both Kune and Nr x . Nr x localization at the septate junctions in 92h AED larvae is dependent on both Kune ($Ap > kune^{RNAi}$, Figure 2-12A) and Cora ($Ap > cora^{RNAi}$, Figure 2-12E). However, in the absence of Kune, we see faint Nr x localization along the lateral membrane (Figure 2-12A, orange arrows), which might reflect an association with Cora, whereas in the absence of Cora, we see less evidence of lateral localization of Nr x (Figure 2-12E, blue arrows). At 116h AED, Nr x localization at the septate junction is entirely dependent on both Kune and Cora (Figure 2-12B,F) and no lateral redistribution of Nr x is seen in either of these mutants. Finally, the septate junction localization of Kune at both 92 and 116h AED is entirely dependent on Nr x ($Ap > nrx^{RNAi}$, Figure 2-12C,D) and, surprisingly, Cora ($Ap > cora^{RNAi}$, Figure 2-12E,F). The requirement for Cora to localize Nr x and Kune at 92h AED is unexpected since Cora is not required for the barrier activity observed at 92h AED (Figure 2-10A). We address some possible explanations of this observation in the Discussion section.

We see a complex interdependence between Kune, Nr x , and Cora that determines their localization as the wing disc epithelial barrier becomes more restrictive during the larval third instar. These data indicate that as the epithelial barrier becomes more mature and restrictive, barrier activity becomes dependent on Cora as it re-localizes to the septate junctions.

Figure 2-10. The role of Cora in epithelial barrier activity changes from 92h and 116h AED.

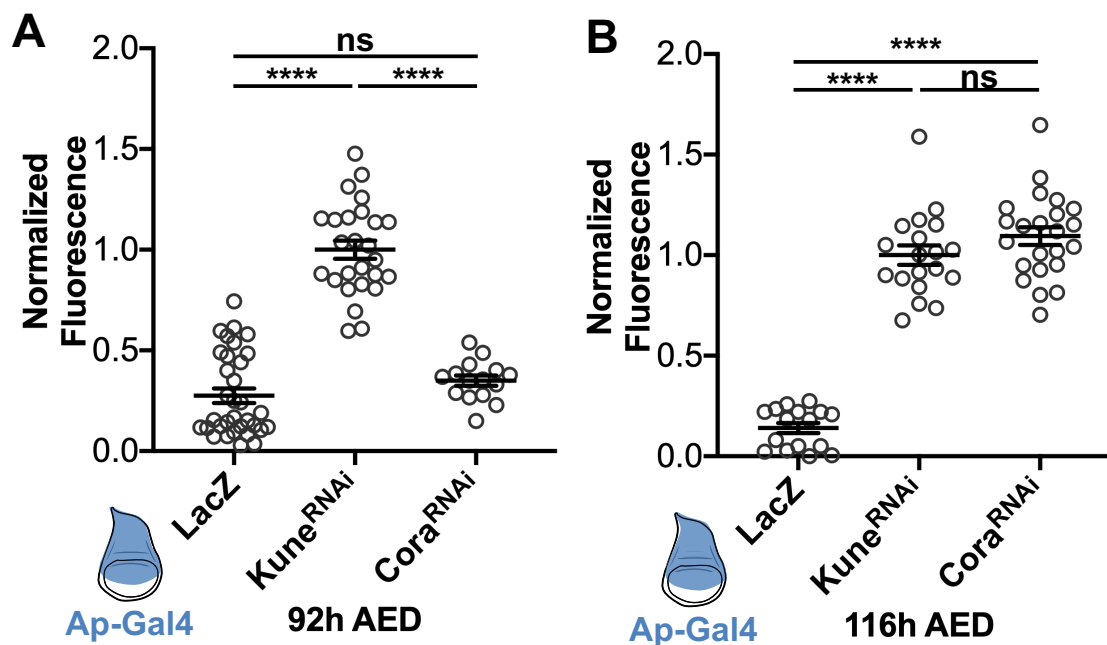


Figure 2-10. The role of Cora in epithelial barrier activity changes from 92h and 116h AED. (A-B) Function of the epithelial barrier in discs expressing *lacZ*, *kune^{RNAi}*, or *cora^{RNAi}* (using Ap-Gal4, expression diagramed in blue) to exclude 10 kDa dextran at (A) 92h and (B) 116h AED. At 92h AED, the barrier of *cora^{RNAi}* expressing discs is similar to *lacZ* expressing discs. At 116h AED, the barrier of *cora^{RNAi}* expressing discs is similar to *kune^{RNAi}* expressing discs. Data are normalized to the mean luminal intensity of *kune^{RNAi}* expressing discs. Graph represents mean \pm SEM, with individual points indicating values of single images. Left to right, n = (A) 33, 26, and 15 images, and (B) 16, 19, and 23 images. ns not significant, **** p < 0.0001 as calculated by Brown-Forsythe and Welch ANOVA with Dunnett's T3 test for multiple comparisons.

Figure 2-11. RNAi inhibition of septate junction components.

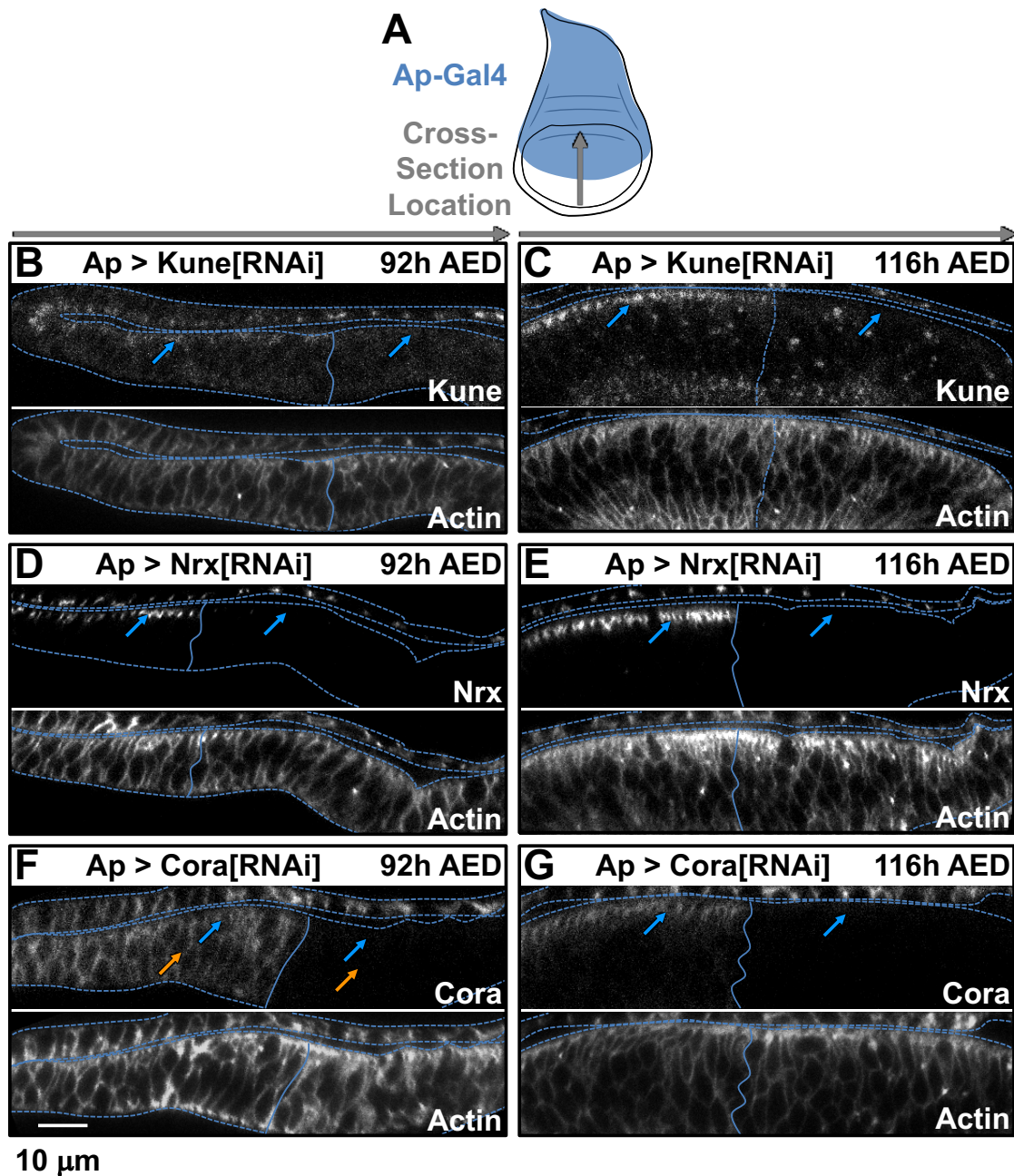


Figure 2-11. RNAi inhibition of septate junction components. (A) Images were taken spanning the dorsal-ventral boundary in the pouch region of wing imaginal discs which includes tissue outside and inside the Ap-Gal4 expression region (blue). Grey arrow indicates approximate image location and orientation, and correlates with the grey arrows above B-G. (B-G) Localization of septate junction

components following RNAi expression and actin localization (defined by rhodamine phalloidin). Images are from the same discs as Figure 2-12. Dotted line represents tissue outline defined by actin staining. Solid line represents dorsal-ventral boundary, expression area (dorsal region) is on the right. Blue arrows indicate apical-lateral localization, orange arrows indicate medial-lateral localization. (B-C) Localization of Kune and Actin in *Ap > kune^{RNAi}* expressing discs at (B) 92h and (C) 116h AED. Kune is depleted in the *kune^{RNAi}* expression region at both times. Images are of the same discs as Figure 2-12A and 2-12B. (D-E) Localization of Nrx and Actin in *Ap > nrx^{RNAi}* expressing discs at (D) 92h and (E) 116h AED. Nrx is depleted in the *nrx^{RNAi}* expression region at both times. Images are of the same discs as Figure 2-12C and 2-12D. (F-G) Localization of Cora and Actin in *Ap > cora^{RNAi}* expressing discs at (F) 92h and (G) 116h AED. Kune is depleted in the *cora^{RNAi}* expression region at both times. Images are of the same discs as Figure 2-12E and 2-12F.

Figure 2-12. The localization of Nr_x and Kune is dependent on Cora at both 92h and 116h AED.

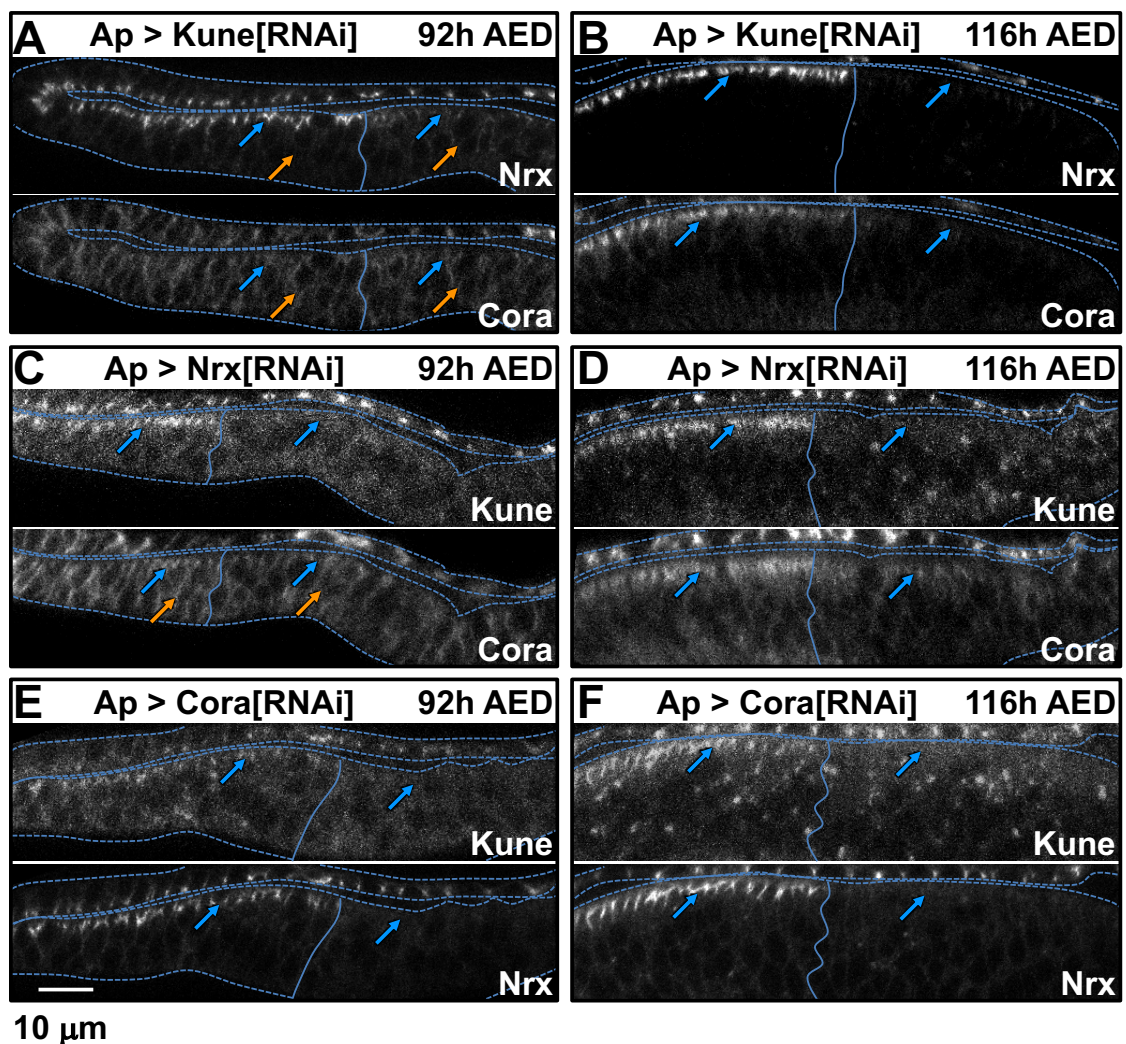


Figure 2-12. The localization of Nr_x and Kune is dependent on Cora at both 92h and 116h AED. Ap-Gal4 was used to express *kune*^{RNAi}, *nr_x*^{RNAi}, or *cora*^{RNAi} and the localization of the Kune, Nr_x, and Cora were assessed (images with same protein as the RNAi are in Figure 2-11). Images were taken spanning the dorsal-ventral boundary (solid line, defined by data in Figure 2-11) and oriented with the dorsal region (expression area) on the right. Dotted lines represent tissue outline defined by Actin staining (Figure 2-11). Blue arrows indicate apical-lateral localization, orange arrows indicate medial-lateral localization. (A-B) Localization of Nr_x and Cora in Ap > *kune*^{RNAi} expressing discs at (A) 92h and (B) 116h AED.

In the portion of the disc without *kune*^{RNAi} expression Nr_x is apical-laterally localized at 92h and 116h AED, without medial-lateral localization. Nr_x intensity localization is lost with *kune*^{RNAi} expression at both times, but at 92h AED, also becomes more diffusely localized. Cora localization is independent of Kune at 92h AED, but is lost with *kune*^{RNAi} expression at 116h AED. (C-D) Localization of Kune and Cora in *Ap > nr_x*^{RNAi} expressing discs at (C) 92h and (D) 116h AED. Kune localization is lost with *nr_x*^{RNAi} expression at both times. Cora localization is independent of Kune at 92h AED, but is lost with *kune*^{RNAi} expression at 116h AED. Cora localization is independent of Kune at 92h AED, but is significantly diminished, although not completely lost, with *kune*^{RNAi} expression at 116h AED. (E-F) Localization of Kune and Nr_x in *Ap > cora*^{RNAi} expressing discs at (E) 92h and (F) 116h AED. Kune and Nr_x localization are lost with *cora*^{RNAi} at both times. (A-F) Images are representative from n = (A) 8, (B) 10, (C) 8, (D) 6, (E) 5, and (F) 11 images.

2.2.5 Ecdysone signaling promotes decreased epithelial barrier permeability and Coracle re-localization

The steroid hormone ecdysone is a critical endocrine regulator of *Drosophila* developmental progression. During the third larval instar, pulses of ecdysone synthesis drive a progressive increase in ecdysone titer throughout the larva that promotes growth and differentiation of the imaginal discs (Burdette, 1962; Colombani et al., 2005; Lavrynenko et al., 2015). During the activation of the regenerative checkpoint following imaginal disc damage, Dilp8 release suppresses ecdysone synthesis through Lgr3 receptors in both the larval brain and PG (Hackney et al., 2012; Halme et al., 2010; Jaszczak et al., 2016).

To assess whether the changes we observe in wing disc epithelial barrier permeability are driven by ecdysone signaling, we first tested whether increasing ecdysone titer in larvae would reduce disc barrier permeability. To do this, we transferred 80h larvae to either food containing 0.6 mg/ml 20-hydroxyecdysone dissolved in ethanol, or food with ethanol alone as a control and assessed wing disc barrier function at 98h AED using our dextran infiltration assay. In previously published work we have seen that this concentration of 20-hydroxyecdysone can alter ecdysone titer, but does not substantially accelerate pupariation timing (Colombani et al., 2005; Jaszczak et al., 2015). When we assessed barrier activity in ecdysone-fed larvae, we see that wing disc permeability is substantially reduced when compared with wing discs from control larvae (Figure 2-13A; Figure 2-14), similar to what we observe in more mature (116h AED) wing discs (compare to Figure 2-1C). This result indicates that increasing ecdysone titers can promote the development of the restrictive barrier we see as the third larval instar progresses.

To determine whether ecdysone acts directly on the wing disc and is necessary for the change in barrier permeability, we assessed barrier function in wing discs expressing the dominant-negative ecdysone receptor allele *EcR.A^{W650A}* in wing discs using *Bx-Gal4*. In 92h AED discs, limiting ecdysone signaling produces little effect on barrier permeability (Figure 2-13B), demonstrating that the barrier function does not rely on ecdysone signaling at this earlier stage. However,

in 116h AED discs we see that blocking ecdysone signaling now produces a substantial increase in epithelial barrier permeability (Figure 2-13C). The expression of *EcR.A^{W650A}* at 116h AED does not produce the same degree of disruption in barrier function as expression of *kune^{RNAi}*, rather it produces barrier permeability similar to that seen in 92h AED discs (compare Figures 2-13B and 2-13C). These results demonstrate that ecdysone signaling in the wing disc is not necessary for barrier activity in 92h AED wing discs, but is required for the maturation of the more restrictive barrier during the third instar.

Since a re-localization of Cora from the lateral membrane to the apical site of the septate junction is associated with the change in barrier permeability, we wanted to determine if this change in Cora localization depends on ecdysone signaling in the wing disc. To do this, we examined the cellular localization of Cora in 116h AED control and *EcR.A^{W650A}* wing discs. Inhibition of ecdysone signaling in the wing disc produces a redistribution of Cora, from tightly localized to the apical lateral membrane, at the site of the septate junction, to a more uniform distribution along the lateral membrane (compare Figure 2-13D and Figure 2-13F; Actin staining Figure 2-15), similar to what is observed in earlier 92h AED discs (Figure 2-7D). This re-localization of Cora is consistent with how ecdysone affects the epithelial barrier, producing an increase in permeability that is similar to what is seen in 92h AED wing discs, but not completely disrupting the epithelial barrier (Figure 2-13A).

In summary, we see that the epithelial barrier activity of the wing disc at 92h AED is not dependent on ecdysone signaling, whereas the re-localization of Coracle to the site of the septate junction, along with the decreased permeability of the epithelial barrier, are both dependent on ecdysone signaling within the wing imaginal disc epithelium.

Figure 2-13. Ecdysone induces barrier maturation and Cora localization.

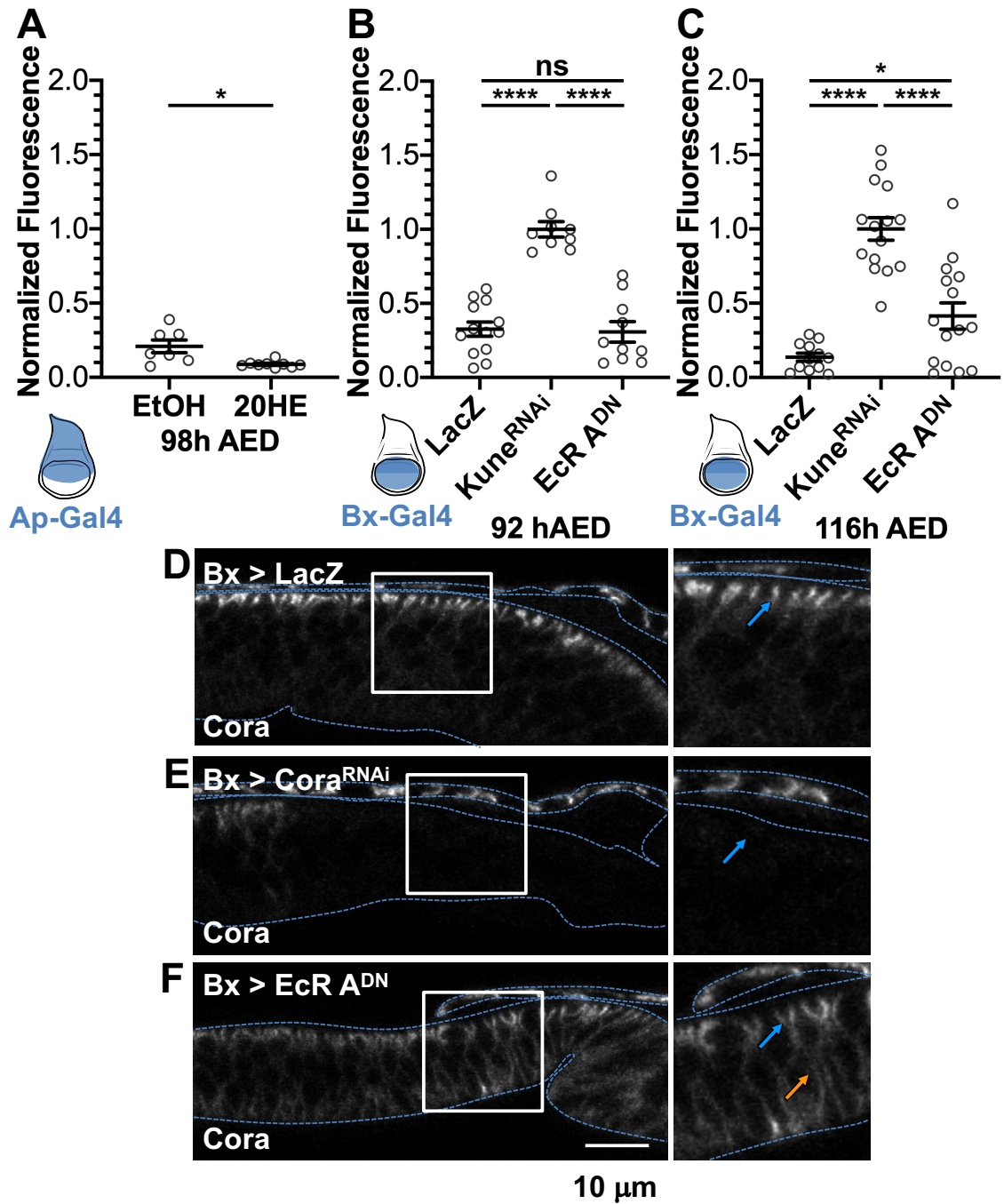


Figure 2-13. Ecdysone induces barrier maturation and Cora localization. (A) Function of the epithelial barrier at 98h AED in the wing imaginal discs of larvae that were switched to food containing ethanol control (EtOH) or 0.6 mg/mL 20-hydroxyecdysone (20HE) at 80h AED. Barrier function is normalized to *Ap* >

kune^{RNAi} expressing discs under the same feeding conditions (complete data in Figure 2-14). Expression area diagramed in blue. (B-C) Epithelial barrier function of *Bx > lacZ* (wild type control), *Bx > kune^{RNAi}*, and *Bx > EcR A^{DN}* at (B) 92h and (C) 116h AED. Barrier function is normalized to *Bx > kune^{RNAi}* expressing discs under the same feeding conditions. Expression area diagramed in blue. (D-F) Localization of Cora in (D) *bx > lacZ* (wild type control), (E) *bx > cora^{RNAi}*, and (F) *bx > EcR A^{DN}* at 116h AED. Dotted lines indicate tissue outline as defined by actin staining (rhodamine phalloidin; Figure 2-15). Tissues are oriented with the dorsal region of the pouch (higher level of Bx expression) on the right. White box indicates zoomed area to the right. Blue arrows indicate apical-lateral Cora localization (or lack thereof in *cora^{RNAi}*), orange arrow indicates medial-lateral localization. (A-C) Graphs represent mean \pm SEM, with individual points indicating values of single images. Left to right, n = (A) 7 and 9, (B) 13, 8, 10, and (C) 12, 15, 15. (A-C) ns not significant, * p < 0.05, **** p < 0.0001 as calculated by (A) Unpaired t-test with Welch's correction, (B) Ordinary one-way ANOVA with Tukey's multiple comparisons test, or (C) Brown-Forsythe and Welch ANOVA tests with Dunnett's T3 multiple comparisons test. (D-F) Images are representative of n = (D) 7, (E) 7, and (F) 5 images.

Figure 2-14. Ecdysone feeding induces barrier maturation early.

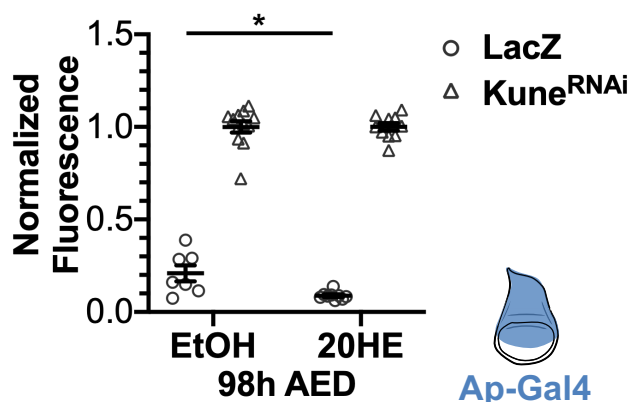


Figure 2-14. Ecdysone feeding induces barrier maturation early. Wing imaginal disc barrier function at 98h AED of larvae fed the EtOH or 20HE food.

Data are from larvae expressing *Ap > lacZ* (data in Figure 2-13A) or *Ap > kune^{RNAi}*. Expression area indicated in blue. Graph represents mean \pm SEM, with individual points indicating values of single images. Left to right, $n = 7, 12, 9, 10$. * $p < 0.05$ as calculated by unpaired t-test with Welch's correction.

Figure 2-15. Actin stain from discs in Figure 2-13.

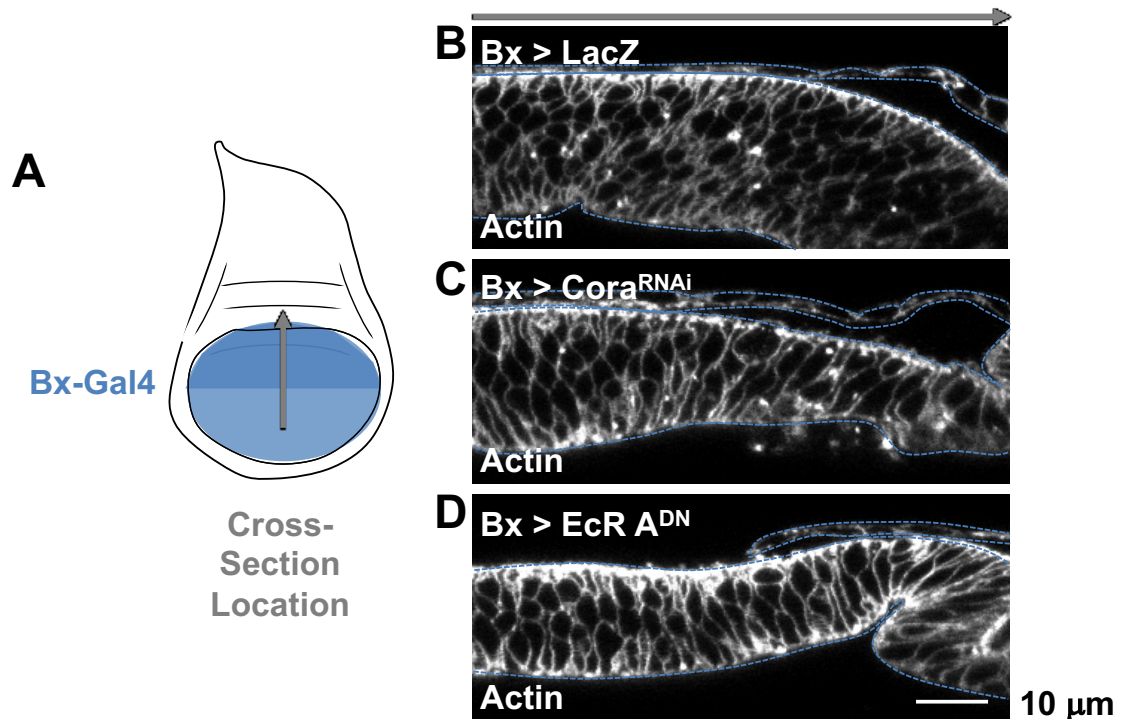


Figure 2-15. Actin stain from discs in Figure 2-13. (A) Approximate image location. Bx-Gal4 expression area (blue). Grey arrow indicates approximate image location and orientation and correlates with the grey arrow above B-D. (B-D) Localization of Actin (rhodamine phalloidin) in (B) *Bx > lacZ* (wild type control), (C) *Bx > kune^{RNAi}*, and (D) *Bx > EcR A^{DN}* at 116h AED. Dotted lines indicate tissue outline. Tissues are oriented with dorsal on the right. Images are from the same discs as Figure 2-13D-F.

2.2.6 The epithelial barrier regulates the end point of regeneration

Our data indicate that ecdysone regulates a maturation of the epithelial barrier and that the epithelial barrier limits Dilp8 signaling. This led us to question

whether the epithelial barrier determines the duration of the regenerative checkpoint. To test this, we targeted damage to the wing discs by using *Bx-Gal4* to express the TNF α homologue Eiger in the pouch of the wing disc (Igaki et al., 2002; Kauppila et al., 2003; Moreno et al., 2002), and examined the effects of barrier disruption on checkpoint duration. As previously observed, *kune*^{RNAi} expression alone produces only a minor effect on delay, whereas Eiger expression produces a substantial delay of 57 hrs. When we combine Eiger and *kune*^{RNAi} expression, we see a synergistic effect on delay that is significantly longer than the expected additive effect of *kune*^{RNAi} and Eiger expression alone (80 hours actual, 62 hours additive; Figure 2-16A). However, this additional delay is not due to increased Dilp8 expression (Figure 2-17). This is consistent with the epithelial barrier limiting Dilp8 signaling at the end of the regenerative checkpoint. We observed a similar result when the epithelial barrier is disrupted with *nrx*^{RNAi} (Figure 2-17; Figure 2-18).

Together, these results demonstrate that a fully-functional epithelial barrier limits the duration of damage-induced checkpoint delay, likely, through the sequestration of Dilp8 within the imaginal disc lumen.

Figure 2-16. The epithelial barrier regulates the end point of regeneration.

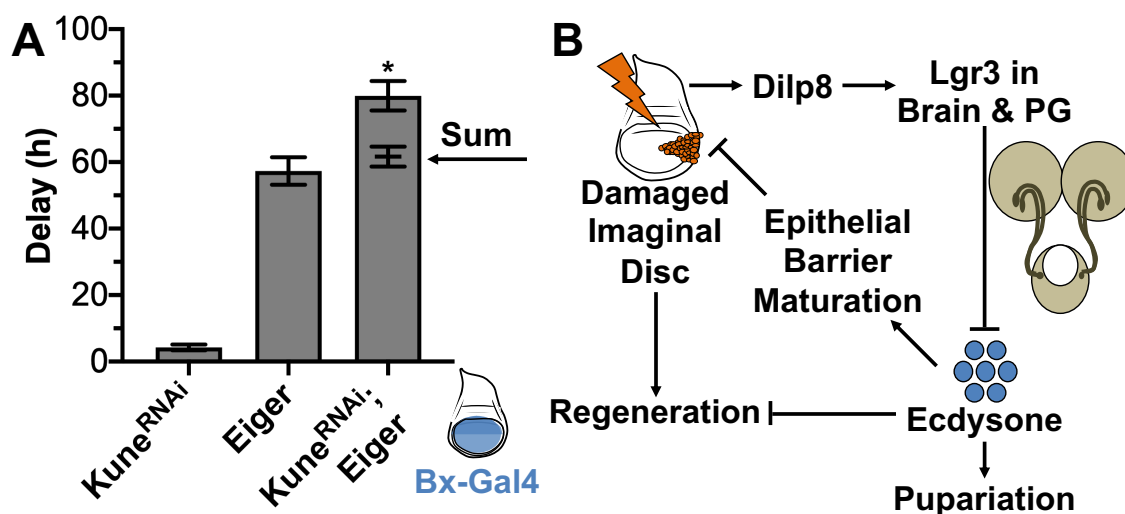


Figure 2-16. The epithelial barrier indirectly regulates the end point of regeneration by regulating the length of the regenerative period. (A) Expression of *kune*^{RNAi} in Eiger-damaged tissues induces synergistic delay. Data were collected from at least three independent experiments, bars represent mean \pm SEM, * $p < 0.05$ from one sample t-test comparing the additive value and observed delay. (B) Model. Following damage to the imaginal discs, regeneration is initiated and Dilp8 is produced in the damaged tissues and is secreted. Dilp8 functions on Lgr3 receptors in the brain and PG to inhibit ecdysone production, resulting in a delay to pupariation. In the late third instar, high levels of ecdysone inhibit regenerative ability and also induce the maturation of the epithelial barrier in imaginal discs. The epithelial barrier inhibits Dilp8 signaling and regulates the duration of the regeneration checkpoint in development. We hypothesize that the maturation of the epithelial barrier in regenerated tissues begins to limit Dilp8 release from the wing disc, and that this is the rate limiting step in ending regeneration checkpoint delay. In future studies, we would be interested in examining if and how barrier maturation in regenerating tissues differs from developing tissues.

Figure 2-17. Coexpression of Eiger and RNAi against septate junction components does not significantly alter measured Dilp8 expression.

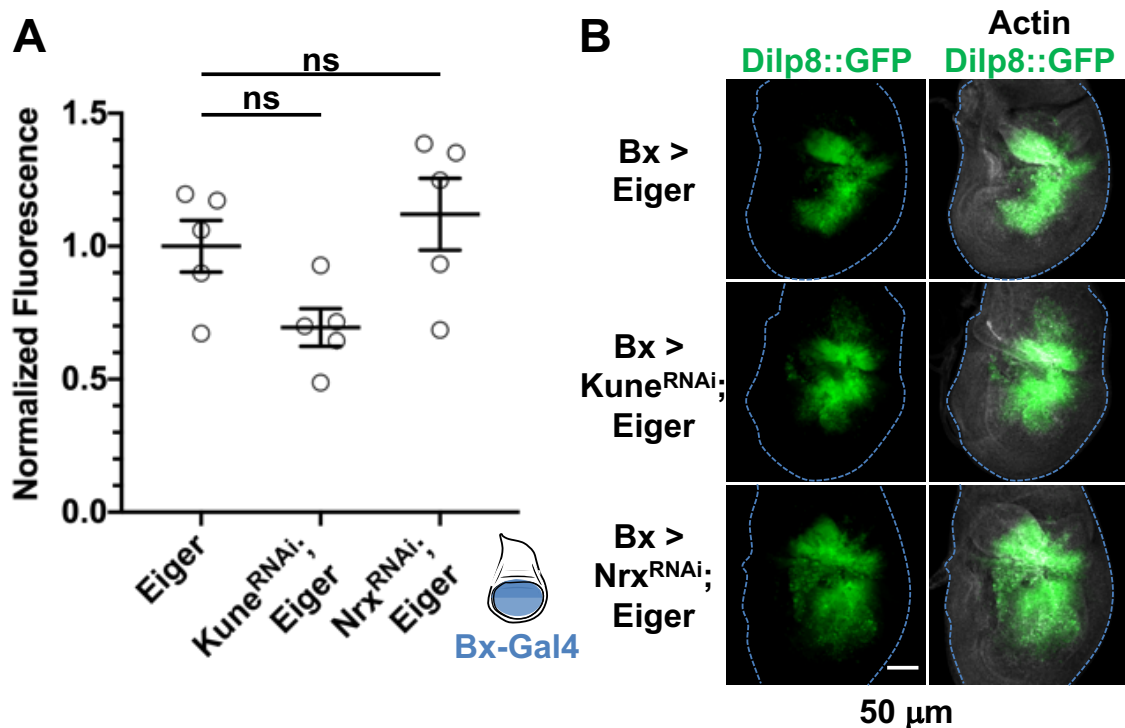


Figure 2-17. Coexpression of Eiger and RNAi against septate junction components does not significantly alter measured Dilp8 expression. Bx-Gal4 (expression area in blue) was used to express Eiger alone, with *kune^{RNAi}*, or with *nrX^{RNAi}* expressing a transcriptional reporter for Dilp8 (*Dilp8^{M100727/+}*; Garelli et al., 2012). (A) Sum GFP intensity was measured and the data were normalized to Eiger alone. (B) Representative images. Discs were collected at 104 hAED. Images represent sum-projected stacks of 5 images. Actin was stained for with rhodamine phalloidin. (A) Graph represents mean \pm SEM, with individual points indicating values of single images, $n = 5$ images in each condition; ns indicates $p > 0.05$ by one-way ANOVA with Tukey test for multiple comparisons.

Figure 2-18. Nr_x limits Eiger-induced delay.

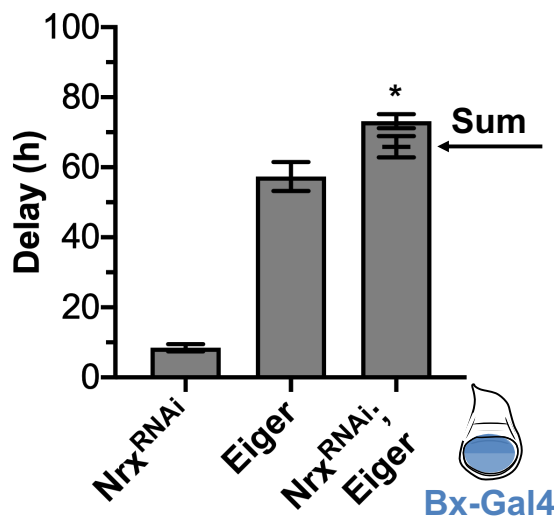


Figure 2-18. Nr_x limits Eiger-induced delay. Co-expression of *nr_x^{RNAi}* and Eiger produces synergistic delay. Ectopic expression of *nr_x^{RNAi}*, Eiger, and co-expression of *nr_x^{RNAi}* and Eiger (*nr_x^{RNAi}*; Eiger) induce developmental delay compared to LacZ controls when expressed in the wing imaginal disc under Bx-Gal4 (expression region in blue). The delay induced by co-expression of *nr_x^{RNAi}* and Eiger (*nr_x^{RNAi}*; Eiger) is significantly more than the sum of the delay induced by *nr_x^{RNAi}* and Eiger expressed alone (sum indicated by arrow. Data were collected from at least four independent experiments, bars represent mean \pm SEM, * $p < 0.01$ from one sample t-test comparing the additive value and observed delay.

2.3 Discussion

2.3.1 How is the end of regeneration determined?

Despite progress towards understanding the cues that initiate regeneration and the signaling pathways that contribute to regenerative growth and repatterning, the mechanisms for determining when the target of regeneration is reached remain poorly understood (Fox et al., 2020). Here, we demonstrate that the formation of a functional, mature epithelial barrier determines the duration of the regenerative period by regulating Dilp8 signaling. Since Dilp8 is seen in the imaginal disc lumen (Colombani et al., 2012; Figure 2-1), it seems likely that the

epithelial barrier limits Dilp8 signaling by physically sequestering Dilp8 protein in the lumen of the imaginal disc, separated from the hemolymph and from access to the prothoracic gland and the brain, where Dilp8 acts through Lgr3 to inhibit ecdysone production (Colombani et al., 2012; Colombani et al., 2015; Garelli et al., 2012; Garelli et al., 2015; Jaszczak et al., 2016). Therefore, we propose that as regeneration is completed, the balance between Dilp8 signaling and ecdysone signaling shifts to favor ecdysone signaling by the establishment of the mature, prepupal epithelial barrier which traps Dilp8 in the regenerated disc lumen. In this way, the re-establishment of a restrictive epithelial barrier would be one mechanism for epithelial tissues to communicate their functional restoration and the completion of regeneration (model, Figure 2-16B). Our current data do not indicate if the epithelial barrier had direct impacts on the ability of a tissue to regenerate, only that the barrier impacts the length of the regenerative period. We are interested in investigating the role of the barrier on regeneration signaling within the tissue in future studies.

2.3.2 Regulated maturation of the epithelial barrier

Our experiments also demonstrate that the function of the epithelial barrier changes during the third instar, growing more restrictive prior to pupariation in response to ecdysone. Although we were unable to determine the direct target of EcR that produces this change in barrier activity, we observe that ecdysone triggers the re-localization of Cora from a pattern of diffuse localization along the length of the lateral membrane to a specific localization at the septate junctions in the apical lateral membrane. This re-localization correlates with the establishment of a mature, restrictive epithelial barrier. This mechanism is similar to observations that Cora re-localizes to the septate junctions during the embryonic stages 12 and 17 in the developing salivary gland and embryonic epidermis, which is when the epithelial barrier is established in these tissues (Hall and Ward, 2016; Oshima and Fehon, 2011; Paul et al., 2003). Similar to the end of larval development, there is a peak of ecdysone production during this embryonic period and EcR is expressed

in both these maturing epithelia (Kozlova and Thummel, 2000; Kozlova and Thummel, 2003; Tan et al., 2014). This leads us to suggest that the regulation of Cora localization by ecdysone may be a general mechanism for the maturation of a restrictive barrier in developing *Drosophila* epithelia.

However, our examination of epithelial barrier maturation in the wing disc also raises some interesting, unanswered questions about the role of individual septate junction components, in particular, the role of the core components Cora and Kune in barrier function earlier in the third instar, at 92h AED. The barrier at this time is not as restrictive as is observed later, but still limits the passage of 10kDa dextran molecules (Figure 2-4B, compare Intact to Punctured). Kune is required for this early barrier activity but Cora is not necessary (Figure 2-10). However, when we block Cora expression with an RNAi, we see that Cora is necessary for the localization of both NrX and Kune at both 92h and 116h AED (Figure 2-11). This suggests that in Cora mutant tissues at 92h AED, the mis-localized Kune (and NrX) still retain some residual barrier activity, which is lost at 116h AED. One possible explanation is that a low level of NrX and Kune localization along the lateral membrane may remain in Cora mutant tissues, but was undetectable by our imaging. This low level of NrX and Kune localization may be sufficient to support early barrier activity in early discs, but not at the end of the third instar. Further study will be necessary to better understand how each of these core components contribute to the barrier as the wing disc matures.

2.3.3 Could other signaling pathways be regulated by epithelial barrier maturation?

Our observation that Dilp8 is constrained by the wing disc epithelial barrier raises the question of whether other signals are regulated by sequestration in the imaginal disc lumen. One interesting possibility is the morphogen Decapentaplegic (Dpp, *Drosophila* BMP2/4 ortholog). Dpp has numerous, critical roles in growth and patterning across development, including in imaginal discs (Hamaratoglu et al., 2014). Setiawan et al. showed that during larval development, Dpp produced in the imaginal tissues inhibits ecdysone production in the prothoracic gland early in

the third larval instar. By the late third instar, Dpp can no longer be detected in the larval hemolymph and the Dpp activity in the prothoracic gland ceases, despite high levels of Dpp expression in imaginal discs. Setiawan et al. hypothesized that this was due in part to the dilution of circulating Dpp as a result of increased hemolymph volume and the trapping of Dpp in imaginal disc tissues, but were unable to identify how the tissues trapped Dpp (Setiawan et al., 2018). Our data suggest that Dpp might be trapped in late third instar discs by the maturing epithelial barrier. Further experiments will be necessary to test this hypothesis.

In summary, our data demonstrate that in *Drosophila*, ecdysone signaling alters the permeability of the wing disc epithelial barrier during the third and final larval instar. We also show that a mature, restrictive wing disc epithelial barrier limits Dilp8 signaling, determining the duration of the regenerative checkpoint. This provides an interesting mechanism by which the barrier, as a primary characteristic of epithelial tissues, can report the successful completion of regeneration.

2.4 Materials and Methods

2.4.1 Drosophila stocks and husbandry

The fly stocks used were, or were generated from crosses with, Ap-Gal4; UAS-LacZ.NZ, UAS-Dcr2/ SM6-TM6B (derived from Bloomington 3041), Bx-Gal4, UAS-Dcr2 (Dr. David Bilder), UAS-LacZ.NZ (Bloomington 3955), UAS-Kune[RNAi] (VDRC GD3962), UAS-NrxIV[RNAi] (VDRC GD8353), UAS-Sinu[RNAi] (VDRC GD44928), UAS-Cora[RNAi] (Bloomington 51845), UAS-EcR.A.W650A (Bloomington 9451), NrxIV-GFP (Bloomington 50798), UAS-eiger, UAS-Dilp8::3xFLAG (Dr. Maria Dominguez) (Garelli et al., 2012), and Dilp8::GFP (Bloomington 33079).

Stocks and crosses were maintained in 25°C incubators with a 12-hour alternating light-dark cycle. Developmental timing was synchronized through egg staging, with collection from a 4-hour egg-laying interval on grape agar plates (Genesee Scientific) with a small amount of baker's yeast paste. At 24h AED, 20-30 first instar larvae were transferred into vials containing cornmeal-yeast-

molasses media (Archon Scientific B101). Ecdysone food was prepared by dissolving 1.2 mg 20-hydroxyecdysone (Sigma) dissolved in 95% ethanol in 2 mL of food media (final concentration 0.6 mg/mL), or an equivalent volume of ethanol for control. Larvae were reared as previously described until 80h AED then transferred to the ecdysone or ethanol-control food, approximately 6 larvae per vial (Halme et al., 2010).

For specific genotypes used in each Figure see 2.4.7.

2.4.2 Pupariation time and developmental delay

Larvae were raised as described. For calculating purposes 0h AED was considered to be the middle of the egg laying interval. The number of pupae in each vial were counted approximately every 12 hours starting around 104h AED and ending 2 days after the most recent pupation. To simplify calculations, data were pooled from multiple vials of the same genotype that were laid on the same day. Data from separate lays were calculated separately, at least three lays are represented in each experiment. Median pupariation time was then calculated (Equation 1). Developmental delay was considered to be the difference between in pupariation time between the experimental and control groups.

Equation 2-1. Median pupariation time calculation.

$$Median = T1 + ((T2 - T1) * \frac{0.5 - S1}{S2 - S1})$$

Equation 2-1. Median pupariation time calculation. Median pupariation time was calculated by first determining the sum fraction of total pupae counted at each timepoint for each genotype. The first timepoint to have sum fraction of total pupae exceeding 50% indicates that the median pupariation time occurred between that timepoint and the preceding timepoint. We next calculated how long past the preceding timepoint 50% of larvae pupated as well as the difference between the sum fractions. To determine how far past the first timepoint the median pupariation time was, we divided the difference from the halfway point by the difference between the sum fractions then multiplied this to by the difference between the

timepoints. We then added this number to the preceding timepoint. T2 indicates the later timepoint, T1 indicates the earlier timepoint, S2 indicates the sum fraction of pupae at T2, S1 indicates the sum fraction of pupae at T1.

2.4.3 Dissection and immunofluorescent staining

Larvae were inverted and cleaned in PBS then fixed with 4% paraformaldehyde in PBS (20 min) and washed with PBS (twice for 5 min each). The tissues were permeabilized with 0.3% Triton in PBS (twice for 10 min each) then washed with a blocking solution of 10% goat and 0.1% Triton in PBS (30 min). Then the tissues were incubated rocking in primary antibody solutions (overnight at 4°C or for two-to-four hours at room temperature). The process was repeated for secondary antibodies and then the tissues were incubated rocking in 80% glycerol in PBS (overnight at 4°C). The tissues were stored at 4°C in 80% glycerol and were mounted for imaging within one week of staining. Imaginal discs were isolated from the stained tissues and mounted on glass slides with Vectashield (Vector Laboratories). Cross-section images were taken from tissues mounted on slides with the coverslips raised by double-sided tape. For experiments with Kune or FLAG staining, the above procedure modified to reduce non-specific staining. In these experiments, larvae were dissected in Schneider's Insect Medium (Sigma-Aldrich), fixed in 4% paraformaldehyde in Schneider's Insect Medium (Sigma-Aldrich), stained in one day within three days of dissection, and imaged within three days of staining.

Antibody solutions were prepared in 10% goat serum and 0.1% Triton in PBS. The primary antibodies that were used are mouse β -Gal (1:250; Promega), mouse anti-Cora C615.16 (1:400; Developmental Studies Hybridoma Bank), mouse anti-FLAG M2 F1804 (1:250; Sigma-Aldrich), rabbit β -Gal (1:400; MP), and rabbit anti-Kune (1:1000; Dr. Mikio Furuse; Nelson et al., 2010). The secondary antibodies that were used are goat anti-mouse or anti-rabbit Alexa405, Alexa488, or Alexa633 (1:1000; ThermoFisher). F-actin was identified by Rhodamine-

conjugated Phalloidin (1:100; ThermoFisher) staining that was performed concurrently with secondary antibody incubations.

2.4.4 Imaging and statistical analysis

Confocal imaging was done using an Olympus FluoView 1000 (Figures 2-3, 2-4AB, 2-5, 2-7FIL, 2-13BCDEF, 2-15) within the University of Virginia Department of Cell Biology or a Zeiss LSM 700 (Figures 2-1, 2-4C, 2-6, 2-7, 2-8, 2-9, 2-10, 2-11, 2-12, 2-13ABC, 2-14, 2-18) in the University of Virginia Advanced Microscopy Facility (RRID:SCR_018736). Laser power and gain settings for each set of stained samples were based on the experimental group with the highest fluorescence intensity in each channel, and kept constant within the experiment. To compare between independently repeated experiments, we normalized within the experiment as indicated. Images were processed and quantified with Fiji/ImageJ (Schindelin et al., 2012).

Prism 8 software was used for Statistical Analysis. The specific tests that were used are listed in the figure descriptions.

2.4.5 Dextran assay

Larvae were inverted and cleaned in Schneider's Insect Medium (Sigma-Aldrich) then transferred into a 1:8 dilution of 10 kDa fluorescein conjugated dextran (Invitrogen) in Schneider's Insect Medium (Sigma-Aldrich) and incubated rocking and covered at room temperature for 30 minutes. The tissues were washed briefly (approximately 1 minute) in Schneider's Insect Medium (Sigma-Aldrich) to remove excess dextran, then fixed with 4% paraformaldehyde in Schneider's Insect Media. Tissues were washed, stained, and imaged as previously described.

Fluorescent dextran infiltration was measured using Fiji/ImageJ (Schindelin et al., 2012), taking the mean intensity along a line in the imaginal disc lumen (identified by rhodamine phalloidin or Cora staining) and subtracting background from outside the disc area. Discs that appeared punctured were either not measured or categorized separately from intact discs. The fluorescence intensity

varies with each experiment, so the data were normalized to the mean from controls that were incubated simultaneously.

2.4.6 Quantification of septate junction component localization

Septate junction localization was quantified using Fiji/ImageJ (Schindelin et al., 2012). Two lines were drawn to collect fluorescence intensity of the junctions. The first across the apical surface of cells near the center of where the septate junctions were localized, and the second along the middle of the cells. Junctional intensity, or membrane intensity for the medial region, was considered as an average of the 7 pixels surrounding local maxima. In this way we hoped to average out misrepresentations in the data that arose from slices that cut through cells approximately parallel to the cell membranes and from slices that cut through tricellular junctions and had more protein from the third cell. None of the proteins we looked at are reported or appeared to have specific tricellular activity. We then took the ratio of the average junctional peak intensity to the average medial peak intensity (Figure 2-9).

Peak identification was adjusted in three steps to reduce false identification of a membrane peak due to the noise within an image, especially with regards to Anti-Kune and Anti-Cora staining. First, to ensure the peak wasn't a result of a slightly brighter random pixel, we removed peaks that were below the median fluorescence of the entire line. Second, to ensure the identified peak was localized at the membrane, we removed points of Anti-Kune and Anti-Cora staining that did not have a Nr_x::GFP peak within the same 7-pixel range. We used Nr_x::GFP instead of Actin (Rhodamine Phalloidin) staining for this because Nr_x::GFP has extremely low noise as it is a membrane bound GFP produced within the cell and does not need to be stained for. Nr_x::GFP also has a very high association with the membrane even away from canonical apical-lateral staining, while this fluorescence is very dim, it is still detectable and highly correlated with the membrane. Finally, to ensure that we took a measurement at the membrane and not at a noisy region within the cell, if no Anti-Kune or Anti-Cora peak was identified

within the 7-pixel range of the Nr_x::GFP peak, a measurement was added at the same placement of the Nr_x::GFP peak. Together these adjustments reduced the number of peak identifications in each image by approximately 1-10 junctions depending on the stain (most images had 40-60 junctions following adjustments).

2.4.7 Genotypes

Figure 2-2A

Bx-Gal4 / + ; UAS-Dcr2 / + ; UAS-LacZ.NZ / +

Bx-Gal4 / + ; UAS-Dcr2 / UAS-Kune^{RNAi}

Bx-Gal4 / + ; UAS-Dcr2 / + ; UAS-Dilp8::3xFLAG / +

Bx-Gal4 / + ; UAS-Dcr2 / UAS-Kune^{RNAi} ; UAS-Dilp8::3xFLAG / +

Figure 2-2B

Bx-Gal4 / + ; UAS-Dcr2 / + ; Dilp8^{MI00727} / Dilp8^{MI00727}

Bx-Gal4 / + ; UAS-Dcr2 / UAS-Kune^{RNAi} ; Dilp8^{MI00727} / Dilp8^{MI00727}

Bx-Gal4 / + ; UAS-Dcr2 / + ; UAS-Dilp8::3xFLAG , Dilp8^{MI00727} / Dilp8^{MI00727}

Bx-Gal4 / + ; UAS-Dcr2 / UAS-Kune^{RNAi} ; UAS-Dilp8::3xFLAG , Dilp8^{MI00727}
/ Dilp8^{MI00727}

Figure 2-4

Ap-Gal4 / + ; UAS-Dcr2 , UAS-LacZ.NZ / UAS-LacZ.NZ

Ap-Gal4 / UAS-Kune^{RNAi} ; UAS-Dcr2 , UAS-LacZ.NZ / +

Figure 2-7

NrxIV-GFP / Nr_xIV-GFP

Figure 2-10

Ap-Gal4 / + ; UAS-Dcr2 , UAS-LacZ.NZ / UAS-LacZ.NZ

Ap-Gal4 / UAS-Kune^{RNAi} ; UAS-Dcr2 , UAS-LacZ.NZ / +

Ap-Gal4 / UAS-Cora^{RNAi} ; UAS-Dcr2 , UAS-LacZ.NZ / +

Figure 2-11A,B

Ap-Gal4 / UAS-Kune^{RNAi} ; UAS-Dcr2 , UAS-LacZ.NZ / Nr_xIV-GFP

Figure 2-11C,D

Ap-Gal4 / UAS-Nrx^{RNAi} ; UAS-Dcr2 , UAS-LacZ.NZ / Nr_xIV-GFP

Figure 2-11E,F

Ap-Gal4 / UAS-Cora^{RNAi} ; UAS-Dcr2 , UAS-LacZ.NZ / NrxF-GFP

Figure 2-13A

Ap-Gal4 / + ; UAS-Dcr2 , UAS-LacZ.NZ / UAS-LacZ.NZ

Ap-Gal4 / UAS-Kune^{RNAi} ; UAS-Dcr2 , UAS-LacZ.NZ / +

Figure 2-13B,C

Bx-Gal4 / + ; UAS-Dcr2 / + ; UAS-LacZ.NZ / +

Bx-Gal4 / + ; UAS-Dcr2 / UAS-Kune^{RNAi}

Bx-Gal4 / + ; UAS-Dcr2 / UAS-EcR.A^{W650A}

Figure 2-13D

Bx-Gal4 / + ; UAS-Dcr2 / + ; UAS-LacZ.NZ / +

Figure 2-13D

Bx-Gal4 / + ; UAS-Dcr2 / UAS-Cora^{RNAi}

Figure 2-13D

Bx-Gal4 / + ; UAS-Dcr2 / UAS-EcR.A^{W650A}

Figure 2-16A

Bx-Gal4 / + ; UAS-Dcr2 / + ; UAS-LacZ.NZ / +

Bx-Gal4 / + ; UAS-Dcr2 / UAS-Kune^{RNAi}

Bx-Gal4 / + ; UAS-Dcr2 / + ; UAS-Eiger / +

Bx-Gal4 / + ; UAS-Dcr2 / UAS-Kune^{RNAi} ; UAS-Eiger / +

Figure 2-1A,C

Ap-Gal4 / + ; UAS-Dcr2 , UAS-LacZ.NZ / UAS-LacZ.NZ

Figure 2-1B,C

Ap-Gal4 / + ; UAS-Dcr2 , UAS-LacZ.NZ / UAS-Dilp8::3xFLAG

Figure 2-2A

Bx-Gal4 / + ; UAS-Dcr2 / + ; UAS-LacZ.NZ / +

Bx-Gal4 / + ; UAS-Dcr2 / UAS-Nrx^{RNAi}

Bx-Gal4 / + ; UAS-Dcr2 / + ; UAS-Dilp8::3xFLAG / +

Bx-Gal4 / + ; UAS-Dcr2 / UAS-Nrx^{RNAi} ; UAS-Dilp8::3xFLAG / +

Figure 2-2B

Bx-Gal4 / + ; UAS-Dcr2 / + ; Dilp8^{MI00727} / Dilp8^{MI00727}

Bx-Gal4 / + ; UAS-Dcr2 / UAS-Nrx^{RNAi} ; Dilp8^{MI00727} / Dilp8^{MI00727}

Bx-Gal4 / + ; UAS-Dcr2 / + ; UAS-Dilp8::3xFLAG , Dilp8^{MI00727} / Dilp8^{MI00727}

Bx-Gal4 / + ; UAS-Dcr2 / UAS-Nrx^{RNAi} ; UAS-Dilp8::3xFLAG , Dilp8^{MI00727} / Dilp8^{MI00727}

Figure 2-3B

Ap-Gal4 / + ; UAS-Dcr2 , UAS-LacZ.NZ / UAS-LacZ.NZ

Ap-Gal4 / UAS-Kune^{RNAi} ; UAS-Dcr2 , UAS-LacZ.NZ / +

Figure 2-5

Ap-Gal4 / + ; UAS-Dcr2 , UAS-LacZ.NZ / UAS-LacZ.NZ

Ap-Gal4 / UAS-Kune^{RNAi} ; UAS-Dcr2 , UAS-LacZ.NZ / +

Figure 2-6

Ap-Gal4 / + ; UAS-Dcr2 , UAS-LacZ.NZ / UAS-LacZ.NZ

Ap-Gal4 / UAS-Kune^{RNAi} ; UAS-Dcr2 , UAS-LacZ.NZ / +

Figure 2-8

NrxIV-GFP / NrxIV-GFP

Figure 2-9

NrxIV-GFP / NrxIV-GFP

Figure 2-11B,C

Ap-Gal4 / UAS-Kune^{RNAi} ; UAS-Dcr2 , UAS-LacZ.NZ / NrxIV-GFP

Figure 2-11D,E

Ap-Gal4 / UAS-Nrx^{RNAi} ; UAS-Dcr2 , UAS-LacZ.NZ / NrxIV-GFP

Figure 2-11F,G

Ap-Gal4 / UAS-Cora^{RNAi} ; UAS-Dcr2 , UAS-LacZ.NZ / NrxIV-GFP

Figure 2-14B

Ap-Gal4 / + ; UAS-Dcr2 , UAS-LacZ.NZ / UAS-LacZ.NZ

Ap-Gal4 / UAS-Kune^{RNAi} ; UAS-Dcr2 , UAS-LacZ.NZ / +

Figure 2-15B

Bx-Gal4 / + ; UAS-Dcr2 / + ; UAS-LacZ.NZ / +

Figure 2-15C

Bx-Gal4 / + ; UAS-Dcr2 / UAS-Cora^{RNAi}

Figure 2-15D

Bx-Gal4 / + ; UAS-Dcr2 / UAS-EcR.A^{W650A}

Figure 2-17

Bx-Gal4 / + ; UAS-Dcr2 / + ; UAS-Eiger / Dilp8^{MI00727}

Bx-Gal4 / + ; UAS-Dcr2 / UAS-Kune^{RNAi} ; UAS-Eiger / Dilp8^{MI00727}

Bx-Gal4 / + ; UAS-Dcr2 / UAS-Nrx^{RNAi} ; UAS-Eiger / Dilp8^{MI00727}

Figure 2-18

Bx-Gal4 / + ; UAS-Dcr2 / + ; UAS-LacZ.NZ / +

Bx-Gal4 / + ; UAS-Dcr2 / UAS-Nrx^{RNAi}

Bx-Gal4 / + ; UAS-Dcr2 / + ; UAS-Eiger / +

Bx-Gal4 / + ; UAS-Dcr2 / UAS-Nrx^{RNAi} ; UAS-Eiger / +

Appendix

Investigating epithelial barrier maturation and recovery during tissue regeneration.

Abstract

The epithelial barrier in *Drosophila* wing imaginal discs grows more restrictive during the third instar in response to ecdysone signaling. This maturation of the epithelial barrier limits the regenerative delay that results from Dilp8 signaling. Based on these data, I hypothesized that if the barrier is disrupted following damage, the recovery of the mature and more restrictive barrier usually found at the end of larval development could trap Dilp8 to communicate the completion of regeneration. Here I demonstrate that damage induced by X-irradiation does indeed disrupt the epithelial barrier. Preliminary data indicate that the barrier likely recovers prior to pupariation, but that the timeframe of recovery is dependent on when the tissues were damaged. When larvae were damaged prior to regeneration restriction, the barrier was disrupted and stayed disrupted for over 36 hours, only beginning to recover at the last timepoint I collected. When larvae were damaged after regeneration restriction, barrier function was restored within 24 hours of damage. To begin to understand the differences between these recovery dynamics, I looked at the localization of two septate junction core complex components, Neurexin-IV and Coracle, following damage. Both were depleted at the septate junctions following X-irradiation before regeneration restriction. The re-localization of Neurexin-IV and Coracle at the septate junctions correlates with my preliminary observation of the restoration of barrier function. In contrast, in larvae irradiated after regeneration restriction, Neurexin-IV and Coracle were not depleted even when the barrier was disrupted. Together these data preliminarily indicate that the localization of the septate junction components are likely regulated during regeneration.

α.1 Introduction

In *Drosophila*, damage to the imaginal tissues, the larval precursors to adult organs, induces the expression and secretion of *Drosophila* insulin-like peptide 8 (Dilp8) (Colombani et al., 2012; Garelli et al., 2012). Dilp8 functions in the brain and prothoracic gland (PG) to inhibit the production of the steroid hormone ecdysone (Colombani et al., 2015; Garelli et al., 2015; Jaszczak et al., 2016; Vallejo et al., 2015). High levels of ecdysone at the end of the larval period initiates changes and cause the transition to pupal development. Consequently, the inhibition of ecdysone by Dilp8 extends the larval developmental period (Colombani et al., 2012; Garelli et al., 2012). This developmental delay provides more time for the damaged tissues to regenerate (Jaszczak et al., 2015; Smith-Bolton et al., 2009). Among the changes ecdysone initiates before pupariation is the loss of regenerative ability, which functions as a developmental checkpoint (regeneration restriction checkpoint) (Halme et al., 2010).

In Chapter 2, I showed that another change that ecdysone initiates in imaginal tissues is the maturation of the epithelial barrier. The epithelial barrier is a semi-permeable diffusion barrier that is formed in *Drosophila* by septate junctions between adjacent epithelial cells (Izumi and Furuse, 2014). The restriction of barrier permeability results from ecdysone induced localization of Coracle (Cora) (Lamb et al., 1998) to the septate junctions. Before barrier restriction, Cora is diffusely localized along the apical-lateral surface of the cells. I found that the timing of barrier maturation correlates with the timing of regeneration restriction. Additionally, I found that the mature barrier could serve as a mechanism for communicating the completion of regenerative growth by restricting Dilp8 signaling. I proposed that the epithelial barrier may be disrupted following damage to the imaginal discs and as the tissues regenerates the barrier re-forms and grows to be capable to sequestering Dilp8 in the imaginal disc lumen. If this hypothesis is correct, then it is likely that the development of prepupal barrier, which is the more mature and restrictive barrier that limits Dilp8, would be highly regulated during the regenerative response.

Here I describe preliminary results that indicate that 1) the barrier is indeed disrupted following damage, regardless of whether damage occurs before or after regeneration restriction; 2) following damage before regeneration restriction, the barrier and its components are downregulated while regeneration is occurring, only recovering towards the end of the regenerative period; and 3) following damage after regeneration restriction, the components are not downregulated, and the barrier functionality recovers more rapidly.

α .2 Results

α .2.1 The epithelial barrier is disrupted following damage and may be restored prior to pupariation

In Chapter 2, I described how the epithelial barrier regulates Dilp8 signaling to communicate the completion of regeneration. I hypothesized a model in which damaged tissues produce Dilp8 to limit ecdysone production in the brain and PG, but once the tissue regenerates the epithelial barrier matures and limits Dilp8. It is unclear if damage disrupts the barrier to facilitate Dilp8 release thereby prolonging regeneration, if the maturation of the barrier is delayed in response to the delay of ecdysone signaling, or if both of these scenarios occur. To first determine if the epithelial barrier is disrupted following damage, I used X-irradiation to damage the larvae, then observed the functionality of the barrier. I modified an assay for epithelial barrier function previously used by Lamb et al. 1998 in embryonic tissues (Lamb et al., 1998). The modified assay assessed the ability of a 10 kDa fluorescein-conjugated dextran to enter the lumen of wing imaginal discs to determine the functionality of the barrier (see Materials and Methods for more details). The experiment had a small sample size, so results should be considered preliminary.

I first collected data on the activity of the epithelial barrier in wing imaginal discs of unirradiated larvae. At 92 hours after egg deposition (h AED), the barrier was permeable to 10 kDa dextran (Figure α -1A), but was more restrictive than a disc punctured during dissection (Figure α -3A). This indicates that the barrier is

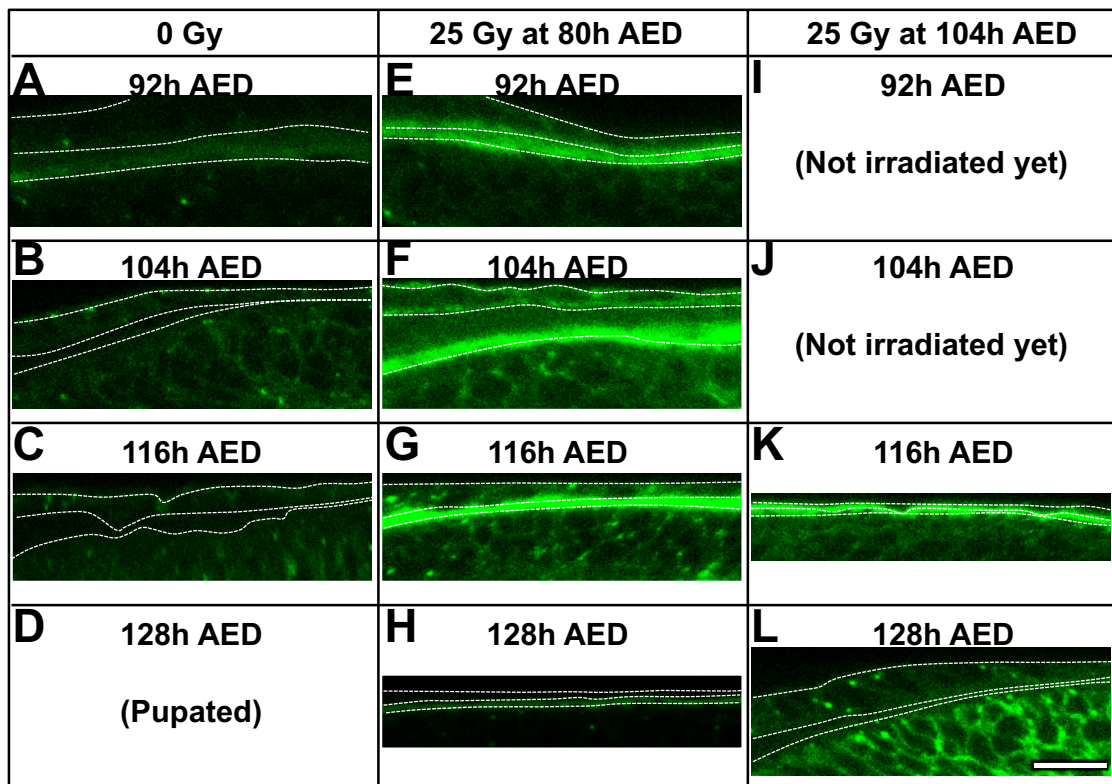
established before 92h AED. At 104h and 116h AED, little to no dextran is detected in the imaginal disc lumen (Figure α -1B,C). These data are consistent with my Chapter 2 conclusion that the barrier becomes more restrictive over time. In Chapter 2, I showed that the 104h AED barrier is more restrictive than the 92h AED barrier, but less restrictive than the 116h AED barrier. The lack of distinction here between the 104h and 116h AED barrier may result from the small sample size of the experiment.

Following damage by X-irradiation before regeneration restriction (25 Gy at 80h AED), barrier activity is disrupted and does not begin to recover until 128h AED, the last timepoint collected (Figure α -1E-H). At 92h AED, 12 hours after damage, the barrier is significantly more permeable to 10 kDa dextran than unirradiated controls, at a level comparable to a disc that was punctured during dissection (compare Figures α -1E and α -3B). The barrier remains highly permeable for at least 36 hours (Figures α -1F,G). At 128h AED, 48 hours after damage and the last timepoint collected in this timecourse, the barrier was permeable to dextran, but was more restrictive than the damaged barrier between 92h and 116h AED or a barrier disrupted by puncturing (compare Figures α -1H, α -1E-G, and α -3C). The level of permeability is similar to the unirradiated 92h AED barrier (compare Figures α -1H and α -1A). Together, these data preliminarily indicate that the activity of the epithelial barrier is disrupted following damage. The data also preliminarily indicate that some functionality may be restored after regenerative growth and before pupariation.

Although these data indicate that barrier activity is disrupted following damage, they do not differentiate between disruption resulting from signaling or morphological changes in tissue, and disruption as a characteristic of regeneration or damage. To distinguish between these possibilities, I observed the functionality of the barrier following X-irradiation (25 Gy) around the time that regeneration is restricted (at 104h AED). Larvae damaged at 104h AED do not regenerate tissue damage, but still undergo slight developmental delay, although less than larvae damaged earlier in development (Halme et al., 2010). At 116h AED, 12 hours after

irradiation, the barrier is permeable to 10 kDa dextran (Figure α -1K). This permeability after irradiation at 104h AED was comparable to the permeability after irradiation at 80h AED (compare Figure α -1K and α -1E-G). At 128h AED, 24 hours after irradiation, the epithelial barrier was impermeable to the dextran, comparable to undamaged controls at 116h AED (compare Figure α -1L to α -1C). These data demonstrate that damage can disrupt the barrier. The data also preliminarily suggest that the barrier may develop or re-develop to exclude dextran even in non-regenerating tissues. However, these data do not indicate how the barrier is disrupted or indicate what aspect of damage or regeneration induces barrier disruption. The data also do not explain why damage-induced barrier disruption in regenerating tissues lasts so much longer than the barrier disruption in damaged, but non-regenerative tissues.

Figure α -1. Damage disrupts the epithelial barrier, but it may recover before pupariation.



10 μ m

Figure α -1. Damage disrupts the epithelial barrier, but it may recover before pupariation. Data are from preliminary experiments using 10 kDa dextran (green) to measure epithelial barrier function following damage. The epithelial barrier of wing imaginal discs was tracked every 12 hours or until pupation (92h, 104h, 116h, and 128h AED) in larvae that were damaged with X-irradiation at (A-D) 0 Gy (control), (E-H) 25 Gy at 80h AED, or (I-L) 25 Gy at 104h AED. White dotted lines indicate tissue outlines as defined by Actin (Rhodamine Phalloidin; Figure α -2). (A-D) The epithelial barrier grows more restrictive over the third instar. (A) At 92h AED, the epithelial barrier is permeable to 10 kDa dextran, but less so than a disrupted disc (Figure α -3A) or the damaged discs. (B-C) At 104h and 116h AED, 10 kDa dextran is not observed in the imaginal disc lumen. (D) Unirradiated larvae pupate before 128h AED. (E-H) The epithelial barrier is disrupted by damage before regeneration restriction (25 Gy at 80h AED) and remains disrupted for a prolonged period of time. (E-G) At 92h, 104h, and 116h AED the epithelial barrier is permeable to 10 kDa dextran at a level similar to a disrupted disc (Figure α -3B). (H) At 128h AED, 48 hours after damage, the epithelial barrier is permeable to 10 kDa dextran. However, the barrier is more restrictive to the 10 kDa dextran than earlier timepoints or punctured discs (Figure α -3C). The barrier is similar to the 92h AED undamaged larvae (A). No discs were collected after 128h AED. (I-J) The epithelial barrier is disrupted by damage after regeneration restriction (25 Gy at 104h AED), but recovers rapidly. (I-J) Larvae were not irradiated until 104h AED. (K) At 116h AED, 12 hours after damage, the epithelial barrier is permeable to 10 kDa dextran at a level similar to a disrupted disc (Figure α -3). (L) At 128h AED, 24 hours after damage, the epithelial barrier is restrictive to the 10 kDa dextran, similar to 116h AED unirradiated larvae. Data are from one experiment in w^{1118} larvae with $n =$ (A) 3, (B) 3, (C) 1, (E) 3, (F) 2, (G) 2, (H) 1, (K) 6, and (L) 1 images. Punctured discs in Figure α -3 are from this same experiment, but punctured discs are not counted among the n of this experiment. Cora images in Figure α -4 are also from this experiment.

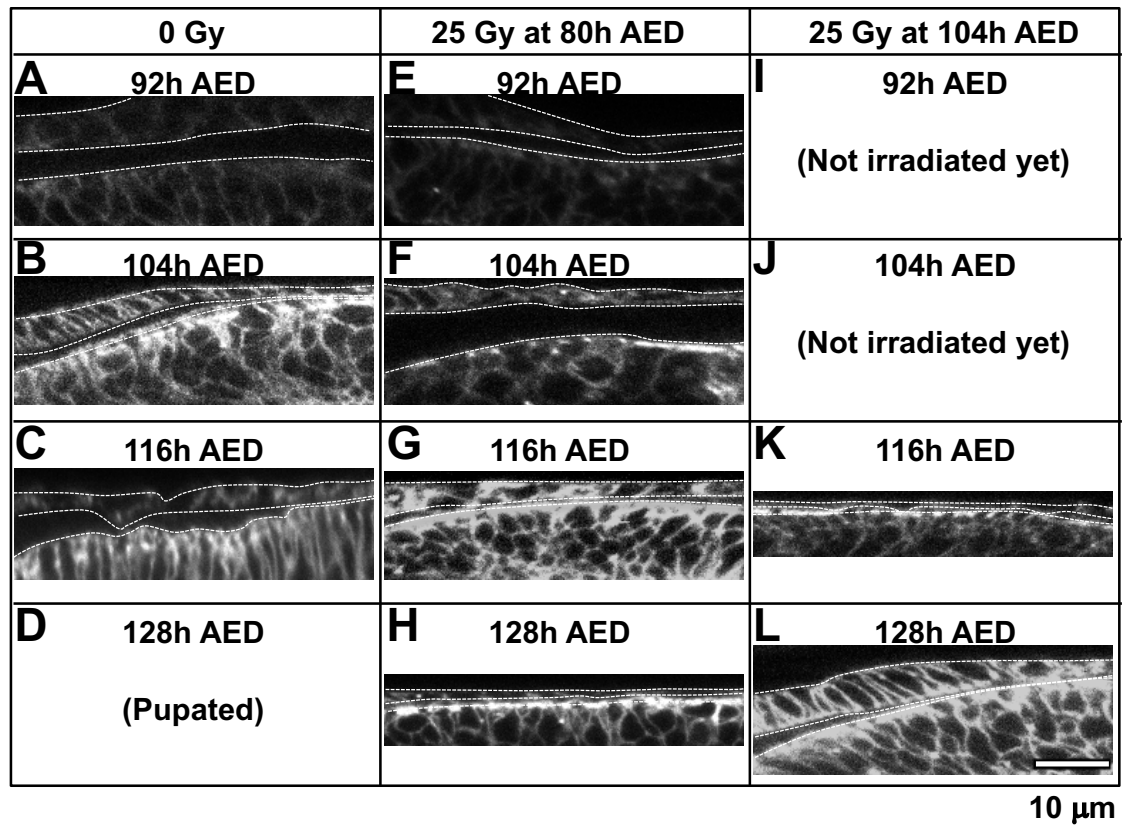
Figure α -2. Actin stain from discs in Figure α -1.

Figure α -2. Actin stain from discs in Figure α -1. Localization of Actin (rhodamine phalloidin) in the discs of Figure α -1 that was used to define the tissue outline (white dotted lines). Larvae were damaged with X-irradiation at (A-D) 0 Gy (control), (E-H) 25 Gy at 80h AED, or (I-L) 25 Gy at 104h AED.

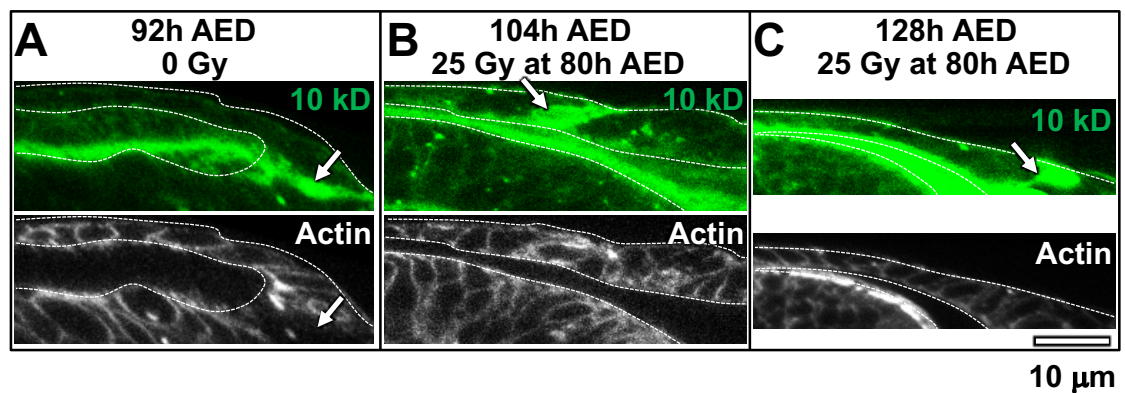
Figure α -3. Epithelial barrier of punctured imaginal discs.

Figure α -3. Epithelial barrier of punctured imaginal discs. Barrier function as defined by 10 kDa assay of wing imaginal discs of discs punctured during dissection. Larvae were damaged with X-irradiation (0 Gy or 25 Gy at 80h AED) along with images of Figures α -1 and α -2, but discs were punctured during dissection before dextran incubation. The punctured discs show disrupted epithelial barriers regardless of the functionality of the barrier in intact discs from the same experiment (Figures α -1 and α -2). Arrows indicate a punctured region, as defined by one or more cells flooded with dextran in a pattern contiguous with the lumen of the imaginal disc, occasionally gaps are visible in the Actin staining as well (A). White dotted lines indicate tissue outline defined by Actin (Rhodamine Phalloidin) staining.

α .2.2 Septate junction components are down-regulated during regeneration

To begin to understand how damage disrupts the barrier and why the barrier in regenerating tissues is disrupted for an extended period of time, I irradiated the larvae as before (25 Gy at 80h or 104h AED) then observed the localization of two septate junction components, Neurexin-IV (Nrx) and Coracle (Cora) (Baumgartner et al., 1996; Lamb et al., 1998). Nrx is necessary for the function of the epithelial barrier (Baumgartner et al., 1996) and for the localization of the other components of the septate junction core complex (Laprise et al., 2009 and Chapter 2). Nrx localizes to the septate junctions in wing imaginal discs by 92h AED (Chapter 2). At 92h AED, Cora is diffusely localized along the apical-lateral surface of cells and is not necessary for the functionality of the barrier; by 116h AED Cora is localized at the septate junctions and is necessary for barrier function (Chapter 2). At both 92h and 116h AED Cora is necessary for the localization of other components, including Nrx, at the septate junctions (Chapter 2).

The localization of Nrx and Cora at 92h and 116h AED in unirradiated larvae was consistent with the observations of Chapter 2. Nrx is localized to the septate junctions by 92h AED and remains so at 104h and 116h AED, although the intensity of Nrx at the junctions increases from 92h AED (Figure α -4A-C). Following

X-irradiation before regeneration restriction (25Gy at 80hAED), Nr_x is depleted in the cells and mislocalized away from the region of the septate junctions relative to unirradiated controls (compare Figures α -4E with α -4A). At 104h AED, Nr_x begins to recover intensity and localization at the junctions, but the staining is less intense than in unirradiated controls at either 92h or 104h AED (compare Figures α -4F with α -4A,B). By 116h AED, 36 hours after damage, Nr_x localization and intensity have recovered (compare Figures α -4G with α -4C). Cora follows a similar trend following damage. In unirradiated controls, at 92h AED Cora is diffusely localized along the apical-lateral surface of the cells, but is localized solely to the septate junctions by 116h AED (Figure α -6A-C). At 104h AED, Cora was localized primarily at the septate junctions in high amounts, as indicated by much brighter staining than at 116h AED (Figure α -6B). It is unclear what role, if any, Cora has on barrier function at 104h AED, therefore it is difficult to interpret this brighter staining, but it may result from whatever mechanism localizes Cora to the septate junctions. At 92h AED following X-irradiation before regeneration (25 Gy at 80h AED), Cora staining is depleted relative to unirradiated controls (compare Figures α -6E and α -6A). By 104h AED, 24 hours after damage, virtually no Cora is detected in the tissue (Figure α -6F). At 116h AED, 36 hours after damage, Cora staining intensity has begun to recover, but the localization is diffuse along the lateral membrane similar to unirradiated controls at 92h AED (compare Figures α -6G and α -6A). By 128h AED, 48 hours after damage, Cora is localized to the septate junctions, and has a bright staining pattern more similar to 104h AED than 116h AED (compare Figures α -6H and α -6B,C). The timeline of Cora localization correlates with the timeframe of epithelial barrier recovery following damage (compare Figures α -6E-H and α -1E-H). The similarity of Cora staining at 128h AED in the wing imaginal discs of irradiated larvae to Cora staining at 104h AED in the wing imaginal discs of unirradiated larvae may explain the slight permeability of the barrier at this time, but further investigation is needed. Additionally, the disruption of Nr_x and Cora appear uniform across the tissue instead of being localized in patches and remain depleted or mislocalized for an extended period of time following damage. This

indicates that the junctional components are depleted or down-regulated by a non-cell autonomous mechanism. If the disruption was autonomous, I would expect to only see a response in cells directly surrounding damaged or replicating cells, which would produce a scattered pattern of disruption. The disruption would be briefer and/or more scattered around cells that were damaged or actively regenerating.

To determine if this depletion of Nr_x and Cora is specific to regenerating tissues, I observed Nr_x and Cora localization following X-irradiation after regeneration is restricted (25 Gy at 104h AED). At both 116h and 128h AED, 12 and 24 hours following irradiation respectively, neither Nr_x nor Cora were mislocalized or depleted in the wing imaginal discs relative to unirradiated larvae (Figures α -4K,L and α -6K,L). I previously observed that the epithelial barrier was disrupted at 116h AED following irradiation at 104h AED (Figure α -1K). Therefore, these data indicate that barrier disruption following damage is not specific to regenerating tissues. However, the septate junction components are not mislocalized or depleted following late damage and barrier activity recovers relatively rapidly. This also indicates that the sustained permeability in the barrier observed following damage before regeneration restriction (Figure α -1E-H) is likely due to a regulated depletion of the septate junction components during the regenerative process.

Figure α -4. Nr_x is depleted and mislocalized following X-irradiation before but not after regeneration restriction.

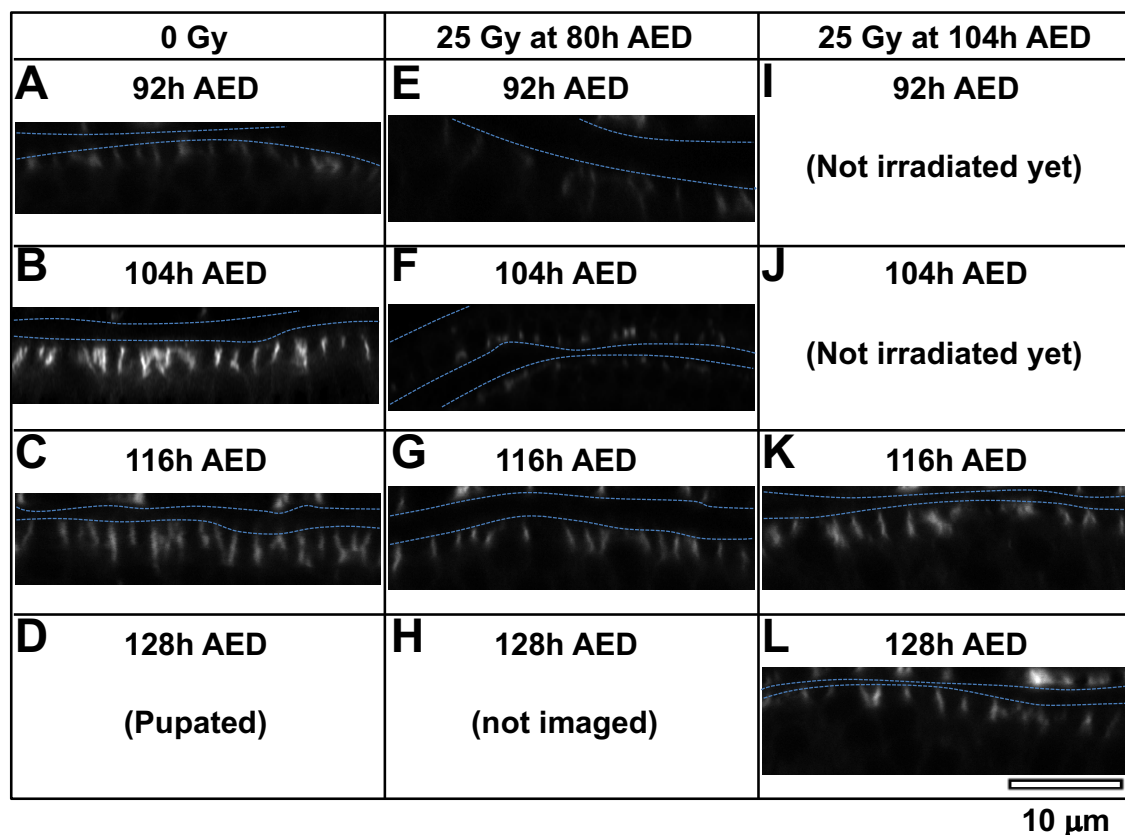


Figure α -4. Nr_x is depleted and mislocalized following X-irradiation before but not after regeneration restriction. Nr_x::GFP localization in wing imaginal discs of larvae were damaged with X-irradiation at (A-D) 0 Gy (control), (E-H) 25 Gy at 80h AED, or (I-L) 25 Gy at 104h AED. Blue dotted lines indicate tissue outlines as defined by Actin (Rhodamine Phalloidin; Figure α -7). (A-D) Between 92h and 116h AED, Nr_x intensity at the septate junctions increases. (A) At 92h AED, Nr_x is localized at the apical-lateral region of the membrane where the septate junctions are expected to localize. (B-C) At 104h and 116h AED, Nr_x is localized at the region of the septate junctions at a greater intensity than observed at 92h AED (D) Unirradiated larvae pupate before 128h AED. (E-H) Following X-irradiation before regeneration restriction (25 Gy at 80h AED), Nr_x localization is depleted, but recovers prior to pupation. (E-F) At 92h and 104h AED, 12 and 24

hours after damage, Nr_x is localized similarly to unirradiated controls, but is significantly depleted. (G) At 116h AED, 36 hours after damage, Nr_x intensity at the septate junctions is similar to unirradiated controls (C). (H) No discs were collected after 116h AED. (I-J) Nr_x localization is not disrupted following X-irradiation after regeneration restriction (25 Gy at 104h AED). (I-J) Larvae were not irradiated until 104h AED. (K-L) At 116h and 128h AED, 12 and 24 hours after damage respectively, Nr_x is not depleted and is localized at the region of the septate junctions. Data are from one experiment in Nr_x::GFP larvae with n = (A) 3, (B) 4, (C) 4, (E) 2, (F) 2, (G) 4, (K) 5, and (L) 4.

Figure α -5. Actin stain from discs in Figure α -4.

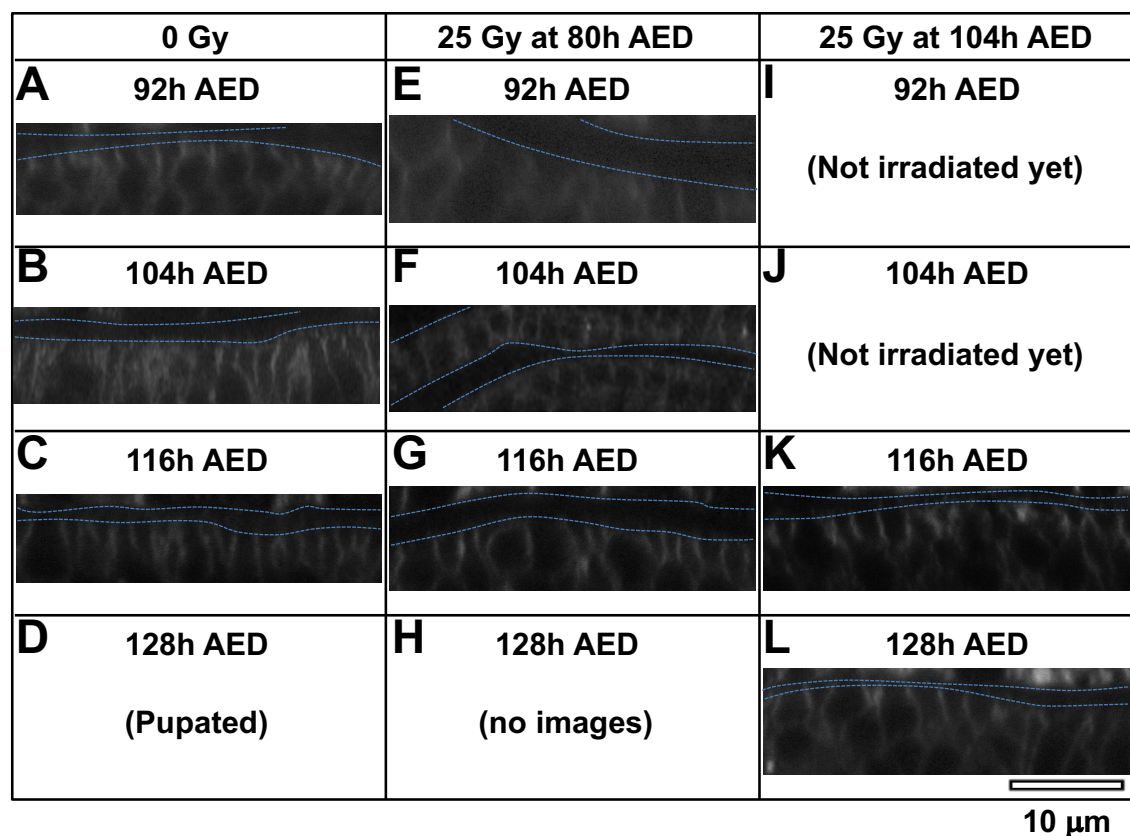


Figure α -5. Actin stain from discs in Figure α -4. Localization of Actin (rhodamine phalloidin) in the discs of Figure α -4 that was used to define the tissue

outline (blue dotted lines). Larvae were damaged with X-irradiation at (A-D) 0 Gy (control), (E-H) 25 Gy at 80h AED, or (I-L) 25 Gy at 104h AED.

Figure α -6. Cora is depleted and mislocalized following X-irradiation before but not after regeneration restriction.

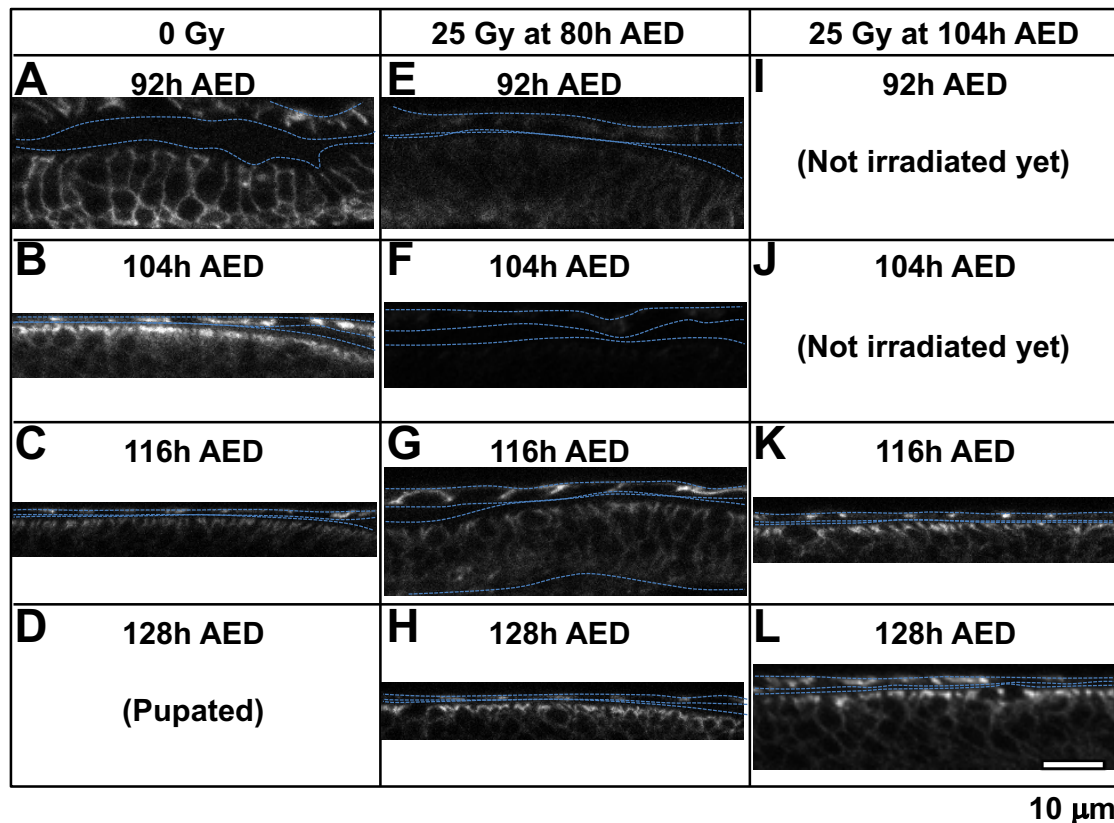


Figure α -6. Cora is depleted and mislocalized following X-irradiation before but not after regeneration restriction. Cora localization in wing imaginal discs of larvae were damaged with X-irradiation at (A-D) 0 Gy (control), (E-H) 25 Gy at 80h AED, or (I-L) 25 Gy at 104h AED. Blue dotted lines indicate tissue outlines as defined by Actin (Rhodamine Phalloidin; Figure α -5). (A-D) Between 92h and 116h AED, Cora localization in the wing imaginal discs of undamaged larvae shifts from diffuse along the membrane to only localized at the septate junctions. (A) At 92h AED, Cora is localized diffusely along the lateral membrane of cells. (B) At 104h AED, Cora is localized at the apical-lateral surface of the cells where the septate junctions are expected to be localize. (C) At 116h AED, Cora is localized at the

region of the septate junctions. The staining is less bright than at 104h AED. (D) Unirradiated larvae pupate before 128h AED. (E-H) Following X-irradiation before regeneration restriction (25 Gy at 80h AED), Cora localization is depleted and mislocalized, but recovers prior to pupation. (E) At 92h AED, 12 hours after damage, Cora staining is reduced compared to unirradiated controls (A). (F) At 104h AED, 24 hours after damage, little-to-no Cora is detectable in the tissue. (G) At 116h AED, 36 hours after damage, Cora localization is diffuse along the lateral membrane of the cells, similar to 92h AED unirradiated larvae (A). (H) At 128h AED, 48 hours after damage, Cora is localized at the apical-lateral membrane where septate junctions are expected to localize. No discs were collected after 128h AED. (I-J) Cora localization is not disrupted following X-irradiation after regeneration restriction (25 Gy at 104h AED). (I-J) Larvae were not irradiated until 104h AED. (K-L) At 116h and 128h AED, 12 and 24 hours after damage respectively, Cora is not depleted and is localized at the region of the septate junctions. Data are from one experiment in w^{1118} larvae with $n =$ (A) 3, (B) 4, (C) 2, (E) 2, (F) 4, (G) 3, (H) 4, (K) 5, and (L) 1 images and are consistent with data from an experiment in $Nrx::GFP$ larvae. $Nrx::GFP$ images from this experiment are shown in Figure α -4, Cora images are not shown. 128h AED following irradiation at 80h AED was not imaged in the $Nrx::GFP$ experiment. n for the $Nrx::GFP$ experiment listed in Figure α -4. Images in Figures α -1, α -2, and α -3 are also from the same experiment w^{1118} larvae.

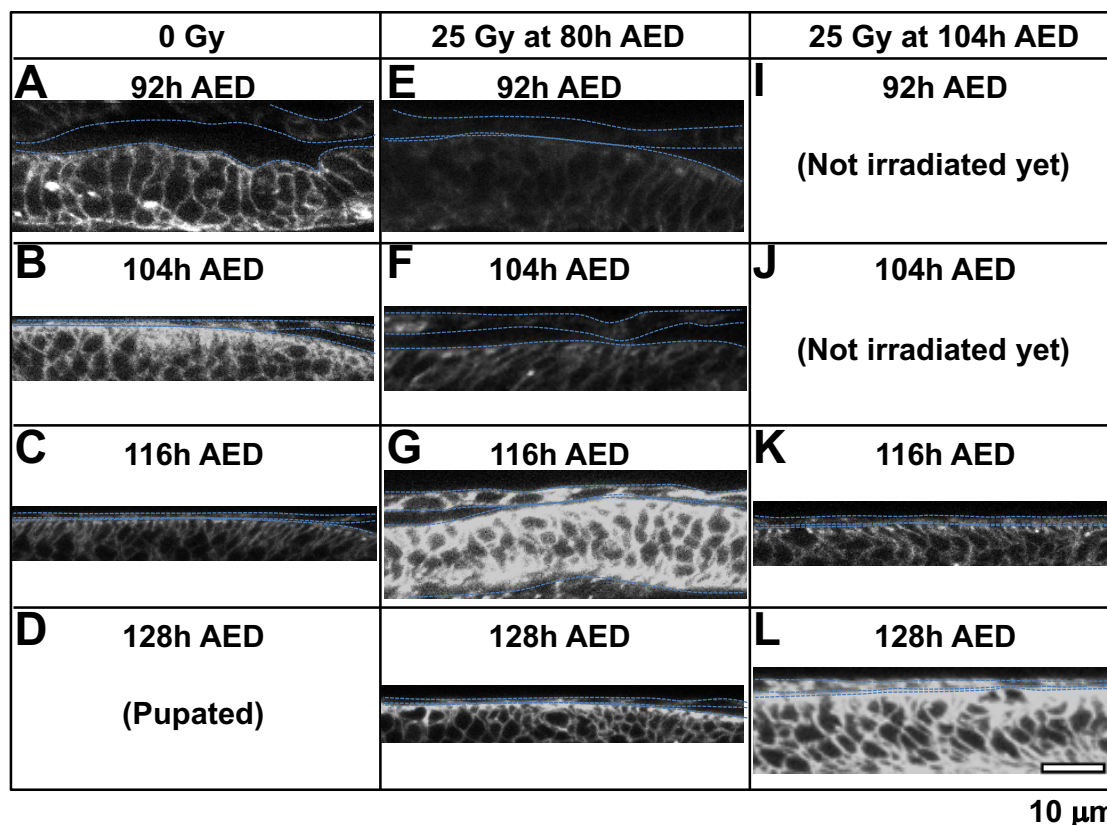
Figure α -7. Actin stain from discs in Figure α -6.

Figure α -7. Actin stain from discs in Figure α -6. Localization of Actin (rhodamine phalloidin) in the discs of Figure α -6 that was used to define the tissue outline (blue dotted lines). Larvae were damaged with X-irradiation at (A-D) 0 Gy (control), (E-H) 25 Gy at 80h AED, or (I-L) 25 Gy at 104h AED.

α .3 Discussion

α .3.1 Disruption of the epithelial barrier following damage

Here I preliminarily demonstrate that the epithelial barrier is disrupted following damage. When the damage occurs before regeneration, the septate junction components are likely downregulated to sustain barrier permeability. This is not entirely surprising. Although, apoptosis does not necessarily compromise the functionality of an epithelial barrier, other aspects of damage are associated with reduced barrier activity. In mice, cells surrounding an apoptotic cell form an epithelial barrier with each other before extruding the dying cell from the cell layer

(Rosenblatt et al., 2001). As a result, the barrier remains intact. It is unclear if this is the case in *Drosophila* as well, but X-irradiation induces both apoptotic and necrotic cell death in wing imaginal discs (Abbott, 1983). The effects of necrosis on barrier function have not been explicitly studied. However, inflammation is a defining characteristic of necrotic cell death and inflammation is associated with weaker epithelial barriers across multiple diseases (Hardyman et al., 2013; Xu et al., 2019; Zeissig et al., 2007; Xie et al., 2020; Duszyc et al., 2017). In mammals, the inflammatory signal TNF- α induces expression of barrier forming components that increase the permeability of the barrier (Al-Sadi et al., 2016; Haines et al., 2016). There may be a similar mechanism regulating barrier activity and the septate junctions in *Drosophila*.

What is more surprising is that the preliminary data indicate that when tissues are damaged after regeneration restriction, the barrier rapidly restores itself and the localization of the components never changes. This indicates that, after regeneration restriction, the initial damage may disrupt the barrier but the junctions themselves are not affected by it. It is not clear how the barrier is disrupted in these tissues, although barrier disruption within the wing discs is non-autonomous (described in Chapter 2), so it is possible that imaging across a wider area may provide insights if there are localized areas of septate junction disruption.

α .3.2 Regulation of the epithelial barrier during regeneration

The septate junction components Cora and Nr x are only disrupted following damage in regenerating tissues which indicates that regenerative processes includes the down-regulation of the epithelial barrier. The most likely candidate for the regulation of the septate junctions during regeneration is *wingless* (*Drosophila* Wnt-1 homolog) (Baker, 1987). Wingless is a morphogen that plays roles in both normal development and tissue regeneration (Schubiger et al., 2010; Smith-Bolton et al., 2009). Regenerative Wingless is activated by cell death and induces proliferative signaling in neighboring cells to produce regenerative growth (Katsuyama et al., 2015; Rodrigues et al., 2012; Smith-Bolton et al., 2009).

Regenerative ability is lost in *Drosophila* as a result of the ecdysone-dependent epigenetic silencing of the enhancer region that induces *wingless* expression during regeneration (Harris et al., 2016). This would explain why the septate junctions would not be down-regulated in non-regenerative tissues. Additionally, since Wingless is a morphogen this would also explain why septate junctions are downregulated across the tissues instead of in patches near damaged cells.

α .3.3 How is the end of regeneration determined?

The mechanisms for determining and communicating the completion of regenerative growth is poorly understood (Fox et al., 2020). In Chapter 2, I demonstrated that epithelial barrier maturation in the late larval period determines the duration of regeneration by limiting Dilp8 signaling. I proposed that following damage to larvae capable of regeneration, the development of the mature epithelial barrier would limit Dilp8 signaling, thereby promoting ecdysone production to initiate late-larval and prepupal developmental events. The data I present here further support this hypothesis. Damage before regeneration restriction disrupts the epithelial barrier and the septate junction components Nr_x and Cora for an extended period of time. This could facilitate the distribution of Dilp8 from the imaginal disc lumen to the brain and PG, where it functions (Colombani et al., 2012; Colombani et al., 2015; Garelli et al., 2012; Garelli et al., 2015; Jaszczak et al., 2016). Prior to pupariation, Nr_x and Cora re-localizes and the epithelial barrier may start to reform. This could serve to trap the remaining Dilp8 in the imaginal disc lumen. However, to determine this conclusively, I would need to repeat the barrier assay quantitatively and measure timepoints past 128h AED, which may require collection in intervals shorter than six hours.

α .4 Methods

The experiments presented here were done chronologically before many of the experiments presented in Chapter 2. As a result, the protocols used in these experiments are less refined than those of Chapter 2; the differences in methods

are explicitly stated here. It should also be noted that some of these experiments have very low n or were done non-quantitatively, and therefore should be considered preliminary. Still, these data are worth assessing as they present very interesting interpretations, especially when contextualized by the more recent data from Chapter 2.

α .4.1 *Drosophila* stocks, husbandry, and irradiation

The fly stocks used were w^{1118} and Nr x IV-GFP (Bloomington 50798). Stocks were maintained in 25° incubators with a 12-hour alternating light-dark cycle. Developmental timing was synchronized through egg staging, with collection from a 4-hour egg-laying interval on grape agar plates (Genesee Scientific) with a small amount of baker's yeast paste. At 24h AED, 10-15 first instar larvae were transferred into 35 mm petri dishes containing cornmeal-yeast-molasses media. At 80h AED, the lids of the petri dishes were removed and the bases containing food and larvae were placed in a 10 cm petri dish to allow airflow while also preventing escape during the wandering phase of the third instar.

At the times indicated, the petri dishes were slightly flooded with distilled water (usually 3-5 drops) to ensure that the larvae came to the surface of the food to receive a full dose of X-irradiation as well as ensure that the food did not dry out following treatment. The petri dishes were then placed on a rotator to ensure even dosage and exposed to 25 Gy X-irradiation in a Faxitron RX-650 operating at 130 kV and 5.0 mA. Following irradiation, excess moisture was removed gently with a kim wipe if necessary. Undamaged controls were treated with distilled water only if the food appeared to be dry.

α .4.2 Dissection and immunofluorescent staining

Larvae were inverted and cleaned in PBS then fixed with 4% paraformaldehyde in PBS (20 min) and washed with PBS (twice for 5 min each). The tissues were permeabilized with 0.3% Triton in PBS (twice for 10 min each) then washed with a blocking solution of 10% goat serum and 0.1% Triton in PBS

(30 min). The tissues were then incubated rocking in primary antibody solutions (overnight at 4°C or for two-to-four hours at room temperature). The process was repeated for secondary antibodies and then the tissues were incubated rocking in 80% glycerol in PBS (overnight at 4°C). The tissues were stored at 4°C in 80% glycerol and were mounted for imaging within one week of staining. Imaginal discs were isolated from the stained tissues and mounted on glass slides with Vectashield (Vector Laboratories). Tissues were mounted on slides with the coverslips raised by double-sided tape.

Antibody solutions were prepared in 10% goat serum and 0.1% Triton in PBS. The primary antibody used was mouse anti-Cora C615.16 (1:500; Developmental Studies Hybridoma Bank). The secondary antibody used was goat anti-mouse Alexa633 (1:1000; ThermoFisher). F-actin was identified by Rhodamine-conjugated Phalloidin (1:100; ThermoFisher) staining that was performed concurrently with secondary antibody incubations.

Differences from Chapter 2: In Chapter 2 Cora staining was done at 1:500 instead of 1:400, which I found imaged slightly more reliably. All staining was mounted with raised coverslips, whereas in Chapter 2 only images assessing the localization of the septate junction components utilized a raised coverslip.

α .4.3 Imaging

Confocal imaging was done at 63x with a Zeiss LSM 700 (Figures α -1, α -2, α -3, α -6, α -7) or a Zeiss LSM 880 (Figures α -4; α -5) within the University of Virginia Advanced Microscopy Facility (RRID:SCR_018736). Laser power and gain settings for each set of stained samples were based on the experimental group with the highest fluorescence intensity in each channel, and kept constant within the experiment. Images were processed and quantified with Fiji/ImageJ (Schindelin et al., 2012).

Differences from Chapter 2: In Chapter 2 the Zeiss LSM 880 was not used when imaging septate junction localization to better assess the nature of the characteristics with the junctions. However, this greatly restricted the field of view

and was dropped to better observe more junctions in a shorter period of time. Images were collected in a cross section approximately along the dorsal-ventral boundary of the pouch region of the wing imaginal discs instead of perpendicular to this region approximately along the anterior-posterior boundary. Most image cross sections were not taken all the way through the tissue, instead focusing only on the luminal space and the apical-lateral region near the septate junctions. As a result, the ratio of localization medial-to-apical in these images is not possible to obtain in most cases.

α .4.4 Dextran assay

Larvae were inverted and cleaned in Schneider's Insect Medium (Sigma-Aldrich) then transferred into a 1:4 dilution of 10 kDa fluorescein conjugated dextran (Invitrogen) in Schneider's Insect Medium (Sigma-Aldrich) and incubated rocking and covered at room temperature for 30 minutes. Then fixed with 4% paraformaldehyde in Schneider's Insect Media. Tissues were washed, stained, and imaged as previously described.

Differences from Chapter 2: In Chapter 2 carcasses were incubated in a 1:8 dilution of dextran instead of a 1:4 dilution and tissues were washed with Schneider's Insect Medium following incubation following incubation and before fixation. I found this removed some background signal by preventing clumping on the outside of the tissue.

α .4.5 Genotypes

Figure 1

w^{1118} / w^{1118}

Figure 2

w^{1118} / w^{1118}

Figure 3

w^{1118} / w^{1118}

Figure 4

w¹¹¹⁸ / w¹¹¹⁸

Figure 5

w¹¹¹⁸ / w¹¹¹⁸

Figure 6

Nrx::GFP / Nrx::GFP

Figure 7

Nrx::GFP / Nrx::GFP

Chapter 3

Conclusions, Discussion, and Future Directions

3.1 Summary

An outstanding question in regenerative biology is how tissues communicate the completion of regeneration. My work demonstrates that, in the developing wing of *Drosophila melanogaster* larvae, one mechanism to communicate the end of regeneration is the maturation of the epithelial barrier. In Chapter 2, I demonstrate that disruption of the epithelial barrier limits the length of the regenerative period by inhibiting signaling by the damage response peptide *Drosophila* insulin-like peptide 8 (Dilp8). Dilp8 functions in the brain and prothoracic gland to inhibit the production of the steroid hormone ecdysone (Colombani et al., 2012; Colombani et al., 2015; Garelli et al., 2012; Garelli et al., 2015; Jaszczak et al., 2016; Vallejo et al., 2015). Ecdysone signaling regulates many of the changes that induce pupation, and its inhibition results in a developmental delay during which damaged tissues are able to regenerate (Colombani et al., 2012; Garelli et al., 2012). The disruption of the epithelial barrier in wing imaginal discs extends Dilp8-induced developmental delay, meaning that the barrier limits Dilp8 signaling. I developed a quantitative assay to measure the exclusivity function of the epithelial barrier, and found that the functionality of the barrier matures during the third instar to become more restrictive, and eventually impermeable, to 10 kDa dextran. The maturation of the barrier results from ecdysone-induced localization of the septate junction component Coracle (Cora) (Fehon et al., 1994).

Since Dilp8 accumulates in the imaginal disc lumen (Colombani et al., 2012; Chapter 2), I hypothesized that the way that the epithelial barrier limits Dilp8 signaling is by sequestering Dilp8 to the imaginal disc lumen following regeneration and restoration of tissue function, including the function of the late-larval epithelial barrier. In the Appendix, I present preliminary data that begin to test this hypothesis. One of the major changes caused by ecdysone in preparation for pupariation is the loss of regenerative capacity, which acts as a developmental checkpoint (Halme et al., 2010). Larvae damaged before regeneration restriction preliminarily showed a sustained loss of barrier function and depletion of septate

junction components, including Cora, in wing imaginal discs which began to recover before pupation. Although preliminary, these data tend to support the hypothesis that following regeneration a restored barrier could exclude Dilp8. In contrast, larvae damaged after regeneration restriction preliminarily showed no depletion of septate junction components and rapid restoration of barrier function. This suggests that in regenerating larvae the functionality of the barrier may be downregulated, which I hypothesized may further facilitate the release of Dilp8.

3.2 Significance and Implications

This work adds interesting insights into regenerative biology, epithelial barrier development, and *Drosophila* development. In this section I will summarize our current understanding in these areas and discuss how my work adds to them.

3.2.1 The role of epithelial barrier maturation in regeneration

In regenerating tissues, damage induces phosphorylation of Basket (*Drosophila* JNK homolog) (Riesgo-Escovar et al., 1996; Sluss et al., 1996). Phosphorylated Basket activates the transcription factor AP-1 (Riesgo-Escovar et al., 1996; Sluss et al., 1996). AP-1 is a dimer of Jun-related antigen (*Drosophila* homolog of Jun) and Kayak (*Drosophila* homolog of Fos) that induces expression of multiple pro-apoptotic and regenerative genes, including the morphogen Wingless (Baker, 1987; Chen et al., 2002; Harris et al., 2016; Hwang and Pallas, 2014; Perkins et al., 1990). Wingless induces proliferative signals like Myc and JAK/STAT in neighboring cells to produce regenerative growth (Katsuyama et al., 2015; Rodrigues et al., 2012; Smith-Bolton et al., 2009). JAK/STAT induces Dilp8 signaling (Katsuyama et al., 2015). Dilp8 is released from the tissue and binds to Lgr3 receptors in the brain and prothoracic gland to inhibit ecdysone and delay development (Colombani et al., 2012; Colombani et al., 2015; Garelli et al., 2012; Garelli et al., 2015; Jaszczak et al., 2016; Vallejo et al., 2015, 3).

This pathway describes how damaged tissues communicate that they need to regenerate and how they coordinate regenerative growth, but do not indicate

how tissues communicate the completion of regeneration. My data presented in Chapter 2 indicate that the length of the regenerative period is regulated by the mature epithelial barrier by limiting Dilp8 signaling. My preliminary data presented in the Appendix indicate that barrier activity is downregulated during regeneration. The downregulation could promote Dilp8 release from the tissue. In this case, the barrier could play roles in facilitating developmental delay during regeneration as well as communicating the completion of regeneration. It is not clear from my work whether barrier activity affects the length of regenerative signaling or instead serves as a mechanism for communicating the completion of regeneration to other tissues.

3.2.2 The regulation and change of function of the epithelial barrier

One key finding that I present in Chapter 2 is that the epithelial barrier of wing imaginal discs grows more restrictive during the third instar. I modified an assay first developed by Lamb et al. 1998 to be quantitative (Lamb et al., 1998). The assay measures the ability of 10 kDa fluorescein-conjugated dextran to permeate the lumen of wing imaginal discs relative to a disc with a barrier disrupted by expressing *kune*^{RNAi} or by puncturing the disc. Between 92 and 116 hours after egg deposition (h AED), the barrier becomes decreasingly permeable to 10 kDa dextran. The change results from increasing levels of the steroid hormone ecdysone during the third instar. Importantly, the barrier at 92h AED is functional, excluding significantly more dextran from the lumen than discs with disrupted barriers. Therefore, this change in epithelial barrier function is not the establishment of the barrier in wing imaginal discs, but an alteration in an existing barrier.

Although this is the first instance observed in *Drosophila*, the alteration of the function of the epithelial barrier after barrier establishment has been observed in other model systems before. In mammals, decreases in progesterone and corticosterone in the mammary duct induces a tightening of the epithelial barrier, which is necessary for milk secretion (Nguyen et al., 2001). This correlates with

upregulation of the tight junction (mammalian septate junction ortholog) components Claudin 1, 3, and 4 in the mammary epithelium (Baumgartner et al., 2017). Likewise, adding Vitamin D to cultured cornea epithelial cell lines increases transepithelial resistance, which indicates a tightening of the barrier (Yin et al., 2011; reviewed in Zhang et al., 2013). The tightening effect continues for at least 5 hours, but is discernable within 1 hour relative to controls (Yin et al., 2011). This correlates with increased expression of the tight junction component Occludin (Yin et al., 2011; reviewed in Zhang et al., 2013). My data indicate that this ability to adapt barrier activity may be consistent between *Drosophila* septate junctions and mammalian tight junctions.

3.2.3 The development of the barrier and ecdysone signaling

In Chapter 2, I demonstrated that increasing levels of ecdysone during the late third instar induces a change in the function of the epithelial barrier in wing imaginal discs. The change in barrier function results from the ecdysone-dependent re-localization of Cora, which changes from being diffusely localized along the lateral membrane to localized only at the septate junctions. This is similar the changes in Cora localization between embryonic stages 14 and 17 in the embryonic salivary gland and the embryonic epidermis. In these tissues, many of the septate junction components become localized to the septate junctions between stages 12 and 14 (Hall and Ward, 2016; Laprise et al., 2009; Oshima and Fehon, 2011). Although Cora localization does shift to become increasingly localized to the septate junctions between stages 12 and 14, it is not localized solely to the septate junctions until stage 17 (Bätz et al., 2014; Hall and Ward, 2016; Oshima and Fehon, 2011).

Between stages 14 and 17 there is also an increase in ecdysone production (Kozlova and Thummel, 2000). At this time, Ecdysone Receptor (EcR) is expressed in these tissues as well (Kozlova and Thummel, 2003; Tan et al., 2014). The connection between ecdysone and barrier function or septate junction localization has not been investigated before my work. I hypothesize that ecdysone

regulates Cora localization during embryonic development, as it does in larval development. We could test this hypothesis using the EcR dominant negative alleles driven under embryonic Gal4 driver lines. The establishment of the embryonic barrier in embryonic development is necessary for embryonic development (Beitel and Krasnow, 2000; Wang et al., 2006; Fehon et al., 1994). Understanding how the barrier is established and regulated would provide insights into how tissue development is coordinated.

3.2.4 The role of the epithelial barrier in regulating signaling and developmental patterns

One of my prominent findings described in Chapter 2 is that the epithelial barrier of the wing imaginal disc grew more restrictive during the third instar. Just prior to pupariation, the barrier is capable of excluding virtually all of the 10 kDa dextran. The timing of this maturation raises questions about the role of the barrier in the morphology of the imaginal discs. The epithelial barrier is likely to be disrupted during early pupal development, which is very soon after the more restrictive barrier forms.

During pupal development, the wing disc evaginates along the midline of the wing pouch (Fristrom and Fristrom, 1975; reviewed in Diaz de la Loza and Thompson, 2017). Within 4 hours the evaginating primary epithelium ruptures the peripodial epithelium (Aldaz et al., 2010). This results in the peripodial epithelium retracting down the sides of expanding primary epithelial tissues, the cells then clump together and undergo apoptosis (Aldaz et al., 2010). My data from Chapter 2 indicate that puncturing the wing disc is sufficient to disrupt the epithelial barrier, so rupturing of the peripodial membrane indicates that the epithelial barrier should be disrupted at this time. This along with the late development of the mature epithelial barrier, indicates that the function of the mature barrier is likely limited to the end of larval development. My data indicate that one role of the mature barrier is limiting Dilp8 signaling (Chapter 2), there are many other changes in signaling pathways that occur around this time in development.

3.3 Proposal for Future Directions

The data presented here raise several questions that could be the framework for follow-up studies focusing on the interplay of epithelial barrier maturation, tissue regeneration, and regeneration restriction. Here I will outline questions for future study and the major experiments that could address them.

3.3.1 How is epithelial barrier maturation regulated during regeneration?

A key question raised by my work is how the barrier acts and is regulated during regeneration. The experiments within the Appendix begin to address this question, but need to be quantitatively repeated using the techniques I developed in Chapter 2. These experiments would utilize X-irradiation to damage the larvae before and after regeneration restriction and measure barrier function and septate junction localization. In the Appendix, I preliminarily observed that following damage before regeneration restriction, the activity of the epithelial barrier was disrupted and septate junction localization was depleted for an extended period of time. Before pupation, septate junction localization recovered and the tissues began excluding dextran from the lumen, although not to the extent that mature undamaged discs did. In contrast, although damage after regeneration restriction disrupted the barrier initially, it recovered quickly and the septate junction components were not depleted or mislocalized. These data preliminarily indicate that the septate junctions are downregulated during regeneration. Performing these experiments quantitatively would help distinguish between the loss of barrier function and the less restrictive, but functional barrier observed in less mature imaginal discs.

Although the data indicate that the septate junctions are regulated during regeneration, they do not indicate how this regulation occurs. The most likely regulatory candidate for the septate junctions during regeneration is the morphogen *wingless* (Baker, 1987). *Wingless* expression following damage is activated by Basket/Jnk activity cell death and initiates proliferative signaling in

neighboring cells to promote regenerative growth (Katsuyama et al., 2015; Rodrigues et al., 2012; Smith-Bolton et al., 2009). A primary cause of the loss of regenerative ability during late larval development is the epigenetic silencing of the enhancer region for *wingless* following damage (Harris et al., 2016). This silencing is ecdysone dependent (Harris et al., 2016) and I have demonstrated that barrier maturation is also ecdysone dependent (Chapter 2). This may explain the correlation between the maturation of the barrier and the inability of damage to disrupt the junctions. Additionally, Wingless is a morphogen which may explain why I observed a downregulation of the septate junction components in regenerating discs across the tissue instead of in patches of damaged cells (Appendix). We could investigate this connection using the *wg*¹ mutant (Sharma, 1973). *Wg*¹ is a genetic deletion of most of the damage-responsive *wingless* enhancer region (Schubiger et al., 2010). *Wg*¹ does not impact developmental Wingless signaling or patterning but eliminates regenerative Wingless signaling (Harris et al., 2016; Schubiger et al., 2010; Sharma and Chopra, 1976). If the septate junction components are not disrupted following damage early (before regeneration restriction in wild type controls) in *wg*¹ mutants, this would indicate that Wingless downregulates the septate junctions during regeneration.

3.3.2 How does tissue damage disrupt the epithelial barrier?

It is not clear how the barrier is disrupted following damage and what down-regulates the septate junctions during regeneration. The impact of cell death on the *Drosophila* epithelial barrier has not been studied, so these studies may also provide additional context for understanding the *Drosophila* epithelial barrier. In mice when apoptosis occurs in an epithelial sheet, the cells around the dying cell form an epithelial barrier with each other before extruding the dying cell from the cell layer (Rosenblatt et al., 2001). As a result, the functionality of the barrier is not compromised (Rosenblatt et al., 2001). This may be the case in *Drosophila* as well.

An important note in these experiments is that apoptosis is not the only form of cell death that occurs during X-irradiation; necrosis occurs as well (Abbott,

1983). The effects of necrosis on barrier function have not been explicitly studied. However, apoptosis is considered to be a non-inflammatory mechanism of cell death while necrosis is considered inflammatory, and diseases that are characterized by inflammation (e.g. Crohn's disease, asthma) are associated with weaker epithelial barriers (Hardyman et al., 2013; Xu et al., 2019; Zeissig et al., 2007; Xie et al., 2020; Duszyc et al., 2017). Necrosis is harder to study than apoptosis due to confusion of terminology and poorer characterization. Necrosis was the original term for all cell death (McCall, 2010). In 1972, apoptosis was distinguished as being non-inflammatory and more controlled than necrosis (Kerr et al., 1972), and is characterized by cleaved caspase signaling (Nicholson and Thornberry, 1997). The term "necrosis" became a catch-all term for inflammatory cell death. Although some types of necrosis are highly regulated (e.g. necroptosis) distinctions between types of necrosis are somewhat uncommon (Cho et al., 2009; Xie et al., 2020). One characteristic shared by all types of necrotic cell death is a lack of cleaved caspase signaling and the blebbing then bursting of the cell membrane, which is what causes the inflammation (Pasparakis and Vandenabeele, 2015). In an imaginal disc, blebbing would be difficult or impossible to detect via confocal microscopy. Therefore, it makes sense to start by looking at the role of apoptosis in barrier disruption, then investigate necrosis if necessary.

The easiest way to determine if apoptotic cells are disrupting the barrier following irradiation would be to first correlate the loss of barrier function with apoptosis. This could be done by performing the dextran assay shortly after damage and staining the tissues for an apoptotic marker, such as cleaved Death Caspase-1 (Dcp1) (Song et al., 1997). At minimum, this experiment will give a timeline of how quickly after damage barrier disruption occurs and if that correlates with cell death. However, it is also possible that this experiment may give more concrete answers as well. When I was developing the dextran assay, I disrupted the epithelial barrier by puncturing the discs and was able to observe the regions where the tissues were damaged by accumulation of dextran in those regions (Chapter 2). The co-localization of an apoptotic marker and these regions of

dextran accumulation would indicate that these cells are responsible for the disruption of the barrier. Dextran accumulation in cells away from the apoptotic marker would indicate that these may be locations of necrosis and that is what causes the disruption of the barrier. However, confirming that conclusion or identifying the type of necrosis responsible may prove more difficult.

We should correlate cell death with barrier disruption both before and after regeneration is restricted. Although barrier disruption may result from the same cause in both situations, I have demonstrated that one of the many ways that the tissue morphology changes is in the functionality of the barrier (Chapter 2). Additionally, my preliminary data indicate that the septate junction components are not depleted or mislocalized following damage after regeneration restriction (Appendix). This indicates a possibility that the disruption of the barrier following damage before and after regeneration restriction results from different initial causes. It would also be worthwhile to observe the localization of the septate junction components in these or parallel experiments to determine whether the disruption of the barrier correlates with the depletion of the septate junction components. My preliminary data only show component depletion following damage before regeneration (Appendix) so it may only be necessary to follow localization after damage early.

3.3.3 What is the role of Coracle in the less restrictive barrier?

It is not clear what Cora is doing at the septate junctions when Cora staining is diffuse. Cora is not necessary for the less restrictive barrier function, but the claudin Kune is (Chapter 2). Surprisingly, knockdown of Cora by RNAi results in the knockdown of Kune at the septate junctions (Chapter 2). This indicates that Cora does play a role in the septate junctions at the early barrier since it is necessary for component localization. These data also indicate redundancy in the functionality of the less restrictive barrier since barrier function is not lost after the loss of Cora disrupts Kune localization. This is confusing though because the

disruption of Kune by *kune*^{RNAi} expression disrupts the barrier, but the disruption of Kune by *cora*^{RNAi} expression does not.

One possibility is that Cora disruption affects turnover kinetics at the junctions. By this hypothesis, *cora*^{RNAi} expression causes Kune to turnover rapidly and reduces Kune at the junctions, but does not eliminate it. Perhaps the amount of Kune at the junctions at any one time is sufficient to provide the less restrictive barrier function, but when Kune is depleted by *kune*^{RNAi} expression then it cannot be replaced. I find this hypothesis unlikely. In this scenario, I would expect to observe significantly more intracellular Kune and some junctional Kune, although less than in wild type expression. This is not consistent with my data (Figure 2-5E).

Another possibility is that Cora impacts the kinetics of the septate junction complex. By this hypothesis, loss of Cora by *cora*^{RNAi} expression causes depletion of Kune at the septate junctions, but the complex forms so that the barrier function is dependent on a different claudin. When Kune is depleted by *kune*^{RNAi} it disrupts the complex too much, the complex cannot reform to become dependent on a different claudin. I think this hypothesis is more likely given our understanding of the septate junction complex as being highly interdependent and Kune being the most central of the known claudins (Nelson et al., 2010a).

Although it would be difficult to investigate these hypotheses, I think it would be possible through a series of experiments. First, to determine if Cora is a part of the septate junction complex when the barrier is functional but less restrictive, we could attempt to co-immunoprecipitate Cora and Kune at this time. This is necessary because Cora localization is diffuse at this point in development. Although its localization does not appear to be specifically away from the septate junctions it is also not specifically localized to the septate junctions. My hypotheses revolve around the role of Cora being specific when it is localized at the septate junctions. However, if Cora is not yet a part of the septate junction complex, then these hypotheses make little sense. This would indicate a more complex regulatory system than we have the ability to analyze without more information. If Cora and Kune do form a complex at this time, then we could next determine if Cora

disruption affects overall Kune levels using western blots, comparing between *cora^{RNAi}*, *kune^{RNAi}*, and *lacZ* control expressing discs. Overall protein levels are not indicative of functionality at the septate junctions: in a preliminary experiment I temporarily expressed *kune^{RNAi}* universally using a heat-shock Gal4 and did not observe a reduction of Kune protein (Figure 3-1) and both under- and overexpression of the tricellular septate junction component Gliotactin disrupts of the barrier and causes significant cell and tissue disruption (delamination, cell migration, and apoptosis) (Sharifkhodaei et al., 2016). Thus, relative protein levels detected by western blot should not be read as indicative of barrier function, but could indicate whether there is Kune available for use at the barrier even if there is rapid turnover.

Next, we should observe the localization of the other claudins (Sinuous and Pickel) when Cora is knocked down early compared to control (Behr et al., 2003; Wu et al., 2004). These are the most likely candidates to provide barrier function in the absence of Kune. If one of the other claudins becomes more concentrated at the junctions, this would indicate a strong likelihood that the barrier is becoming dependent on that component. However, it is also possible that the claudin(s) were already providing barrier function as a redundancy method. In this case the depletion of Kune in *cora^{RNAi}* expressing discs may not present a notable change in the localization, intensity, or pattern of Sinuous and/or Pickel. In this situation, we could screen the known septate junction components for components that are not affected by *cora^{RNAi}* expression when the barrier is less restrictive. Then we would need to demonstrate that this component is necessary for the localization of Sinuous and/or Pickel by knocking down the component with RNAi and observing Sinuous and/or Pickel expression. This would need to be followed by an assessment of the functionality of the epithelial barrier following RNAi knockdown. If the functionality of the less restrictive barrier has redundancy, the barrier should remain functional, even though the claudin is mislocalized. This would be similar to what I observed with *cora^{RNAi}* where Kune is knocked down but the barrier remains functional. Finally, we could co-express the candidate RNAi

with *cora*^{RNAi} and observe for a loss of barrier function. Co-expression of the RNAi with *cora*^{RNAi} should disrupt Kune function as well as the function of the other claudin. This would indicate that Cora stabilizes the septate junctions even before it has become localized solely to the septate junctions.

Figure 3-1. Kune protein levels following temporal knockdown.

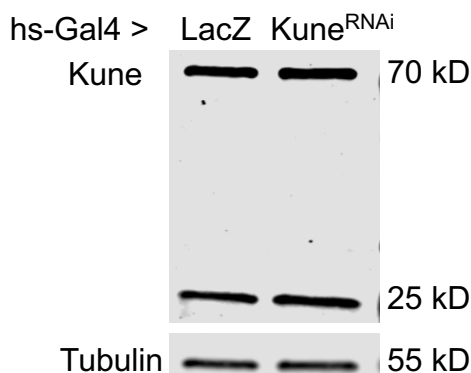


Figure 3-1. Kune protein levels following temporal knockdown. Western blot of extracts from the cleaned carcasses of wandering third instar larvae expressing UAS-*lacZ* or UAS-*kune*^{RNAi} under the hs-Gal4 promoter. No obvious loss of kune is observed. No control for Kune is presented as global knockdown of Kune is embryonic lethal. The efficacy of *kune*^{RNAi} was tested via immunofluorescence in Chapter 2 (Figure 2-12B,C).

Figure 3-1. Materials and methods. Small crosses (approximately 10 females by 10 males) were made from hs-Gal4 (Bloomington 1799) crossed to UAS-LacZ.NZ (Bloomington 3955) or UAS-Kune[RNAi]; UAS-Dcr2 (derived from VDRC GD3962 and VDRC 60009). Flies were maintained in 25°C incubators with a 12-hour alternating light-dark cycle. Adult flies were transferred daily to fresh vials containing cornmeal-yeast-molasses media (Archon Scientific B101). Heat shock was performed on vials with mostly wandering larvae for 45 minutes in a water bath at 37°C. 3-5 relatively large wandering third instar larvae were collected one hour after heat shock. The larvae were halved and inverted, the posterior half was discarded. The intestines were stripped from the anterior half. The cleaned carcasses were immediately put on dry ice.

To extract protein, the samples were sonicated in lysis buffer (2% SDS, 60 mM Tris-HCl, pH 6.8) with phosphatase and protease inhibitors (Roche). Protein concentration was measured using a BCA assay (Pierce). 10 μ g of protein from each sample was separated by SDS-PAGE using a Mini-Protean® TGX™ 4–15% gel (BioRad), and transferred to a nitrocellulose membrane with pore size 0.2 μ m at 100 V for 70 minutes. The membrane was incubated in blocking solution (1% cold fish gelatin in Tris buffered saline with 0.1% Tween, pH 7.6) for 30 minutes. Primary antibody incubation was done in blocking solution in 4°C rocking overnight. The membrane was again incubated in blocking solution for 30 minutes, then was washed in TBS-T (three times for 5 minutes) before being incubated in secondary antibody in blocking solution for 45 minutes. The membrane was again washed in TBS-T (three times for 5 minutes), before being visualized by Li-COR Odyssey® CLx Imaging System (UVA Cell Biology Department).

The primary antibodies that were used are rabbit anti-Kune (1:2,000; Dr. Mikio Furuse; Nelson et al., 2010) and mouse anti- α -Tubulin (1:5,000; Sigma T6074). The secondary antibodies that were used are IRDye 800CW goat anti-rabbit IgG (1:20,000; LI-COR) and IRDye 680RD goat anti-mouse IgG (1:20,000; LI-COR).

Figure 3-1. Acknowledgements. Thank you to Brittany Martínez (Michelle Bland lab) for performing the protein isolation from the prepared samples, Faith Karanja (Adrian Halme lab) for running the western blot, and the Xiaowei Lu and Noelle Dwyer labs for lending us various reagents and equipment.

3.3.4 How does ecdysone regulate Coracle localization and barrier maturation?

It is unclear how ecdysone regulates the localization of Cora to change the function of the barrier. EcR is a transcription factor so the change must result from changes in the expression of Cora itself or of a regulator of Cora (perhaps a scaffolding protein). The gene locus for Cora contains multiple predicted binding sites for EcR and Broad, another transcription factor regulated by EcR (Galcerán et al., 1990) (Figure 3-2). This could indicate that Cora is directly regulated by EcR

(or Broad), but protein levels do not necessarily correlate with improved barrier function. If EcR regulates a regulator of Cora, it may be difficult to determine which protein is responsible for the regulation. EcR regulates the expression of many genes including other transcription factors (Gauhar et al., 2009) and the Cora phenotype during barrier maturation does not lend itself to a large-scale genetic screen. However, it may be possible to determine how EcR regulates Cora localization. One possibility is that EcR regulates differential expression of Cora isoforms and that relative expression levels drive localization. Cora has six splice isoforms (Consortium, 2019; Thurmond et al., 2019) (Figure 3-2), and the role of these isoforms has not been investigated. The available antibody for Cora is specific to the heavy isoform (Developmental Studies Hybridoma Bank). However, it would be possible to determine relative expression levels of the isoforms over time within the wing using RT-PCR and compare those levels in wild type control wings to wings expressing the EcR dominant negative allele.

Figure 3-2. Cora isoforms and binding site predictions.

Coracle (2R:19,227,437..19,246,125)

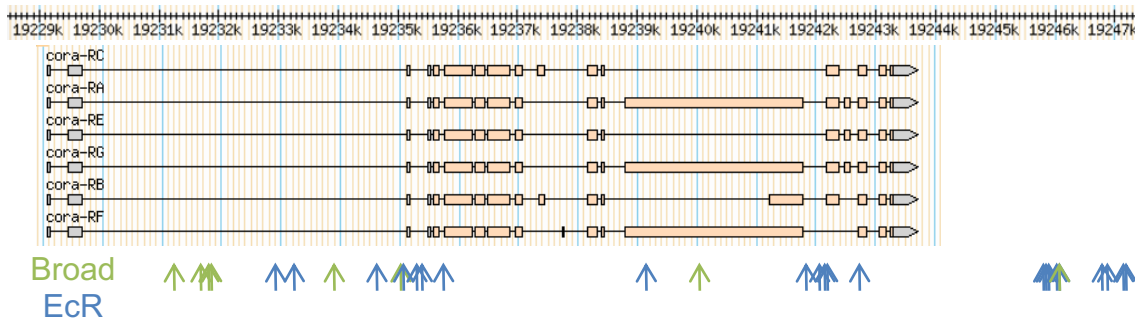


Figure 3-2. Cora isoforms and binding site predictions. The *cora* gene locus is on 2R and contains six splice isoforms. Binding site predictions within the gene locus and surrounding regions are also indicated for the transcription factors Broad (green) or EcR (blue). Note that binding site predictions are highly sensitive, but not selective. As such, many of these predicted binding sites may not be functional but the data set is very likely to include any functional binding sites.

Methods: The binding sites were predicted by aligning the Cora sequence from Flybase (Thurmond et al., 2019) to the JASPAR 2016 curated matrix for Broad or EcR::usp (Mathelier et al., 2016). Ultraspiracle (Usp) must form a dimer with EcR in order for EcR to bind to DNA with high affinity (Yao et al., 1993).

3.3.5 Does the mature barrier limit Dpp signaling in late third instar larvae?

In Chapter 2 I showed that the epithelial barrier limits Dilp8 signaling, possibly by containing Dilp8 to the lumen of the imaginal discs. It is possible that the barrier impacts other signaling pathways in a similar manner. One likely candidate is the morphogen Decapentaplegic (Dpp; *Drosophila* ortholog of BMP2/4) (Hoffmann and Goodman, 1987). Dpp is necessary for wing growth and induces proliferation within the wing imaginal disc (Burke and Basler, 1996; Zecca et al., 1995). Setiawan et al. recently found that Dpp from the wing also signals in the prothoracic gland (Setiawan et al., 2018). Dpp in the prothoracic gland inhibits ecdysone production but this signaling decreases during the third instar (Setiawan et al., 2018). By the end of the third instar Dpp signaling in the prothoracic gland is negligible even though Dpp signaling still occurs within the wing (Setiawan et al., 2018b). They were unable to determine how this decrease occurred, but proposed a combination of factors: proliferation within the wing may consume an increasing amount of Dpp to dilute the signal leaving the wing disc, increased volume of the hemolymph may dilute Dpp further, and some mechanism of the late larval wing may cause increase retention of Dpp within the wing (Setiawan et al., 2018b).

The timeframe and characteristics of the decrease in Dpp signal within the prothoracic gland is very similar to Dilp8, which is also produced in the wing and functions in the prothoracic gland (Colombani et al., 2015; Garelli et al., 2015; Jaszczak et al., 2016b, 3; Vallejo et al., 2015, 3). These similarities and my data indicating that Dilp8 signaling in the prothoracic gland is limited by the mature epithelial barrier (Chapter 2), lead me to hypothesize that Dpp signaling within the prothoracic gland may be also limited by the maturation of the wing epithelial

barrier. This would explain why Dpp function in the prothoracic gland decreases in the late third instar, and why there is no decrease in Dpp signaling within the wing. The mature epithelial barrier could be the mechanism for the system they proposed that retains Dpp signal to the wing. This hypothesis does not exclude the other options they presented. We could test if Dpp is limited by the wing epithelial barrier by disrupting the barrier and observing for Dpp signaling within the brain after Dpp signaling decreases in wild type controls.

3.3.6 What is the role of the less restrictive barrier?

It is not clear what the role of the less restrictive barrier is in the wing disc. It may be beneficial to look at barrier development in the embryo for this aspect of the problem. In the embryonic trachea the establishment of the epithelial barrier (occurs at embryonic stage 15) is necessary for tube elongation and proper branching patterns, defects in which are embryonic lethal (Luschnig et al., 2006; Wang et al., 2006). These aspects of tracheal development are controlled by the deposition of the chitin deacetylases Vermiform and Serpentine within the trachea (Luschnig et al., 2006; Wang et al., 2006). In septate junction mutants, Vermiform and Serpentine do not accumulate in the tracheal lumen. Cora does localize to the septate junctions in trachea, but the refinement of Cora localization between stages 14 and 17 has only been studied in the epidermis and salivary glands (Hall and Ward, 2016; Lamb et al., 1998a; Paul et al., 2003). If Cora localization refines in embryonic tracheal development as it does in the embryonic epidermis and salivary glands or the larval wing and if embryonic barrier function refines over time, then the less restrictive barrier may be sufficient to sequester Vermiform and Serpentine to the tracheal lumen. However, this would be difficult to test because we do not know how the barrier is initially established or how to induce barrier establishment.

There is another aspect of this problem even if the embryonic barrier is established at stage 15 in a functional, but less restrictive form that grows more restrictive after Cora localization at stage 17, and if the less restrictive barrier is

sufficient to sequester Vermiform and Serpentine. It still would not be clear how the less restrictive barrier sequesters Vermiform or Serpentine. One option is size exclusion, but this is not backed by my data in Chapter 2 within the wing. The epithelial barrier of wings excludes 10 kDa dextran and 70 kDa dextran at similar levels (compare Figure 2-2C with 2-S4), and Vermiform and Serpentine fall within this size range (Vermiform is 60 or 63 kDa depending on the isoform and Serpentine is 62 kDa) (Consortium, 2019; Luschnig et al., 2006). Additionally, I observed that the less restrictive barrier was able to exclude dextran, just not to the same extent that I observed later in development. Another possibility is charge exclusion, but again this is not supported by my data. The 10 kDa dextran I used is anionically charged and the 70 kDa dextran is neutrally charged (Invitrogen). Vermiform and Serpentine are predicted to both be anionically charged (calculated by Protein Calculator v3.4 using UniProt sequences).²

A third option is that the restrictiveness of the barrier does not impact size or charge, but diffusion kinetics. This could function to concentrate signals within the lumen or dilute signals from outside the lumen of the tissue, but is contrary to what is understood of the barrier being exclusive based on size and charge. By this hypothesis, diffusion occurs very quickly in a disrupted or unestablished barrier, more slowly in the less restrictive barrier, and so slowly in the mature barrier as to be negligible. During the dextran assay in Chapter 2 and the Appendix, I fixed my samples after a 30-minute incubation period. Perhaps if we did a timecourse of incubation times, we would observe an early timeframe where the less restrictive and mature barrier behave similarly and another timeframe where the functional barrier behaves similarly to a disrupted barrier.

3.4 Thesis conclusions and perspectives

The data presented within this thesis describe a novel characteristic of the *Drosophila* epithelial barrier where the functionality of the barrier changes over

² Protein Calculator v3.4 is free to use and does not provide a reference paper. Link: <http://protcalc.sourceforge.net/>

time and demonstrate that this maturation results from a change in hormone signaling. In and of itself, this is an interesting finding that provides a new model to study the regulation of the epithelial barrier and opens the door to studies targeted towards better understanding the development of the barrier. My data also indicate that this maturation of the barrier is a mechanism to communicate the completion of regeneration within a damaged tissue. The question of how the completion of regeneration is communicated to other tissues is longstanding and this work provides one mechanism. Further investigations branching from this aspect of my data could focus on understanding how regenerating tissues regulate the barrier so that this communication occurs at the proper time.

I see my thesis work as a bridge between two fields. It answers several questions and in doing so brings up many more. I am excited to see future studies that branch from this work.

References

- Abbott, L. A.** (1983). Ultrastructure of cell death in gamma- or X-irradiated imaginal wing discs of *Drosophila*. *Radiat. Res.* **96**, 611–627.
- Aldaz, S., Escudero, L. M. and Freeman, M.** (2010). Live imaging of *Drosophila* imaginal disc development. *PNAS* **107**, 14217–14222.
- Ali, S. R., Hippenmeyer, S., Saadat, L. V., Luo, L., Weissman, I. L. and Ardehali, R.** (2014). Existing cardiomyocytes generate cardiomyocytes at a low rate after birth in mice. *PNAS* **111**, 8850–8855.
- Al-Sadi, R., Guo, S., Ye, D., Rawat, M. and Ma, T. Y.** (2016). TNF- α Modulation of Intestinal Tight Junction Permeability Is Mediated by NIK/IKK- α Axis Activation of the Canonical NF- κ B Pathway. *The American Journal of Pathology* **186**, 1151–1165.
- Ambrose, A. F., Cruz, L. and Paul, G.** (2015). Falls and Fractures: A systematic approach to screening and prevention. *Maturitas* **82**, 85–93.
- Angelow, S., Ahlstrom, R. and Yu, A. S. L.** (2008). Biology of claudins. *American journal of physiology. Renal physiology* **295**, F867–F876.
- Auld, V. J., Fetter, R. D., Broadie, K. and Goodman, C. S.** (1995). Gliotactin, a novel transmembrane protein on peripheral glia, is required to form the blood-nerve barrier in *Drosophila*. *Cell* **81**, 757–767.
- Ayyaz, A., Li, H. and Jasper, H.** (2015). Haemocytes control stem cell activity in the *Drosophila* intestine. *Nature Cell Biology* **17**, 736–748.
- Baena-López, L. A., Pastor-Pareja, J. C. and Resino, J.** (2003). Wg and Egrf signalling antagonise the development of the peripodial epithelium in *Drosophila* wing discs. *Development* **130**, 6497–6506.
- Baena-Lopez, L. A., Nojima, H. and Vincent, J.-P.** (2012). Integration of morphogen signalling within the growth regulatory network. *Current Opinion in Cell Biology* **24**, 166–172.
- Baker, N. E.** (1987). Molecular cloning of sequences from wingless, a segment polarity gene in *Drosophila*: the spatial distribution of a transcript in embryos. *The EMBO Journal* **6**, 1765–1773.
- Balda, M. S., Whitney, J. A., Flores, C., González, S., Cereijido, M. and Matter, K.** (1996). Functional dissociation of paracellular permeability and transepithelial electrical resistance and disruption of the apical-basolateral

intramembrane diffusion barrier by expression of a mutant tight junction membrane protein. *J Cell Biol* **134**, 1031–1049.

Banerjee, S., Sousa, A. D. and Bhat, M. A. (2006a). Organization and function of septate junctions: an evolutionary perspective. *CBB* **46**, 65–78.

Banerjee, S., Pillai, A. M., Paik, R., Li, J. and Bhat, M. A. (2006b). Axonal ensheathment and septate junction formation in the peripheral nervous system of *Drosophila*. *J. Neurosci.* **26**, 3319–3329.

Bätz, T., Förster, D. and Luschig, S. (2014). The transmembrane protein Macroglobulin complement-related is essential for septate junction formation and epithelial barrier function in *Drosophila*. *Development (Cambridge, England)* **141**, 899–908.

Baumgartner, S., Littleton, J. T., Broadie, K., Bhat, M. A., Harbecke, R., Lengyel, J. A., Chiquet-Ehrismann, R., Prokop, A. and Bellen, H. J. (1996). A *Drosophila* Neurexin is required for septate junction and blood-nerve barrier formation and function. *Cell* **87**, 1059–1068.

Baumgartner, H. K., Rudolph, M. C., Ramanathan, P., Burns, V., Webb, P., Bitler, B. G., Stein, T., Kobayashi, K. and Neville, M. C. (2017). Developmental expression of claudins in the mammary gland. *Journal of Mammary Gland Biology and Neoplasia* **22**, 141.

Behr, M., Riedel, D. and Schuh, R. (2003). The Claudin-like Megatrachea is essential in septate junctions for the epithelial barrier function in *Drosophila*. *Developmental Cell* **5**, 611–620.

Beira, J. V. and Paro, R. (2016). The legacy of *Drosophila* imaginal discs. *Chromosoma* **125**, 573–592.

Beitel, G. J. and Krasnow, M. A. (2000). Genetic control of epithelial tube size in the *Drosophila* tracheal system. *Development* **3282**, 3271–3282.

Ben-Yosef, T., Belyantseva, I. A., Saunders, T. L., Hughes, E. D., Kawamoto, K., Van Itallie, C. M., Beyer, L. A., Halsey, K., Gardner, D. J., Wilcox, E. R., et al. (2003). Claudin 14 knockout mice, a model for autosomal recessive deafness DFNB29, are deaf due to cochlear hair cell degeneration. *Human Molecular Genetics* **12**, 2049–2061.

Bergmann, O., Zdunek, S., Felker, A., Salehpour, M., Alkass, K., Bernard, S., Sjostrom, S. L., Szewczykowska, M., Jackowska, T., dos Remedios, C., et al. (2015). Dynamics of Cell Generation and Turnover in the Human Heart. *Cell* **161**, 1566–1575.

- Bieber, A. J., Snow, P. M., Hortsch, M., Patel, N. H., Jacobs, J. R., Traquina, Z. R., Schilling, J. and Goodman, C. S.** (1989). Drosophila neuroglian: a member of the immunoglobulin superfamily with extensive homology to the vertebrate neural adhesion molecule L1. *Cell* **59**, 447–460.
- Bohn, H.** (1976). Tissue interactions in the regenerating cockroach leg. In *Insect Development* (ed. P. A. Lawrence), .
- Borgens, R. B.** (1982). Mice regrow the tips of their foretoes. *Science* **217**, 747–750.
- Brockes, J. P. and Kumar, A.** (2005). Appendage regeneration in adult vertebrates and implications for regenerative medicine. *Science* **310**, 1919–1923.
- Bryant, P. J.** (1971). Regeneration and duplication following operations in situ on the imaginal discs of *Drosophila melanogaster*. *Developmental Biology* **26**, 637–651.
- Burdette, W. J.** (1962). Changes in Titer of Ecdysone in *Bombyx mori* during Metamorphosis. *Science* **135**, 432–432.
- Burke, R. and Basler, K.** (1996). Dpp receptors are autonomously required for cell proliferation in the entire developing *Drosophila* wing. *Development* **122**, 2261–2269.
- Buszczak, M., Paterno, S., Lighthouse, D., Bachman, J., Planck, J., Owen, S., Skora, A. D., Nystul, T. G., Ohlstein, B., Allen, A., et al.** (2007). The carnegie protein trap library: A versatile tool for drosophila developmental studies. *Genetics* **175**, 1505–1531.
- Butler, M. J., Jacobsen, T. L., Cain, D. M., Jarman, M. G., Hubank, M., Whittle, J. R. S., Phillips, R. and Simcox, A.** (2003). Discovery of genes with highly restricted expression patterns in the *Drosophila* wing disc using DNA oligonucleotide microarrays. *Development* **130**, 659–670.
- Byri, S., Misra, T., Syed, Z. A., Bätz, T., Shah, J., Boril, L., Glashauser, J., Aegerter-Wilmsen, T., Matzat, T., Moussian, B., et al.** (2015). The triple-repeat protein Anakonda controls epithelial tricellular junction formation in *Drosophila*. *Developmental Cell*.
- Carlson, M. R., Bryant, S. V. and Gardiner, D. M.** (1998). Expression of Msx-2 during development, regeneration, and wound healing in axolotl limbs. *J. Exp. Zool.* **282**, 715–723.

- Cereijido, M., Robbins, E. S., Dolan, W. J., Rotunno, C. A. and Sabatini, D. D.** (1978). Polarized monolayers formed by epithelial cells on a permeable and translucent support. *J Cell Biol* **77**, 853–880.
- Chen, H.-W., Marinissen, M. J., Oh, S.-W., Chen, X., Melnick, M., Perrimon, N., Gutkind, J. S. and Hou, S. X.** (2002). CKA, a novel multidomain protein, regulates the JUN N-terminal kinase signal transduction pathway in *Drosophila*. *MCB* **22**, 1792–1803.
- Cherbas, L., Hu, X., Zhimulev, I., Belyaeva, E. and Cherbas, P.** (2003). EcR isoforms in *Drosophila*: testing tissue-specific requirements by targeted blockade and rescue. *Development* **130**, 271–284.
- Chernomordik, L. V. and Kozlov, M. M.** (2005). Membrane Hemifusion: Crossing a Chasm in Two Leaps. *Cell* **123**, 375–382.
- Chirayath, M. V., Gajdzik, L., Hulla, W., Graf, J., Cross, H. S. and Peterlik, M.** (1998). Vitamin D increases tight-junction conductance and paracellular Ca²⁺ transport in Caco-2 cell cultures. *American Journal of Physiology-Gastrointestinal and Liver Physiology* **274**, G389–G396.
- Cho, Y., Challa, S., Moquin, D., Genga, R., Ray, T. D., Guildford, M. and Chan, F. K.-M.** (2009). Phosphorylation-driven assembly of the RIP1-RIP3 complex regulates programmed necrosis and virus-induced inflammation. *Cell* **137**, 1112–1123.
- Claude, P.** (1978). Morphological factors influencing transepithelial permeability: A model for the resistance of the Zonula Occludens. *J. Membrin Biol.* **39**, 219–232.
- Claude, P. and Goodenough, D. A.** (1973). Fracture faces of zonulae occludentes from “tight” and “leaky” epithelia. *Journal of Cell Biology* **58**, 390–400.
- Cohen, B., McGuffin, M. E., Pfeifle, C., Segal, D. and Cohen, S. M.** (1992). *apterous*, a gene required for imaginal disc development in *Drosophila* encodes a member of the LIM family of developmental regulatory proteins. *Genes and Development* **6**, 715–729.
- Cohen, B., Simcox, A. A. and Cohen, S. M.** (1993). Allocation of the thoracic imaginal primordia in the *Drosophila* embryo. 597–608.
- Cohen, E., Allen, S. R., Sawyer, J. K. and Fox, D. T.** (2018). Fizzy-Related dictates A cell cycle switch during organ repair and tissue growth responses in the *Drosophila* hindgut. *eLife* **7**, e38327.

- Colombani, J., Bianchini, L., Layalle, S., Pondeville, E., Dauphin-Villemant, C., Antoniewski, C., Carré, C., Noselli, S. and Léopold, P.** (2005). Antagonistic actions of ecdysone and insulins determine final size in *Drosophila*. *Science* **310**, 667–670.
- Colombani, J., Andersen, D. S. and Léopold, P.** (2012). Secreted Peptide Dilp8 Coordinates *Drosophila* Tissue Growth with Developmental Timing. *Science* **336**, 582–585.
- Colombani, J., Andersen, D. S., Boulan, L., Boone, E., Romero, N., Virolle, V., Texada, M. and Léopold, P.** (2015). *Drosophila* Lgr3 Couples Organ Growth with Maturation and Ensures Developmental Stability. *Current biology : CB* **25**, 2723–9.
- Consortium, T. U.** (2019). UniProt: a worldwide hub of protein knowledge. *Nucleic Acids Res* **47**, D506–D515.
- Couso, J. P., Knust, E. and Martinez Arias, A.** (1995). Serrate and wingless cooperate to induce vestigial gene expression and wing formation in *Drosophila*. *Current Biology* **5**, 1437–1448.
- Crawford, K. and Stocum, D. L.** (1988). Retinoic acid proximalizes level-specific properties responsible for intercalary regeneration in axolotl limbs. *Development* **104**, 703–712.
- da Silva, P. P. and Kachar, B.** (1982). On tight-junction structure. *Cell* **28**, 441–450.
- da Silva, S. M., Gates, P. B. and Brockes, J. P.** (2002). The Newt Ortholog of CD59 Is Implicated in Proximodistal Identity during Amphibian Limb Regeneration. *Developmental Cell* **3**, 547–555.
- Dentice, M., Ambrosio, R., Damiano, V., Sibilio, A., Luongo, C., Guardiola, O., Yennek, S., Zordan, P., Minchiotti, G., Colao, A., et al.** (2014). Intracellular Inactivation of Thyroid Hormone Is a Survival Mechanism for Muscle Stem Cell Proliferation and Lineage Progression. *Cell Metabolism* **20**, 1038–1048.
- Diaz de la Loza, M. C. and Thompson, B. J.** (2017). Forces shaping the *Drosophila* wing. *Mechanisms of Development* **144**, 23–32.
- Diaz-Benjumea, F. J. and Cohen, S. M.** (1993). Interaction between dorsal and ventral cells in the imaginal disc directs wing development in *Drosophila*. *Cell* **75**, 741–752.

- Duszyc, K., Gomez, G. A., Schroder, K., Sweet, M. J. and Yap, A. S.** (2017). In life there is death: How epithelial tissue barriers are preserved despite the challenge of apoptosis. *Tissue Barriers* **5**,.
- Ebnet, K., Schulz, C. U., Brickwedde, M.-K. M. zu, Pendl, G. G. and Vestweber, D.** (2000). Junctional Adhesion Molecule Interacts with the PDZ Domain-containing Proteins AF-6 and ZO-1. *J. Biol. Chem.* **275**, 27979–27988.
- Eschenhagen, T., Bolli, R., Braun, T., Field, L. J., Fleischmann, B. K., Frisé, J., Giacca, M., Hare, J. M., Houser, S., Lee, R. T., et al.** (2017). Cardiomyocyte Regeneration: A Consensus Statement. *Circulation* **136**, 680–686.
- Farquhar, M. G. and Palade, G. E.** (1963). Junctional complexes in various epithelia. *J Cell Biol* **17**, 375–412.
- Fehon, R. G., Dawson, I. A. and Artavanis-Tsakonas, S.** (1994). A Drosophila homologue of membrane-skeleton protein 4.1 is associated with septate junctions and is encoded by the coracle gene. *Development (Cambridge, England)* **120**, 545–557.
- Filshie, B. K. and Flower, N. E.** (1977). Junctional structures in hydra. *Journal of Cell Science* **23**, 151–172.
- Fox, D. T., Cohen, E. and Smith-Bolton, R.** (2020). Model systems for regeneration: Drosophila. *Development* **147**,.
- French, V., Bryant, P. J. and Bryant, S. V.** (1976). Pattern Regulation in Epimorphic Fields. *Science* **193**, 969–981.
- Fristrom, D. and Fristrom, J. W.** (1975). The mechanism of evagination of imaginal discs of *Drosophila melanogaster*: I. General considerations. *Developmental Biology* **43**, 1–23.
- Furuse, M. and Tsukita, S.** (2006). Claudins in occluding junctions of humans and flies. *Trends in cell biology* **16**, 181–8.
- Furuse, M., Fujita, K., Hiiragi, T., Fujimoto, K. and Tsukita, S.** (1998). Claudin-1 and -2: novel integral membrane proteins localizing at tight junctions with no sequence similarity to occludin. *The Journal of cell biology* **141**, 1539–50.
- Galcerán, J., Llanos, J., Sampedro, J., Pongs, O. and Izquierdo, M.** (1990). Transcription at the ecdysone-inducible locus 2B5 in *Drosophila*. *Nucleic Acids Res* **18**, 539–545.

- Garelli, A., Gontijo, A. M., Miguela, V., Caparros, E. and Dominguez, M.** (2012). Imaginal Discs Secrete Insulin-Like Peptide 8 to Mediate Plasticity of Growth and Maturation. *Science* **336**, 579–582.
- Garelli, A., Heredia, F., Casimiro, A. P., Macedo, A., Nunes, C., Garcez, M., Mantas Dias, A. R., Volonte, Y. A., Uhlmann, T., Caparros, E., et al.** (2015). Dilp8 requires the neuronal relaxin receptor Lgr3 to couple growth to developmental timing.
- Gauhar, Z., Sun, L. V., Hua, S., Mason, C. E., Fuchs, F., Li, T.-R., Boutros, M. and White, K. P.** (2009). Genomic mapping of binding regions for the Ecdysone receptor protein complex. *Genome Res* **19**, 1006–1013.
- Genova, J. L. and Fehon, R. G.** (2003). Neuroglian, Gliotactin, and the Na⁺/K⁺ ATPase are essential for septate junction function in *Drosophila*. *Journal of Cell Biology* **161**, 979–989.
- Gibson, M. C., Lehman, D. A. and Schubiger, G.** (2002). Luminal Transmission of Decapentaplegic in *Drosophila* Imaginal Discs. *Developmental Cell* **3**, 451–460.
- Gilbert, L. I.** (2004). Halloween genes encode P450 enzymes that mediate steroid hormone biosynthesis in *Drosophila melanogaster*. *Molecular and Cellular Endocrinology* **215**, 1–10.
- Girgis, S. M.** (1975). Spontaneous Reanastomosis of the Vas Deferens after Surgery: A Case Report. *Fertility and Sterility* **26**, 182–185.
- Gödel, M., Hartleben, B., Herbach, N., Liu, S., Zschiedrich, S., Lu, S., Debreczeni-Mór, A., Lindenmeyer, M. T., Rastaldi, M.-P., Hartleben, G., et al.** (2011). Role of mTOR in podocyte function and diabetic nephropathy in humans and mice. *J Clin Invest* **121**, 2197–2209.
- González-Mariscal, L., Betanzos, A. and Ávila-Flores, A.** (2000). MAGUK proteins: structure and role in the tight junction. *Seminars in Cell & Developmental Biology* **11**, 315–324.
- Goodenough, D. A. and Revel, J. P.** (1970). A fine structural analysis of intracellular junctions in the mouse liver. *J Cell Biol* **45**, 272–290.
- Graubert, M. D., Asuncion Ortega, M., Kessel, B., Mortola, J. F. and Iruela-Arispe, M. L.** (2001). Vascular Repair After Menstruation Involves Regulation of Vascular Endothelial Growth Factor-Receptor Phosphorylation by sFLT-1. *Am J Pathol* **158**, 1399–1410.
- Green, C. R. and Bergquist, P. R.** (1982). Phylogenetic relationships within the invertebrata in relation to the structure of septate junctions and the

development of “occluding” junctional types. *Journal of Cell Science* **53**, 279–305.

- Guo, Z., Driver, I. and Ohlstein, B.** (2013). Injury-induced BMP signaling negatively regulates Drosophila midgut homeostasis. *J Cell Biol* **201**, 945–961.
- Haas, A. J., Zihni, C., Ruppel, A., Hartmann, C., Ebnet, K., Tada, M., Balda, M. S. and Matter, K.** (2020). Interplay between Extracellular Matrix Stiffness and JAM-A Regulates Mechanical Load on ZO-1 and Tight Junction Assembly. *Cell Reports* **32**, 107924.
- Hackney, J. F. and Cherbas, P.** (2014). Injury response checkpoint and developmental timing in insects. *Fly* **8**, 226–231.
- Hackney, J. F., Zolali-Meybodi, O. and Cherbas, P.** (2012). Tissue damage disrupts developmental progression and ecdysteroid biosynthesis in Drosophila. *PloS one* **7**, e49105.
- Hadorn, E. and Buck, D.** (1962). Ueber Entwicklungsleistungen transplantiertes Teilstücke von Flügel-Imaginalscheiben von *Drosophila melanogaster* [On the differentiation of transplanted wing imaginal disc fragments of *Drosophila melanogaster*]. *Revue suisse de zoologie* **69**, 302–310.
- Haines, R. J., Jr, R. S. B., Eitner, R. A., Chen, L. and Wu, M. H.** (2016). TNF α /IFN γ Mediated Intestinal Epithelial Barrier Dysfunction Is Attenuated by MicroRNA-93 Downregulation of PTK6 in Mouse Colonic Epithelial Cells. *PLOS ONE* **11**, e0154351.
- Hall, S. and Ward, R. E.** (2016). Septate Junction Proteins Play Essential Roles in Morphogenesis Throughout Embryonic Development in Drosophila. *G3 (Bethesda, Md.)* **6**, 2375–84.
- Halme, A., Cheng, M. and Hariharan, I. K.** (2010). Retinoids Regulate a Developmental Checkpoint for Tissue Regeneration in Drosophila. *Current Biology* **20**, 458–463.
- Hamada, Y., Bando, T., Nakamura, T., Ishimaru, Y., Mito, T., Noji, S., Tomioka, K. and Ohuchi, H.** (2015). Leg regeneration is epigenetically regulated by histone H3K27 methylation in the cricket *Gryllus bimaculatus*. *Development* **142**, 2916–2927.
- Hamaratoglu, F., Affolter, M. and Pyrowolakis, G.** (2014). Dpp/BMP signaling in flies: From molecules to biology. *Seminars in Cell & Developmental Biology* **32**, 128–136.

- Han, M., Yang, X., Lee, J., Allan, C. H. and Muneoka, K.** (2008). Development and regeneration of the neonatal digit tip in mice. *Developmental Biology* **315**, 125–135.
- Hardyman, M. A., Wilkinson, E., Martin, E., Jayasekera, N. P., Blume, C., Swindle, E. J., Gozzard, N., Holgate, S. T., Howarth, P. H., Davies, D. E., et al.** (2013). TNF- α -mediated bronchial barrier disruption and regulation by src-family kinase activation. *Journal of Allergy and Clinical Immunology* **132**, 665-675.e8.
- Harris, R. E., Setiawan, L., Saul, J. and Hariharan, I. K.** (2016). Localized epigenetic silencing of a damage-activated WNT enhancer limits regeneration in mature *Drosophila* imaginal discs. *eLife* **5**,.
- Haynie, J. L. and Bryant, P. J.** (1977). The effects of X-rays on the proliferation dynamics of cells in the imaginal wing disc of *Drosophila melanogaster*. *Wilhelm Roux' Archiv* **183**, 85–100.
- Heron, M.** (2019). *Deaths: Leading Causes for 2017*. U.S. Department of Health and Human Services, Centers for Disease Control and Prevention, National Center for Health Statistics, National Vital Statistics System.
- Herrera, S. C. and Bach, E. A.** (2019). JAK/STAT signaling in stem cells and regeneration: from *Drosophila* to vertebrates. *Development* **146**,.
- Higashi, T. and Chiba, H.** (2020). Molecular organization, regulation and function of tricellular junctions. *Biochimica et Biophysica Acta (BBA) - Biomembranes* **1862**, 183143.
- Higashi, T., Tokuda, S., Kitajiri, S., Masuda, S., Nakamura, H., Oda, Y. and Furuse, M.** (2013). Analysis of the 'angulin' proteins LSR, ILDR1 and ILDR2 – tricellulin recruitment, epithelial barrier function and implication in deafness pathogenesis. *J Cell Sci* **126**, 966–977.
- Hijazi, A., Masson, W., Augé, B., Waltzer, L., Haenlin, M. and Roch, F.** (2009). boudin is required for septate junction organisation in *Drosophila* and codes for a diffusible protein of the Ly6 superfamily. *Development (Cambridge, England)* **136**, 2199–209.
- Hoffmann, F. M. and Goodman, W.** (1987). Identification in transgenic animals of the *Drosophila* decapentaplegic sequences required for embryonic dorsal pattern formation. *Genes Dev.* **1**, 615–625.
- Hu, X., Cherbas, L. and Cherbas, P.** (2003). Transcription Activation by the Ecdysone Receptor (EcR/USP): Identification of Activation Functions. *Molecular Endocrinology* **17**, 716–731.

- Hwang, J. and Pallas, D. C.** (2014). STRIPAK complexes: Structure, biological function, and involvement in human diseases. *The International Journal of Biochemistry & Cell Biology* **47**, 118–148.
- Igaki, T., Kanda, H., Yamamoto-Goto, Y., Kanuka, H., Kuranaga, E., Aigaki, T. and Miura, M.** (2002). Eiger, a TNF superfamily ligand that triggers the Drosophila JNK pathway. *EMBO Journal* **21**, 3009–3018.
- Ikenouchi, J., Furuse, M., Furuse, K., Sasaki, H., Tsukita, S. and Tsukita, S.** (2005). Tricellulin constitutes a novel barrier at tricellular contacts of epithelial cells. *J Cell Biol* **171**, 939–945.
- Illingworth, C. M.** (1974). Trapped fingers and amputated finger tips in children. *Journal of Pediatric Surgery* **9**, 853–858.
- Inoki, K., Mori, H., Wang, J., Suzuki, T., Hong, S., Yoshida, S., Blattner, S. M., Ikenoue, T., Rüegg, M. A., Hall, M. N., et al.** (2011). mTORC1 activation in podocytes is a critical step in the development of diabetic nephropathy in mice. *J Clin Invest* **121**, 2181–2196.
- Itoh, M., Furuse, M., Morita, M., Kubota, K., Saitou, M. and Tsukita, S.** (1999). Direct binding of three tight junction-associated MAGUKs, ZO-1, ZO-2, and ZO-3, with the COOH termini of claudins. *The Journal of cell biology* **147**, 1351–63.
- Izumi, Y. and Furuse, M.** (2014). Molecular organization and function of invertebrate occluding junctions. *Seminars in Cell & Developmental Biology* **36**, 186–193.
- Izumi, Y., Yanagihashi, Y. and Furuse, M.** (2012). A novel protein complex, Mesh–Ssk, is required for septate junction formation in the Drosophila midgut. *J Cell Sci* **125**, 4923–4933.
- Izumo, S., Nadal-Ginard, B. and Mahdavi, V.** (1986). All members of the MHC multigene family respond to thyroid hormone in a highly tissue-specific manner. *Science* **231**, 597–600.
- Jaszczak, J. S., Wolpe, J. B., Dao, A. Q. and Halme, A.** (2015). Nitric oxide synthase regulates growth coordination during Drosophila melanogaster imaginal disc regeneration. *Genetics* **200**, 1219–1228.
- Jaszczak, J. S., Wolpe, J. B., Bhandari, R., Jaszczak, R. G. and Halme, A.** (2016). Growth coordination during Drosophila melanogaster imaginal disc regeneration is mediated by signaling through the relaxin receptor Lgr3 in the prothoracic gland. *Genetics* **204**, 703–709.

- Jin, H. J. and Park, H.-S.** (2018). Claudin may be a Potential Biomarker for Epithelial Barrier Dysfunction in Asthma. *Allergy Asthma Immunol Res* **10**, 4–5.
- Johnson, H. A. and Vera Roman, J. M.** (1966). Compensatory renal enlargement. Hypertrophy versus hyperplasia. *Am J Pathol* **49**, 1–13.
- Kaarteenaho, R., Merikallio, H., Lehtonen, S., Harju, T. and Soini, Y.** (2010). Divergent expression of claudin -1, -3, -4, -5 and -7 in developing human lung. *Respir. Res.* **11**, 59.
- Kachar, B. and Reese, T. S.** (1982). Evidence for the lipidic nature of tight junction strands. *Nature* **296**, 464–466.
- Kan, F. W.** (1993). Cytochemical evidence for the presence of phospholipids in epithelial tight junction strands.: *Journal of Histochemistry & Cytochemistry*.
- Kashio, S., Obata, F., Zhang, L., Katsuyama, T., Chihara, T. and Miura, M.** (2016). Tissue nonautonomous effects of fat body methionine metabolism on imaginal disc repair in *Drosophila*. *PNAS* **113**, 1835–1840.
- Katoonizadeh, A., Nevens, F., Verslype, C., Pirenne, J. and Roskams, T.** (2006). Liver regeneration in acute severe liver impairment: a clinicopathological correlation study. *Liver International* **26**, 1225–1233.
- Katsuyama, T., Comoglio, F., Seimiya, M., Cabuy, E. and Paro, R.** (2015). During *Drosophila* disc regeneration, JAK/STAT coordinates cell proliferation with Dilp8-mediated developmental delay. *Proceedings of the National Academy of Sciences of the United States of America* **112**, E2327–36.
- Kauppila, S., Maaty, W. S. A., Chen, P., Tomar, R. S., Eby, M. T., Chapo, J., Chew, S., Rathore, N., Zachariah, S., Sinha, S. K., et al.** (2003). Eiger and its receptor, Wengen, comprise a TNF-like system in *Drosophila*. *Oncogene* **22**, 4860–4867.
- Kerr, J. F. R., Wyllie, A. H. and Currie, A. R.** (1972). Apoptosis: A Basic Biological Phenomenon with Wideranging Implications in Tissue Kinetics. *British Journal of Cancer* **26**, 239–257.
- Kertesz, M., Iovino, N., Unnerstall, U., Gaul, U. and Segal, E.** (2007). The role of site accessibility in microRNA target recognition. *Nature Genetics* **39**, 1278–1284.

- Khadilkar, R. J. and Tanentzapf, G.** (2019). Septate junction components control *Drosophila* hematopoiesis through the Hippo pathway. *Development* **146**,.
- Klein, T.** (2001). Wing disc development in the fly: the early stages. *Current Opinion in Genetics & Development* **11**, 470–475.
- Klein, T. and Arias, A. M.** (1998a). Different spatial and temporal interactions between Notch, wingless, and vestigial specify proximal and distal pattern elements of the wing in *Drosophila*. *Dev. Biol.* **194**, 196–212.
- Klein, T. and Arias, A. M.** (1998b). Interactions among Delta, Serrate and Fringe modulate Notch activity during *Drosophila* wing development. *Development* **125**, 2951–2962.
- Koelle, M. R., Talbot, W. S., Segraves, W. A., Bender, M. T., Cherbas, P. and Hogness, D. S.** (1991). The *drosophila* EcR gene encodes an ecdysone receptor, a new member of the steroid receptor superfamily. *Cell* **67**, 59–77.
- Kozlova, T. and Thummel, C. S.** (2000). Steroid Regulation of Postembryonic Development and Reproduction in *Drosophila*. *Trends in Endocrinology & Metabolism* **11**, 276–280.
- Kozlova, T. and Thummel, C. S.** (2003). Essential Roles for Ecdysone Signaling During *Drosophila* Mid-Embryonic Development. *Science* **301**, 1911–1914.
- Kragl, M., Knapp, D., Nacu, E., Khattak, S., Maden, M., Epperlein, H. H. and Tanaka, E. M.** (2009). Cells keep a memory of their tissue origin during axolotl limb regeneration. *Nature* **460**, 60–65.
- Lamb, R. S., Ward, R. E., Schweizer, L. and Fehon, R. G.** (1998). *Drosophila* coracle, a member of the protein 4.1 superfamily, has essential structural functions in the septate junctions and developmental functions in embryonic and adult epithelial cells. *Molecular biology of the cell* **9**, 3505–3519.
- Lane, N. J.** (1979). Freeze-fracture and tracer studies on the intercellular junctions of insect rectal tissues. *Tissue and Cell* **11**, 481–506.
- Lane, N. J. and Swales, L. S.** (1982). Stages in the assembly of pleated and smooth septate junctions in developing insect embryos. *Journal of cell science* **56**, 245–62.
- Laprise, P., Lau, K. M., Harris, K. P., Silva-Gagliardi, N. F., Paul, S. M., Beronja, S., Beitel, G. J., McGlade, C. J. and Tepass, U.** (2009). Yurt,

Coracle, Neurexin-IV and the Na⁺,K⁺-ATPase form a novel group of epithelial polarity proteins. *Nature* **459**, 1141–1145.

- Lavrynenko, O., Rodenfels, J., Carvalho, M., Dye, N. A., Lafont, R., Eaton, S. and Shevchenko, A.** (2015). The ecdysteroidome of *Drosophila*: influence of diet and development. *Development (Cambridge, England)* **142**, 3758–68.
- Lee, S.-R., Hong, S.-T. and Choi, K.-W.** (2020). Regulation of epithelial integrity and organ growth by Tctp and Coracle in *Drosophila*. *PLOS Genetics* **16**, e1008885.
- Luschnig, S., Bätz, T., Armbruster, K. and Krasnow, M. A.** (2006). serpentine and vermiform Encode Matrix Proteins with Chitin Binding and Deacetylation Domains that Limit Tracheal Tube Length in *Drosophila*. *Current Biology* **16**, 186–194.
- Maden, M.** (1980). Intercalary regeneration in the amphibian limb and the rule of distal transformation. *Development* **56**, 201–209.
- Maden, M.** (1997). Retinoic acid and its receptors in limb regeneration. *Seminars in Cell & Developmental Biology* **8**, 445–453.
- Malt, R. A.** (1969). Compensatory Growth of the Kidney. *N Engl J Med* **280(26)**, 1446-59.
- Mandaravally Madhavan, M. and Schneiderman, H. A.** (1977). Histological analysis of the dynamics of growth of imaginal discs and histoblast nests during the larval development of *Drosophila melanogaster*. *Wilhelm Roux' Archiv* **183**, 269–305.
- Masuda, S., Oda, Y., Sasaki, H., Ikenouchi, J., Higashi, T., Akashi, M., Nishi, E. and Furuse, M.** (2011). LSR defines cell corners for tricellular tight junction formation in epithelial cells. *J Cell Sci* **124**, 548–555.
- Mathelier, A., Fornes, O., Arenillas, D. J., Chen, C.-Y., Denay, G., Lee, J., Shi, W., Shyr, C., Tan, G., Worsley-Hunt, R., et al.** (2016). JASPAR 2016: a major expansion and update of the open-access database of transcription factor binding profiles. *Nucleic Acids Res.* **44**, D110-115.
- Mayerl, S., Schmidt, M., Doycheva, D., Darras, V. M., Hüttner, S. S., Boelen, A., Visser, T. J., Kaether, C., Heuer, H. and von Maltzahn, J.** (2018). Thyroid Hormone Transporters MCT8 and OATP1C1 Control Skeletal Muscle Regeneration. *Stem Cell Reports* **10**, 1959–1974.
- McBrayer, Z., Ono, H., Shimell, M., Parvy, J.-P., Beckstead, R. B., Warren, J. T., Thummel, C. S., Dauphin-Villemant, C., Gilbert, L. I. and O'Connor,**

- M. B.** (2007). Prothoracicotropic Hormone Regulates Developmental Timing and Body Size in *Drosophila*. *Developmental Cell* **13**, 857–871.
- McCall, K.** (2010). Genetic control of necrosis – another type of programmed cell death. *Curr Opin Cell Biol* **22**, 882–888.
- McCarthy, K. M., Skare, I. B., Stankewich, M. C., Furuse, M., Tsukita, S., Rogers, R. A., Lynch, R. D. and Schneeberger, E. E.** (1996). Occludin is a functional component of the tight junction. *Journal of Cell Science* **109**, 2287–2298.
- McGuire, S. E., Mao, Z. and Davis, R. L.** (2004). Spatiotemporal Gene Expression Targeting with the TARGET and Gene-Switch Systems in *Drosophila*. *Sci. STKE* **2004**, pl6–pl6.
- Milán, M., Diaz-Benjumea, F. J. and Cohen, S. M.** (1998). Beadex encodes an LMO protein that regulates Apterous LIM-homeodomain activity in *Drosophila* wing development: A model for LMO oncogene function. *Genes and Development* **12**, 2912–2920.
- Monteiro, A. C., Sumagin, R., Rankin, C. R., Leoni, G., Mina, M. J., Reiter, D. M., Stehle, T., Dermody, T. S., Schaefer, S. A., Hall, R. A., et al.** (2013). JAM-A associates with ZO-2, afadin, and PDZ-GEF1 to activate Rap2c and regulate epithelial barrier function. *MBoC* **24**, 2849–2860.
- Moonwiryakit, A., Wattanaphichet, P., Chatsudthipong, V. and Muanprasat, C.** (2018). GPR40 receptor activation promotes tight junction assembly in airway epithelial cells via AMPK-dependent mechanisms. *Tissue Barriers* **6**, 1–12.
- Morata, G. and Lawrence, P. A.** (1975). Control of compartment development by the engrailed gene in *Drosophila*. *Nature* **255**, 614–617.
- Moreno, E., Yan, M. and Basler, K.** (2002). Evolution of TNF signaling mechanisms: JNK-dependent apoptosis triggered by Eiger, the *Drosophila* homolog of the TNF superfamily. *Current Biology* **12**, 1263–1268.
- Morin, X., Daneman, R., Zavortink, M. and Chia, W.** (2001). A protein trap strategy to detect GFP-tagged proteins expressed from their endogenous loci in *Drosophila*. *Proceedings of the National Academy of Sciences of the United States of America* **98**, 15050–15055.
- Narasimha, M., Uv, A., Krejci, A., Brown, N. H. and Bray, S. J.** (2008). Grainy head promotes expression of septate junction proteins and influences epithelial morphogenesis. *J Cell Sci* **121**, 747–752.

- Nellen, D., Burke, R., Struhl, G. and Basler, K.** (1996). Direct and Long-Range Action of a DPP Morphogen Gradient. *Cell* **85**, 357–368.
- Nelson, K. S., Furuse, M. and Beitel, G. J.** (2010). The Drosophila Claudin Kune-kune is required for septate junction organization and tracheal tube size control. *Genetics* **185**, 831–9.
- Nguyen, D. A., Parlow, A. F. and Neville, M. C.** (2001). Hormonal regulation of tight junction closure in the mouse mammary epithelium during the transition from pregnancy to lactation. *Journal of Endocrinology* **170**, 347–356.
- Nicholson, D. W. and Thornberry, N. A.** (1997). Caspases: killer proteases. *Trends in Biochemical Sciences* **22**, 299–306.
- Niimi, T., Nagashima, K., Ward, J. M., Minoo, P., Zimonjic, D. B., Popescu, N. C. and Kimura, S.** (2001). claudin-18, a novel downstream target gene for the T/EBP/NKX2.1 homeodomain transcription factor, encodes lung- and stomach-specific isoforms through alternative splicing. *Mol. Cell. Biol.* **21**, 7380–7390.
- Nilton, A., Oshima, K., Zare, F., Byri, S., Nannmark, U., Nyberg, K. G., Fehon, R. G. and Uv, A. E.** (2010). Crooked, coiled and crimped are three Ly6-like proteins required for proper localization of septate junction components. *Development (Cambridge, England)* **137**, 2427–37.
- Noirot-Timothee, C. and Noirot, C.** (1980). Septate and Scalariform Junctions in Arthropods. In *International Review of Cytology*, pp. 97–140.
- Okamoto, N., Viswanatha, R., Bittar, R., Li, Z., Haga-Yamanaka, S., Perrimon, N. and Yamanaka, N.** (2018). A Membrane Transporter Is Required for Steroid Hormone Uptake in Drosophila. *Developmental Cell* **47**, 294–305.e7.
- Oshima, K. and Fehon, R. G.** (2011). Analysis of protein dynamics within the septate junction reveals a highly stable core protein complex that does not include the basolateral polarity protein Discs large. *Journal of Cell Science* **124**, 2861–2871.
- Pan, X., Connacher, R. P. and O'Connor, M. B.** (2020). Control of the insect metamorphic transition by ecdysteroid production and secretion. *Current Opinion in Insect Science*.
- Pasparakis, M. and Vandenabeele, P.** (2015). Necroptosis and its role in inflammation. *Nature* **517**, 311–320.

- Pastor-Pareja, J. C., Grawe, F., Martín-Blanco, E. and García-Bellido, A.** (2004). Invasive cell behavior during *Drosophila* imaginal disc eversion is mediated by the JNK signaling cascade. *Developmental Cell* **7**, 387–399.
- Paul, S. M., Ternet, M., Salvaterra, P. M. and Beitel, G. J.** (2003). The Na⁺/K⁺ ATPase is required for septate junction function and epithelial tube-size control in the *Drosophila* tracheal system. *Development (Cambridge, England)* **130**, 4963–4974.
- Pérez-Garijo, A., Shlevkov, E. and Morata, G.** (2009). The role of Dpp and Wg in compensatory proliferation and in the formation of hyperplastic overgrowths caused by apoptotic cells in the *Drosophila* wing disc. *Development* **136**, 1169–1177.
- Perkins, K. K., Admon, A., Patel, N. and Tjian, R.** (1990). The *Drosophila* Fos-related AP-1 protein is a developmentally regulated transcription factor. *Genes Dev.* **4**, 822–834.
- Pesic, M. and Greten, F. R.** (2016). Inflammation and cancer: tissue regeneration gone awry. *Current Opinion in Cell Biology* **43**, 55–61.
- Pessemesse, L., Tintignac, L., Blanchet, E., Cortade, F., Jublanc, E., Demangel, R., Py, G., Sar, C., Cabello, G., Wrutniak-Cabello, C., et al.** (2019). Regulation of mitochondrial activity controls the duration of skeletal muscle regeneration in response to injury. *Sci Rep* **9**, 12249.
- Porrello, E. R., Mahmoud, A. I., Simpson, E., Hill, J. A., Richardson, J. A., Olson, E. N. and Sadek, H. A.** (2011). Transient Regenerative Potential of the Neonatal Mouse Heart. *Science* **331**, 1078–1080.
- Poss, K. D., Wilson, L. G. and Keating, M. T.** (2002). Heart Regeneration in Zebrafish. *Science* **298**, 2188–2190.
- Potter, C. J., Tasic, B., Russler, E. V., Liang, L. and Luo, L.** (2010). The Q system: a repressible binary system for transgene expression, lineage tracing, and mosaic analysis. *Cell* **141**, 536–548.
- Rajasekaran, A. K., Hojo, M., Huima, T. and Rodriguez-Boulan, E.** (1996). Catenins and zonula occludens-1 form a complex during early stages in the assembly of tight junctions. *J Cell Biol* **132**, 451–463.
- Resino, J., Salama-Cohen, P. and García-Bellido, A.** (2002). Determining the role of patterned cell proliferation in the shape and size of the *Drosophila* wing. *PNAS* **99**, 7502–7507.
- Riesgo-Escovar, J. R., Jenni, M., Fritz, A. and Hafen, E.** (1996). The *Drosophila* Jun-N-terminal kinase is required for cell morphogenesis but

not for DJun-dependent cell fate specification in the eye. *Genes Dev.* **10**, 2759–2768.

Rochard, P., Rodier, A., Casas, F., Cassar-Malek, I., Marchal-Victorion, S., Daury, L., Wrutniak, C. and Cabello, G. (2000). Mitochondrial Activity Is Involved in the Regulation of Myoblast Differentiation through Myogenin Expression and Activity of Myogenic Factors. *J. Biol. Chem.* **275**, 2733–2744.

Rodrigues, A. B., Zoranovic, T., Ayala-Camargo, A., Grewal, S., Reyes-Robles, T., Krasny, M., Wu, D. C., Johnston, L. A. and Bach, E. A. (2012). Activated STAT regulates growth and induces competitive interactions independently of Myc, Yorkie, Wingless and ribosome biogenesis. *Development* **139**, 4051–4061.

Rojas-Canales, D. M., Li, J. Y., Makuei, L. and Gleadle, J. M. (2019). Compensatory renal hypertrophy following nephrectomy: When and how? *Nephrology* **24**, 1225–1232.

Rosenblatt, J., Raff, M. C. and Cramer, L. P. (2001). An epithelial cell destined for apoptosis signals its neighbors to extrude it by an actin- and myosin-dependent mechanism. *Current Biology* **11**, 1847–1857.

Rouaud, F., Sluysmans, S., Flinois, A., Shah, J., Vasileva, E. and Citi, S. (2020). Scaffolding proteins of vertebrate apical junctions: structure, functions and biophysics. *Biochimica et Biophysica Acta (BBA) - Biomembranes* **1862**, 183399.

Rouka, E., Gourgoulianni, N., Lüpold, S., Hatzoglou, C., Gourgouliannis, K., Blanckenhorn, W. U. and Zarogiannis, S. G. (2020). The Drosophila Septate Junctions beyond barrier function: Review of the literature, prediction of human orthologs of the SJ-related proteins, and identification of protein domain families. *Acta Physiologica n/a*, e13527.

Ruiz-Losada, M., Blom-Dahl, D., Córdoba, S. and Estella, C. (2018). Specification and Patterning of Drosophila Appendages. *Journal of Developmental Biology* **6**, 17.

Schindelin, J., Arganda-Carreras, I., Frise, E., Kaynig, V., Longair, M., Pietzsch, T., Preibisch, S., Rueden, C., Saalfeld, S., Schmid, B., et al. (2012). Fiji: an open-source platform for biological-image analysis. *Nature Methods* **9**, 676–682.

Schlingmann, B., Molina, S. A. and Koval, M. (2015). Claudins: gatekeepers of lung epithelial function. *Semin Cell Dev Biol* **42**, 47–57.

- Schneeberger, E. E. and Lynch, R. D.** (2004). The tight junction: a multifunctional complex. *American journal of physiology. Cell physiology* **286**, C1213–C1228.
- Schubiger, M., Sustar, A. and Schubiger, G.** (2010). Regeneration and transdetermination: The role of wingless and its regulation. *Developmental Biology* **347**, 315–324.
- Schwedes, C. C. and Carney, G. E.** (2012). Ecdysone signaling in adult *Drosophila melanogaster*. *Journal of Insect Physiology* **58**, 293–302.
- Senga, K., Mostov, K. E., Mitaka, T., Miyajima, A. and Tanimizu, N.** (2012). Grainyhead-like 2 regulates epithelial morphogenesis by establishing functional tight junctions through the organization of a molecular network among claudin3, claudin4, and Rab25. *Mol Biol Cell* **23**, 2845–2855.
- Sensiate, L. A. and Marques-Souza, H.** (2019). Bone growth as the main determinant of mouse digit tip regeneration after amputation. *Scientific Reports* **9**, 9720.
- Setiawan, L., Pan, X., Woods, A. L., O’connor, M. B. and Hariharan, I. K.** (2018). The BMP2/4 ortholog Dpp can function as an inter-organ signal that regulates developmental timing.
- Sharifkhodaei, Z., Padash-Barmchi, M., Gilbert, M. M., Samarasekera, G., Fulga, T. A., Van Vactor, D. and Auld, V. J.** (2016). The *Drosophila* tricellular junction protein Gliotactin regulates its own mRNA levels through BMP-mediated induction of miR-184. *Journal of cell science* **129**, 1477–89.
- Sharifkhodaei, Z., Gilbert, M. M. and Auld, V. J.** (2019). Scribble and Discs Large mediate tricellular junction formation. *Development (Cambridge)* **146**,.
- Sharma, R. P.** (1973). Wingless - a new mutant in *D. melanogaster*. *DIS* **50**, 134.
- Sharma, R. P. and Chopra, V. L.** (1976). Effect of the wingless (*wg1*) mutation on wing and haltere development in *Drosophila melanogaster*. *Developmental Biology* **48**, 461–465.
- Shen, L.** (2012). Tight junctions on the move: molecular mechanisms for epithelial barrier regulation. *Annals of the New York Academy of Sciences* 9–18.
- Shen, L., Weber, C. R. and Turner, J. R.** (2008). The tight junction protein complex undergoes rapid and continuous molecular remodeling at steady state. *J Cell Biol* **181**, 683–695.

- Simon, H. G., Nelson, C., Goff, D., Laufer, E., Morgan, B. A. and Tabin, C.** (1995). Differential expression of myogenic regulatory genes and Msx-1 during dedifferentiation and redifferentiation of regenerating amphibian limbs. *Dev. Dyn.* **202**, 1–12.
- Siparsky, P. N., Kirkendall, D. T. and Garrett, W. E.** (2014). Muscle Changes in Aging. *Sports Health* **6**, 36–40.
- Sluss, H. K., Han, Z., Barrett, T., Davis, R. J. and Ip, Y. T.** (1996). A JNK signal transduction pathway that mediates morphogenesis and an immune response in *Drosophila*. *Genes Dev.* **10**, 2745–2758.
- Smith-Bolton, R. K., Worley, M. I., Kanda, H. and Hariharan, I. K.** (2009). Regenerative growth in *Drosophila* imaginal discs is regulated by Wingless and Myc. *Dev Cell* **16**, 797–809.
- Song, Z., McCall, K. and Steller, H.** (1997). DCP-1, a *Drosophila* Cell Death Protease Essential for Development. *Science* **275**, 536–540.
- Staehein, L. A.** (1973). Further Observations on the Fine Structure of Freeze-Cleaved Tight Junctions. *Journal of Cell Science* **13**, 763–786.
- Stenderup, K., Justesen, J., Clausen, C. and Kassem, M.** (2003). Aging is associated with decreased maximal life span and accelerated senescence of bone marrow stromal cells. *Bone* **33**, 919–926.
- Stevens, L. J. and Page-McCaw, A.** (2012). A secreted MMP is required for reepithelialization during wound healing. *MBoC* **23**, 1068–1079.
- Stocum, D. L.** (2017). Mechanisms of urodele limb regeneration. *Regeneration (Oxf)* **4**, 159–200.
- Strigini, M. and Cohen, S. M.** (2000). Wingless gradient formation in the *Drosophila* wing. *Current Biology* **10**, 293–300.
- Sugie, H. and Verity, M. A.** (1985). Postnatal histochemical fiber type differentiation in normal and hypothyroid rat soleus muscle. *Muscle & Nerve* **8**, 654–660.
- Suzuki, H., Nishizawa, T., Tani, K., Yamazaki, Y., Tamura, A., Ishitani, R., Dohmae, N., Tsukita, S., Nureki, O. and Fujiyoshi, Y.** (2014). Crystal Structure of a Claudin Provides Insight into the Architecture of Tight Junctions. *Science* **344**, 304–307.
- Suzuki, H., Tani, K., Tamura, A., Tsukita, S. and Fujiyoshi, Y.** (2015). Model for the Architecture of Claudin-Based Paracellular Ion Channels through Tight Junctions. *Journal of Molecular Biology* **427**, 291–297.

- Swarup, S. and Verheyen, E. M.** (2012). Wnt/Wingless Signaling in *Drosophila*. *Cold Spring Harb Perspect Biol* **4**, a007930.
- Tabata, T., Eaton, S. and Kornberg, T. B.** (1992). The *Drosophila* hedgehog gene is expressed specifically in posterior compartment cells and is a target of engrailed regulation. *Genes Dev.* **6**, 2635–2645.
- Takeo, M., Chou, W. C., Sun, Q., Lee, W., Rabbani, P., Loomis, C., Taketo, M. M. and Ito, M.** (2013). Wnt activation in nail epithelium couples nail growth to digit regeneration. *Nature* **499**, 228–232.
- Tan, K. L., Vlisidou, I. and Wood, W.** (2014). Ecdysone Mediates the Development of Immunity in the *Drosophila* Embryo. *Current Biology* **24**, 1145–1152.
- Tepass, U. and Hartenstein, V.** (1994). The Development of Cellular Junctions in the *Drosophila* Embryo. *Developmental Biology* **161**, 563–596.
- Tepass, U., Tanentzapf, G., Ward, R. and Fehon, R.** (2001). *EPITHELIAL CELL POLARITY AND CELL JUNCTIONS IN DROSOPHILA*.
- Terada, N., Saitoh, Y., Ohno, N., Komada, M., Saitoh, S., Peles, E. and Ohno, S.** (2012). Essential Function of Protein 4.1G in Targeting of Membrane Protein Palmitoylated 6 into Schmidt-Lanterman Incisures in Myelinated Nerves. *Mol Cell Biol* **32**, 199–205.
- Thurmond, J., Goodman, J. L., Strelets, V. B., Attrill, H., Gramates, L. S., Marygold, S. J., Matthews, B. B., Millburn, G., Antonazzo, G., Trovisco, V., et al.** (2019). FlyBase 2.0: the next generation. *Nucleic Acids Res* **47**, D759–D765.
- Tracy Cai, X., Li, H., Safyan, A., Gawlik, J., Pyrowolakis, G. and Jasper, H.** (2019). AWD regulates timed activation of BMP signaling in intestinal stem cells to maintain tissue homeostasis. *Nature Communications* **10**, 2988.
- Tsukita, S., Furuse, M. and Itoh, M.** (2001). Multifunctional strands in tight junctions. *Nature Reviews Molecular Cell Biology* **2**, 285–293.
- Turksen, K. and Troy, T.-C.** (2004). Barriers built on claudins. *Journal of cell science* **117**, 2435–2447.
- Ursprung, H.** (1962). Einfluss des Wirtsaiters auf die Entwicklungsleistung von Sagittalhilften männlicher Genitalscheiben von *Drosophila melanogaster* [Influence of the host string on the development performance of sagittal halves of male genital discs from *Drosophila melanogaster*]. *Developmental Biology* **4**, 22–39.

- Vallejo, D. M., Juarez-Carreño, S., Bolivar, J., Morante, J. and Dominguez, M.** (2015). A brain circuit that synchronizes growth and maturation revealed through Dilp8 binding to Lgr3. *Science (New York, N.Y.)* 1–16.
- Vallon, V. and Thomson, S. C.** (2012). Renal Function in Diabetic Disease Models: The Tubular System in the Pathophysiology of the Diabetic Kidney. *Annu. Rev. Physiol.* **74**, 351–375.
- Van Itallie, C. M., Rogan, S., Yu, A., Vidal, L. S., Holmes, J. and Anderson, J. M.** (2006). Two splice variants of claudin-10 in the kidney create paracellular pores with different ion selectivities. *American Journal of Physiology-Renal Physiology* **291**, F1288–F1299.
- Vergheze, S. and Su, T. T.** (2016). Drosophila Wnt and STAT Define Apoptosis-Resistant Epithelial Cells for Tissue Regeneration after Irradiation. *PLoS Biol* **14**,.
- Vuuren, S. H. van, Sol, C. M., Broekhuizen, R., Lillen, M. R., Oosterveld, M. J. S., Nguyen, T. Q., Goldschmeding, R. and Jong, T. P. V. M. de** (2012). Compensatory Growth of Congenital Solitary Kidneys in Pigs Reflects Increased Nephron Numbers Rather Than Hypertrophy. *PLOS ONE* **7**, e49735.
- Wada, N., Kimura, I., Tanaka, H., Ide, H. and Nohno, T.** (1998). Glycosylphosphatidylinositol-anchored cell surface proteins regulate position-specific cell affinity in the limb bud. *Dev. Biol.* **202**, 244–252.
- Wagner, D. E., Wang, I. E. and Reddien, P. W.** (2011). Clonogenic Neoblasts Are Pluripotent Adult Stem Cells That Underlie Planarian Regeneration. *Science* **332**, 811–816.
- Wang, S., Jayaram, S. A., Hemphälä, J., Senti, K.-A., Tsarouhas, V., Jin, H. and Samakovlis, C.** (2006). Septate-junction-dependent luminal deposition of chitin deacetylases restricts tube elongation in the *Drosophila* trachea. *Current biology : CB* **16**, 180–5.
- Wang, Y., Wang, R., Jiang, S., Zhou, W., Liu, Y., Wang, Y., Gu, Q., Gu, Y., Dong, Y., Liu, M., et al.** (2011). Gecko CD59 Is Implicated in Proximodistal Identity during Tail Regeneration. *PLOS ONE* **6**, e17878.
- Ward IV, R. E., Schweizer, L., Lamb, R. S. and Fehon, R. G.** (2001). The protein 4.1, ezrin, radixin, moesin (FERM) domain of *drosophila* coracle, a cytoplasmic component of the septate junction, provides functions essential for embryonic development and imaginal cell proliferation. *Genetics* **159**, 219–228.

- Warren, J. T., Petryk, A., Marqués, G., Jarcho, M., Parvy, J.-P., Dauphin-Villemant, C., O'Connor, M. B. and Gilbert, L. I.** (2002). Molecular and biochemical characterization of two P450 enzymes in the ecdysteroidogenic pathway of *Drosophila melanogaster*. *PNAS* **99**, 11043–11048.
- Wigglesworth, V. B.** (1951). Source of Moulting Hormone in *Rhodnius*. *Nature* **168**, 558–558.
- Williams, J. A., Bell, J. B. and Carroll, S. B.** (1991). Control of *Drosophila* wing and haltere development by the nuclear vestigial gene product. *Genes Dev.* **5**, 2481–2495.
- Wood, R. L.** (1959). Intercellular Attachment in the Epithelium of *Hydra* As Revealed by Electron Microscopy. *J Biophys Biochem Cytol* **6**, 343–352.
- Woods, D. F., Hough, C., Peel, D., Callaini, G. and Bryant, P. J.** (1996). Dlg protein is required for junction structure, cell polarity, and proliferation control in *Drosophila* epithelia. *The Journal of cell biology* **134**, 1469–82.
- Worley, M. I., Setiawan, L. and Hariharan, I. K.** (2012). Regeneration and Transdetermination in *Drosophila* Imaginal Discs. *Annual Review of Genetics* **46**, 289–310.
- Wu, V. M., Schulte, J., Hirschi, A., Tepass, U. and Beitel, G. J.** (2004). Sinuous is a *Drosophila* claudin required for septate junction organization and epithelial tube size control. *The Journal of Cell Biology* **164**, 313–323.
- Wu, V. M., Yu, M. H., Paik, R., Banerjee, S., Liang, Z., Paul, S. M., Bhat, M. A. and Beitel, G. J.** (2007). *Drosophila* Varicose, a member of a new subgroup of basolateral MAGUKs, is required for septate junctions and tracheal morphogenesis. *Development (Cambridge, England)* **134**, 999–1009.
- Xie, Y., Zhao, Y., Shi, L., Li, W., Chen, K., Li, M., Chen, X., Zhang, H., Li, T., Matsuzawa-Ishimoto, Y., et al.** (2020). Gut epithelial TSC1/mTOR controls RIPK3-dependent necroptosis in intestinal inflammation and cancer. *Journal of Clinical Investigation* **130**, 2111–2128.
- Xu, P., Elamin, E., Elizalde, M., Bours, P. P. H. A., Pierik, M. J., Masclee, A. A. M. and Jonkers, D. M. A. E.** (2019). Modulation of Intestinal Epithelial Permeability by Plasma from Patients with Crohn's Disease in a Three-dimensional Cell Culture Model. *Scientific Reports* **9**, 2030.
- Yajima, H., Yoneitamura, S., Watanabe, N., Tamura, K. and Ide, H.** (1999). Role of N-cadherin in the sorting-out of mesenchymal cells and in the

positional identity along the proximodistal axis of the chick limb bud. *Dev. Dyn.* **216**, 274–284.

- Yao, T.-P., Segraves, W. A., Oro, A. E., McKeown, M. and Evans, R. M.** (1992). *Drosophila* ultraspiracle modulates ecdysone receptor function via heterodimer formation. *Cell* **71**, 63–72.
- Yao, T.-P., Forman, B. M., Jiang, Z., Cherbas, L., Chen, J.-D., McKeown, M., Cherbas, P. and Evans, R. M.** (1993). Functional ecdysone receptor is the product of EcR and Ultraspiracle genes. *Nature* **366**, 476–479.
- Yin, Z., Pinteá, V., Lin, Y., Hammock, B. D. and Watsky, M. A.** (2011). Vitamin D Enhances Corneal Epithelial Barrier Function. *Invest Ophthalmol Vis Sci* **52**, 7359–7364.
- Yun, M. H.** (2015). Changes in Regenerative Capacity through Lifespan. *Int J Mol Sci* **16**, 25392–25432.
- Zecca, M., Basler, K. and Struhl, G.** (1995). Sequential organizing activities of engrailed, hedgehog and decapentaplegic in the *Drosophila* wing. *Development* **121**, 2265–2278.
- Zeissig, S., Burgel, N., Gunzel, D., Richter, J., Mankertz, J., Wahnschaffe, U., Kroesen, A. J., Zeitz, M., Fromm, M. and Schulzke, J.-D.** (2007). Changes in expression and distribution of claudin 2, 5 and 8 lead to discontinuous tight junctions and barrier dysfunction in active Crohn's disease. *Gut* **56**, 61–72.
- Zhang, Y.-G., Wu, S. and Sun, J.** (2013). Vitamin D, Vitamin D Receptor, and Tissue Barriers. *Tissue barriers* **1**, 1–6.
- Ziegler-Graham, K., MacKenzie, E. J., Ephraim, P. L., Trivison, T. G. and Brookmeyer, R.** (2008). Estimating the Prevalence of Limb Loss in the United States: 2005 to 2050. *Archives of Physical Medicine and Rehabilitation* **89**, 422–429.
- Zihni, C., Mills, C., Matter, K. and Balda, M. S.** (2016). Tight junctions: from simple barriers to multifunctional molecular gates. *Nature Reviews Molecular Cell Biology* **17**, 564–580.